WMO/TCP/WWW

NINTH INTERNATIONAL WORKSHOP ON TROPICAL CYCLONES (IWTC-9)

Topic (3.1): Intensity Change: Internal Influences

Rapporteur: Jonathan L. Vigh
National Center for Atmospheric Research
jvigh@ucar.edu
+1 +303 +497 8205

Working Group:
Haiyan Jiang (Florida International University)
Yi-Hsuan Huang
Yoshiaki Miyamoto (Keio University)
Ryo Oyama (Meteorological Research Institute)
Qinqing Li (Nanjing University of Information Science and Technology)
Eric Hendricks (NCAR)
Konstantinos Menelaou (McGill University)
Christopher Slocum (Cooperative Institute for Research in the Atmosphere)
Kristen L. Corbosiero (State University of New York–Albany)
Michael Bell (Colorado State University)
Yuqing Wang (University of Hawaiʻi at Mānoa)
Jing Xu (State Key Laboratory of Severe Weather)
Olivier Bousquet (Laboratoire de l'Atmosphère et des Cyclones)
Roger Smith (Ludwig–Maximilians–University of Munich)
Rochelle Coronel (Ateneo de Davao University)
Jeffrey D. Kepert (Bureau of Meteorology)

Abstract:

The past four years have witnessed considerable scientific progress in the area of internal influences on tropical cyclone (TC) intensity change. Observational studies of satellite-sensed cloud and precipitation features, as well as new analyses of lightning data, have improved understanding of the convective morphology before and during RI, particularly with regard to the degree of axisymmetry, the importance of shallow convection around the center, and the radial and azimuthal distribution and evolution of convective bursts and hot towers prior to and during RI. Numerical simulations have increased appreciation of the probabilistic nature of RI processes. The impacts of secondary eyewall formation (SEF) and eyewall replacement cycles (ERCs) on intensity change have become better understood through an expanded climatology of ERCs and the different wind-pressure-relationships that occur in intense and less intense TCs. Improved understanding of the ERC climatology has translated into better operational forecasts of ERC-induced intensity changes. With regard to rainbands and intensity change, recent observational work has shown that outer rainband lightning is positively correlated with subsequent 24-h TC intensity change. Idealized numerical simulations have demonstrated that convective heating in the inner rainband region generally promotes intensification, while evaporative cooling in inner rainbands tends to hinder TC intensification.

Numerical studies on the impacts of inner core instability processes have expanded from 2D barotropic frameworks to more realistic 3D frameworks that include moisture and parameterized mass sinks. Results from simulations in more realistic frameworks show that instability processes may cause intensification under certain assumptions, although considerable uncertainties remain, particularly as to the role of the secondary circulation in either preventing relaxation of the vortex to a monopole (or how quickly it might restore the vortex back to an annular state) and as to the effects of moist convective processes on instability. Advances in modeling and observations of surface fluxes have improved our understanding of the relationships between TC intensification and the drag and enthalpy coefficients, as well with the sea surface temperature response.

The mechanisms by which TCs intensify has been an area of considerable research, resulting in refinements to existing frameworks for understanding TC intensification (e.g., the rotating-convection framework). Vigorous debate has recently occurred as to the suitability of using balanced frameworks to understand intensification, whether or not WISHE is an essential part of TC intensification, and the exact role of the boundary layer in TC spin-up. This report also includes several new topics that have recently emerged, such as the role of TC outflow, the role of vortex structure on a TC’s IR, and a new theory for what sets the fastest rate at which TCs may intensify.

3.1.1 Introduction

The goal of this Rapporteur Report is to summarize the research progress on internal influences of tropical cyclone (TC) intensity change since IWTC-VIII. Intensity change is a broad topic that does not lend itself to artificial delineation between “internal processes” (this report, Topic 3.1) and “external influences” (Topic 3.2). Indeed, close connections exist between TC intensity change and several other topics in IWTC-IX, such as TC structure analysis and change (Topic 4), secondary eyewall formation and the expansion of the wind field (Topic 4.1), and operational perspectives on intensity change (Topic 3.3). Naturally, there will be some overlap between the Rapporteur reports. At the possible expense of some duplication between reports, we have preferred to avoid letting any studies remain uncovered.

The past four years has witnessed a considerable increase in research activity on internal processes of intensity change. Whereas the previous IWTC-VIII Rapporteur Report for this subtopic (Stern et al. 2014) contained references to 77 new studies since the previous IWTC report, the current report contains 183 references to new studies. To identify the publications on this topic that have been published since 2014, our Working Group (WG) followed a rigorous process to screen a list of papers compiled from Web of Science. The list was compiled by Maggie Lien (see acknowledgments) by searching for all papers that contained one of the following TC-related terms in either the paper’s title or topic: “tropical cyclone”, “hurricane”, and “typhoon” (and their plurals). To further narrow the scope of papers to be screened, a further criterion was added by requiring that papers be from the “Meteorological and Atmospheric Science” discipline. The resulting list of 3417 papers was reviewed by the WG for possible relevance to internal intensity change processes, with approximately 300 papers identified as being possibly relevant. The WG then screened the paper titles/abstracts for relevance to this subtopic and grouped the publications into smaller topical divisions.

The WG was then organized into teams, with each team having the responsibility to write a synthesis of the papers for one section of the subtopic. Although this report focuses mainly on research progress, rather than operational perspectives, we have attempted to make the writing accessible to a broad audience (including forecasters). In order to properly put the recent studies into context, each synthesis includes an introduction with brief discussion of earlier studies, as well as a brief summary with recommendations (if any) for future research directions. Finally, it is also important to note that a reader interested in one particular section below need not read the entire report—each synthesis can be read as a stand-alone document.

These literature syntheses form the following seven sections of this Rapporteur Report:

- 3.1.2 Rapid Intensification
- 3.1.3 Eyewall Replacement Cycles
- 3.1.4 Relation of Rainbands to Intensity Change
- 3.1.5 Eyewall Instability and Inner-Core Mixing
- 3.1.6 Relationship between Surface Fluxes and Intensity Change
- 3.1.7 Mechanisms of Tropical Cyclone Intensification
- 3.1.8 New and Emerging Research Topics

This report concludes with a summary and conclusions section, overall recommendations for future research directions, acknowledgements, a list of the primary contributors to each section, a list of acronyms used in this report, and references.

3.1.2 Rapid Intensification (RI)

a) Introduction and Definition of RI

Although the prediction of TC track has improved substantially due to more accurate numerical models and more satellite observations over the open ocean, predictions of TC intensity change have proven to be much more challenging. Our understanding of TC intensity changes is very limited, especially during the RI phase because of a lack of understanding of the physical mechanisms that are responsible for these relatively rare events. RI is first defined by Kaplan and DeMaria (2003) using the 95th percentile of the cumulative distribution functions of the 24-h intensity change derived from historical best track data (Landsea and Franklin 2013). In the North Atlantic (NA) basin, the 95th percentile of the 24-h intensity change is 30 kt (Kaplan and DeMaria 2003). Therefore, in this basin RI is defined as a 24-h period with an intensity increase ≥ 30 kt in this basin. Many following studies found that the same 30 kt (or 15.4 m/s) threshold can be used globally (Jiang 2012; Jiang et al. 2013; Zagrodnik and Jiang 2014) or for other basins such as the northwest Pacific (Shu et al. 2012; Wang et al. 2015), northeast Pacific (Kaplan et al. 2010), and the southwest Indian Ocean (Leroux et al. 2018). In contrast, Hendricks et al. (2010) found that the 95th percentile of the 24-h intensity change for TCs during a five-year period (2003–2008) in the northwest Pacific basin was 19 m/s (36.9 kt). The Hendricks et al. (2010) study period is much shorter than other studies, however, so this could be the reason that they found a higher RI threshold.

The topic of RI has seen significant interest from researchers. Since the previous report for this subtopic (Stern et al. 2014), more than 60 refereed papers have been published about RI. This subsection synthesizes results from these publications during the past four years (2014–2018) to summarize the advancements in understanding physical processes associated with RI and how to better forecast these rare events. This synthesis includes subsections on RI climatology (subsection b), observational and idealized and non-idealized numerical perspectives of RI (subsections c, d and e), and new developments in the operational prediction of RI (subsection f), followed by a summary and recommendations for future research.

b) **RI Climatology**

This subsection reports new insights on TC RI based on recent climatological studies investigating intensification rate (IR) dependence on various internal and external parameters in the North Atlantic (NA) and Western North Pacific (WNP) basins.

Using six decades of NA TC observations from the Hurricane Database (HURDAT2; Landsea and Franklin 2013), Yaukey (2014) found that the onset of intensification (defined as a 15 kt (7.7 m/s) increase over 24 h) was most likely to occur shortly after midnight local time, and least likely to occur shortly before midnight. This statistical analysis also shows that RI is influenced by TC age from genesis, as well as by the wind speed deficit relative to speeds expected for the TC's central pressure.[1] In the NA basin, Qin et al. (2016) used the Extended Best Track (EBT) dataset during the 25-year period of 1990–2014 to perform a statistical analysis of steady state-radius of maximum wind (S-RMWs) associated with rapidly intensifying TCs. In S-RMW cases, the contraction of the RMW during intensification ceases before TCs reach their peak intensities, resulting in nearly steady state RMWs; such features were notably observed in major hurricanes such as Katrina (2005), Megi (2010), and Andrew (1992). An analysis of 55 rapidly intensifying hurricanes that exhibited steady state-RMWs shows that S-RMWs comprise about 53% of the 139 RI events of 24-h duration and 69% of 12-h RI events. Also, S-RMWs tend to occur more frequently in intense storms and when RMWs have already contracted to less than 50 km.

Carrasco et al. (2014) used the NA Hurricane Database (HURDAT2; Landsea and Franklin 2013) to investigate possible connections between TC size and their subsequent propensity to undergo RI. Comparisons between RI and non-RI TCs over a 20-year period of analysis (1990–2010) show that TCs undergoing RI are more likely to be smaller initially than those that do not. For various inner and outer measures of size, such as RMW and average 34-kt radius (AR34), TCs that do not experience RI are approximately 10 n mi (18.5 km) larger than cyclones undergoing RI. They found that RI is unlikely when the initial RMW > 50 n mi (~90 km) and AR34 > 140 n mi (250 km). They also showed that for both size parameters, these thresholds lay near the boundary (RMW = 48 n mi, 89 km) separating medium and large TC, suggesting that RI becomes unlikely once a TC has a large RMW and/or AR34. In contrast, when using the radius of the outermost-closed isobar (ROCI) as the size parameter, the size difference between RI and non-RI cases is negligible (this suggests that intensity forecasts and RI predictions may be improved by the use of the initial size as measured by RMW and AR34). Xu and Wang (2018a) conducted a similar study in the WNP using the Joint Typhoon Warning Center (JTWC) best track database during 1982–2015. RI was found to occur only in a relatively narrow range of the parameter space in storm intensity and both inner-and outer-core sizes, with the highest intensification rate (IR) occurring when Vmax = 70 kt (36 m/s), RMW ≤ 40 km, and AR34 = 150 km. Consistent with the findings for NA TCs, RI was found to occur only for TCs with moderate intensity and small inner-core size, while storms with RMWs > 120 km almost never intensify rapidly (Fig. 1).

[1] Yaukey's results suggests that taking into account additional storm characteristics such as age, strength, and time of day could help increase the performance of RI forecast schemes such as NHC's operational Statistical Hurricane Intensity Prediction Scheme (SHIPS) model.

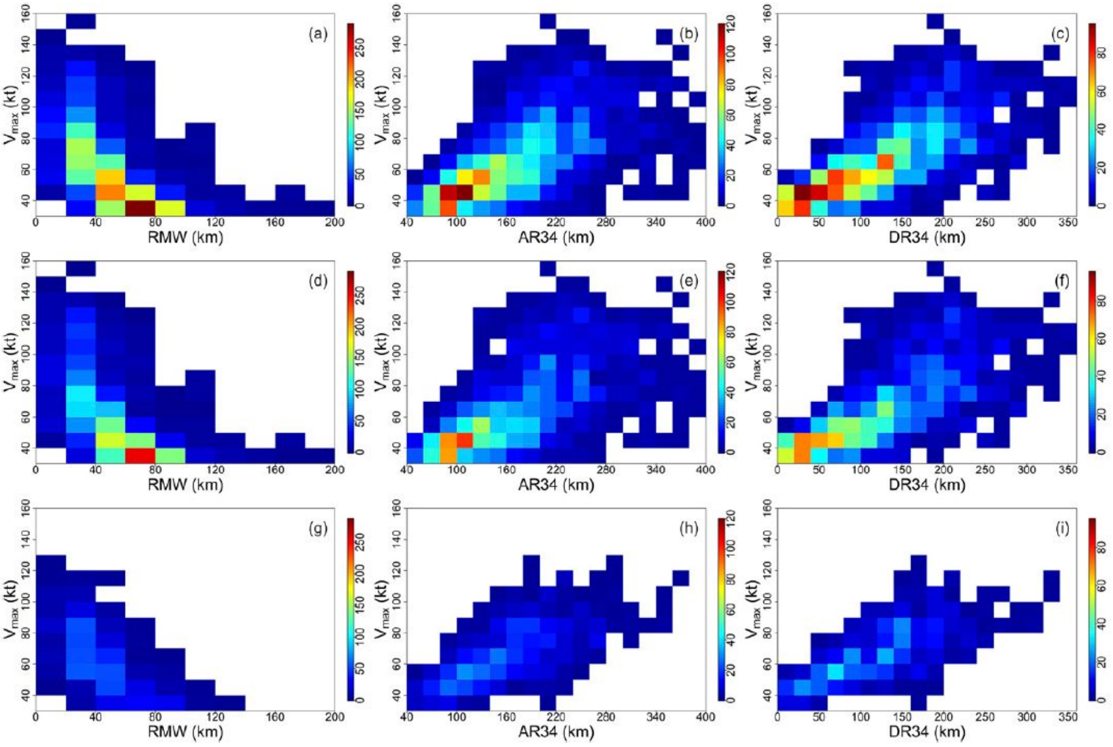

Fig 1. Distributions of numbers of (a)–(c) all intensifying TC cases, (d)–(f) non-RI TC cases [with IR less than 30 kt (15.4 m/s) per 24 h], and (g)–(i) RI TC cases for the parameter spaces of (left) Vmax–RMW, (center) Vmax–AR34, and (right) Vmax–DR34 [where DR34 is the outer-core wind skirt parameter computed as AR34−RMW]. Figure 9 of Xu and Wang (2018a).

c) Observational Perspectives on RI

This subsection reports new insights on RI from observational studies. A key aspect of this topic is the relationship between RI and the distribution of inner-core convection and precipitation. Satellite-based statistical studies have often demonstrated that the degree of axisymmetry of convection and precipitation is a vital indicator of RI. Some pioneering studies that were summarized in the previous IWTC-VIII report include Kieper and Jiang (2012) and Zagrodnik and Jiang (2014). Using 15 years of passive microwave satellite data for Atlantic and east Pacific storms, Alvey et al. (2015) found that, compared to TCs with lower IRs, TCs with higher IRs (including RI) possess more symmetric distributions of precipitation prior to the onset of intensification, as well as a greater overall areal coverage of precipitation. Using 14 years of Tropical Rainfall Measuring Mission (TRMM) Precipitation Radar (PR) data, Tao and Jiang (2015) compared the contributions to RI by shallow to moderate precipitation versus the contributions by moderately deep to very deep convection. They found that increased and widespread shallow convection around the storm center is a first indication of RI and can be used as a predictor for the onset of RI. The contribution to total volumetric rain and latent heating from shallow and moderately shallow precipitation in the inner core is greater in RI storms than in non-RI storms, while the opposite is true for moderately deep and very deep precipitation. Therefore, Tao and Jiang (2015) argued that RI is more likely triggered by the increase of shallow-moderate precipitation, and that the appearance of more moderately to very deep convection in the middle of RI is more likely a response, or positive feedback, to changes in the vortex (rather than a cause of RI). Harnos and Nesbitt (2016) used 37-

and 85-GHz passive microwave data to quantify the relative prevalence of cold clouds (i.e., deep convection and stratiform clouds) versus predominantly warm clouds (i.e., shallow cumulus and cumulus congestus). They found that TCs undergoing subsequent RI or intensification possessed a greater presence of combined liquid and frozen hydrometeors associated with cold clouds. Compared to the full intensity change distribution, TCs undergoing RI episodes exhibited approximately an order of magnitude increase of inner-core cold cloud frequency relative to warm cloud presence.

Conventionally, RI is defined as a 24-h period with intensity increase ≥ 30 kt (15.4 m/s), by following Kaplan and DeMaria's (2003) pioneering work on RI, with each 24-h period treated as a separate case. The main drawback of this approach is that it neglects storm evolution information. In reality, RI usually happens as an event, which can last 48–60 h or longer. In order to place the individual 24-h RI cases within the context of the entire RI event, Tao et al. (2017) first introduced an RI event-based definition. An RI event was defined as multiple, continuous, and overlapping 24-h periods where the maximum sustained winds of each period increased by at least 30 kt (15.4 m/s), as illustrated in Tao et al. (2017)'s figure 1 (not shown). They used this definition to examine the relative importance of stratiform and convective precipitation with respect to the evolution of RI events from a 16-y TRMM PR dataset. They found that the onset of RI follows a significant increase in the occurrence and azimuthal coverage of stratiform rainfall in all shear-relative quadrants, especially upshear left (Fig. 2). They also found that rainfall intensity and total volumetric rain, which are mainly contributed by convective precipitation, do not increase until several hours after RI onset. Therefore, they argued that the convective precipitation is more likely a response, or positive feedback, rather than the trigger of RI. Jiang et al. (2018) used the same RI event-based definition as in Tao et al. (2017) to examine the evolution of different precipitation types during RI events. By further separating convective precipitation into shallow and deep types, Jiang et al. (2018) found a significant increase in the inner-core coverage of stratiform precipitation and shallow convection 3 to 21 h before the onset of RI.

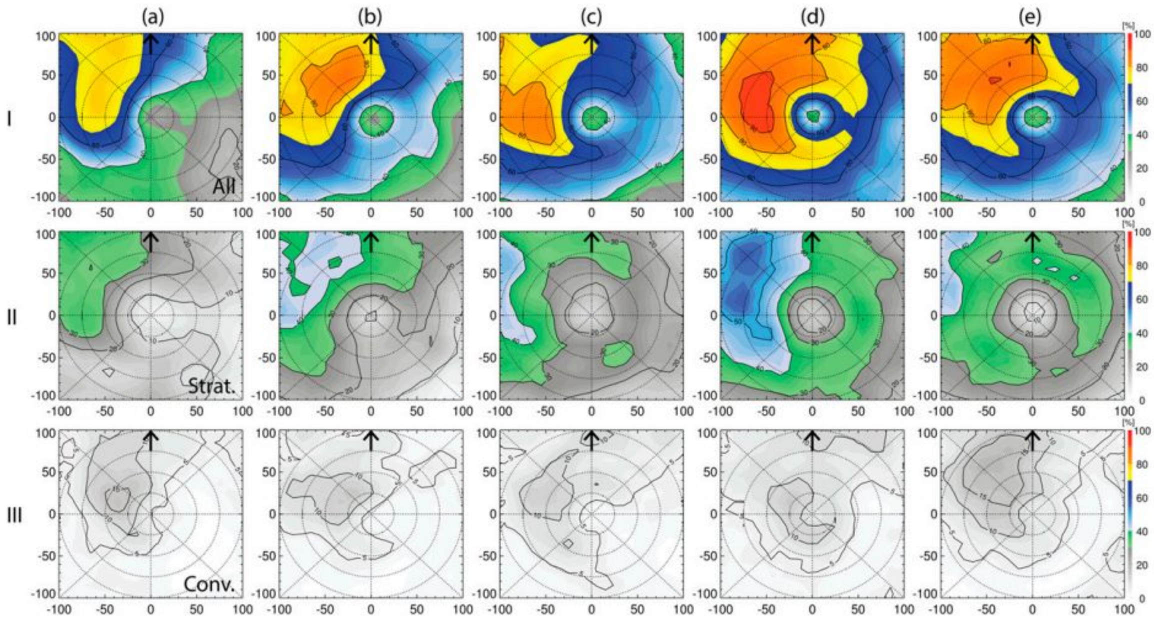

Fig 2. Composite shear-relative distribution of the rainfall coverage from (I) all precipitation, (II) stratiform precipitation, and (III) convective precipitation. From left to right: (a) 12–24 h before RI onset, (b) 0–12 h before RI onset, (c) RI onset, (d) RI continuing, and (e) 12–24 h before RI ends. Dotted range rings represent the 25-, 50-, 75-, and 100-km radii. Figure 4 of Tao et al. (2017).

A normalization technique was used by Fischer et al. (2018) to analyze anomalous TC convective characteristics and their relationship to TC intensity change. They showed that anomalously cold infrared and 85-GHz brightness temperatures, as well as anomalously warm 37-GHz brightness temperatures, in the upshear quadrants of the TC are associated with increased rates of TC intensification, including RI. For RI episodes in the NA basin, they found that an increase in anomalous liquid hydrometeor content precedes anomalous ice hydrometeor content by approximately 12 h, suggesting that convection deep enough to produce robust ice scattering is a symptom of, rather than a precursor to, RI. In the eastern North Pacific basin, they found that the amount of anomalous liquid and ice hydrometeors increases in tandem near the onset of RI. Fischer et al.'s (2018) study suggests that normalized infrared and passive microwave brightness temperatures could be utilized to skillfully predict episodes of RI.

Oyama (2017) examined the relationship between TC intensification and cloud-top outflow revealed by upper-tropospheric atmospheric motion vectors (AMVs) derived from geostationary satellite observations of 44 TCs during 2011–2014. He found that the IRs of 66% of the TCs peaked 0–36 h after the maximum outflow was observed. For TCs undergoing RI, the peak IR also occurred after the maximum outflow. He also found that the correlation between outflow and the TC IR was higher for TCs accompanied by convective bursts (CBs) than for those without CBs, implying that a rapid deepening of inner-core convection is important for intensification of a TC's secondary circulation. Gao et al. (2017) undertook a water budget analysis of TCs to examine four water-budget components (total precipitable water, surface evaporation, precipitation, and column-integrated moisture flux convergence) associated with WNP TCs of different intensity change categories. The water budget parameters were derived from satellite observations and model reanalysis data during 2001–2009. Their results showed that surface evaporation plays an important role in storm RI and the highest evaporation rates are associated with rapidly intensifying TCs over the highest sea surface temperatures (SSTs). They also found that total precipitable water in the outer environment, where moisture is mainly provided by surface evaporation, is also vital to storm RI because RI is favored when there is less dry air intruding into the storm circulation.

Lightning serves as an important proxy of convective intensity. The relationship between the spatial and temporal distribution of lightning activity and RI has been examined statistically across specific basins and globally. Using 16 years of TRMM Lightning Imager Sensor data, Xu et al. (2017) found that rapidly intensifying TCs showed significantly smaller inner-core flash density and volume of 30 dBZ echoes in the mixed phase region than slowly intensifying TCs, indicating the potential use of these parameters in forecasting RI. They also found that inner-core (outer-rainband) flash density decreases (increases) 12–18 h preceding the onset of RI, while inner-core (outer-rainband) flash density increases (decreases) 6–12 h prior to TC weakening (Fig. 3). Using lightning data from the World Wide Lightning Location Network (WWLLN), Zhang et al. (2015) investigated the relationship between inner-core lightning and TC intensity changes over the WNP basin. They found that the differences in lightning density between RI and rapidly weakening (RW) storms are largest in the inner core, and that the lightning density for RI cases is larger than for RW cases in the inner core (0–100km). Using WWLLN data for TCs in the Southwest Indian Ocean (SWIO), Bovalo et al. (2014) found that the proportion of periods with lightning activity is higher during rapid intensity changes of TCs. They also found that during tropical storm stage, lightning activity in the outer rainbands begins increasing 18 h before a RI period. The WWLLN data were also used to examine the characteristics of lightning activity in TCs over North Indian Ocean (NIO) by Ranalkar et al. (2017). They discovered that during RI, TCs exhibit high lightning flash rates.

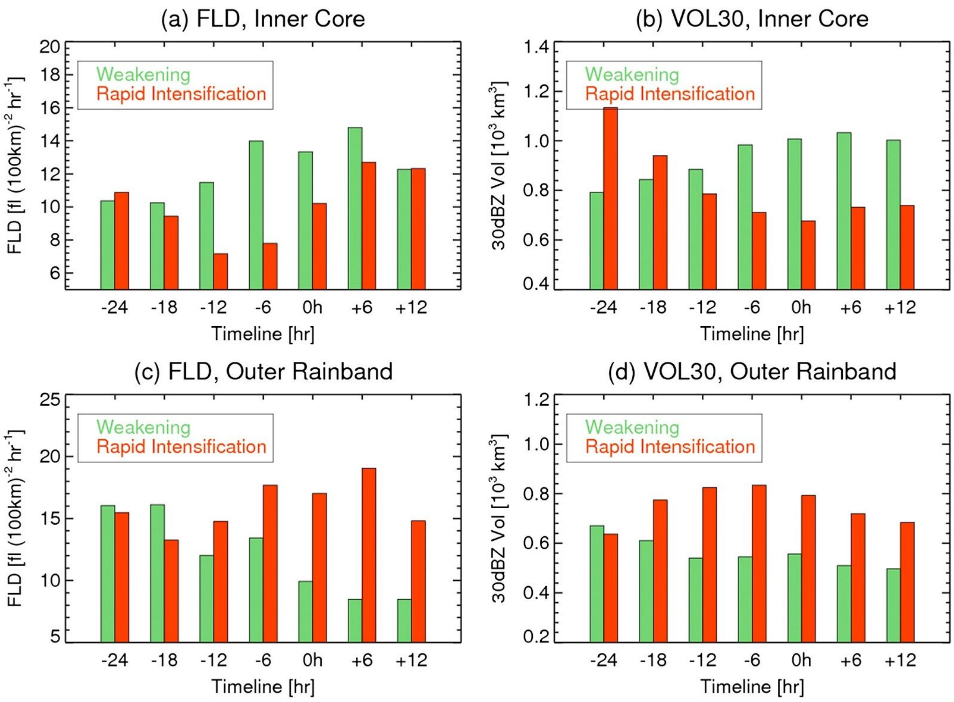

Fig 3. (a, c) Flash density (FLD) and (b, d) 30-dBZ echo volume (VOL30) between -5 and -40°C in the inner-core region (a and b) and outer-rainband region (c and d), as a function of time period relative to the onset of TC weakening (green bars) and RI (red bars). Figure 9 of Xu et al. (2017).

During the IWTC-IX reporting period, two field experiments were dedicated to collecting data for TC intensity and intensity change, including RI: 1) the National Aeronautics and Space Administration's (NASA) Hurricane and Severe Storm Sentinel (HS3) during 2012–2014 (Braun et al. 2016), and 2) the Office of Naval Research Tropical Cyclone Intensity (TCI) field program during 2015 (Doyle et al. 2017). These two field campaigns, along with many previous ones, have provided crucial flight-level, dropsonde, and remote sensing data for RI case studies. Using NASA HS3 data, the relationship between thermodynamic and dynamic structures, and convection and precipitation during the symmetrization process of Hurricane Edouard (2014) and its association with RI was investigated by Zawislak et al. (2016) and Rogers et al. (2016). Zawislak et al. (2016) found that the precipitation distribution is intimately linked to the thermodynamic symmetry, which becomes greater as the frequency, areal coverage, and, in particular, rainfall rate increases upshear. Their results suggest that the upshear moisture content could be a predictor for RI. Rogers et al. (2016) demonstrated that deep convection was located farther inside the RMW during the intensifying period than the weakening period. Their results highlighted the importance of the azimuthal coverage of precipitation and the radial location of deep convection for RI. Using ONR TCI data, Duran and Molinari (2018) studied the dramatic inner-core tropopause variability during the RI of Hurricane Patricia (2015). Based on the observations of eyewall penetrations into the stratosphere during RI, the existence of a narrow inflow layer near the tropopause and the role of subsidence from the stratosphere in developing an upper-level warm core, they hypothesized three mechanisms of inner-core tropopause variability: destabilization of the tropopause inversion layer (TIL) through turbulent mixing, weakening of the TIL over the eye through upper-tropospheric subsidence warming, and increasing tropopause height forced by overshooting updrafts in the eyewall. They further argued that none of these processes are seen as the direct cause of RI, but rather are a part of the RI process that features strong increases in boundary layer moist entropy.

The RI of Hurricane Earl (2010) was extensively examined by Stevenson et al. (2014), Susca–Lopata et al. (2015), and Rogers et al. (2015) using a variety of available data sources. Stevenson et al. (2014) found that the inner-core lightning activity in the inner core of Earl precessed from left-of-shear to upshear beginning just prior to the onset of RI, which was considered to be an extremely rare event since it differed markedly from previous studies. They hypothesized that Earl's RI may have occurred, in part, because the vertical wind shear acted to reduce the upshear tilt, and the occurrence of convection inside the RMW helped to enhance the warm core. The role of deep convection in Earl's RI was further investigated by Susca–Lopata et al. (2015), and Rogers et al. (2015). Both studies found that asymmetric deep convection in the initially vertically misaligned vortex, initially left-of-shear but not distinctly up- or down-shear, subsequently rotated into upshear regions. By the end of this stage, the vortex was aligned and extended over a deep layer, the precipitation symmetry increased, and RI commenced.

Guimond et al. (2016) documented a similar rotation of deep CBs from the downshear quadrants into the upshear quadrants during the RI Hurricane Karl (2010). Guimond et al. (2016) argued that the bursts form and are maintained through a combination of two main processes: 1) convergence generated from counter-rotating mesovortex circulations and the larger vortex-scale flow, and 2) the turbulent transport of anomalously warm, buoyant air from the eye out into the eyewall at low levels. They also documented the development of a pronounced axisymmetric vortex following the pulsing CBs; this vortex included a sloped eyewall structure and the formation of a clear, wide eye.

Sanger et al. (2014) found that vortical updrafts were common before and during RI of Super Typhoon Jangmi (2008). They further claimed that rotating convective clouds are important elements in the TC spin-up process. Similarly, Shimada et al. (2018) found enhanced eyewall convection inside the RMW during the RI of Typhoon Goni (2015).

d) Idealized Numerical Perspectives on RI

Most recent studies are based on idealized, or real-case, ensemble TC simulations using convection-permitting models. For instance, a large ensemble of 270 idealized TC simulations was used by Miyamoto and Nolan (2018) to study the structural changes of TCs preceding RI. The ensemble average of RI cases had two distinct intensification phases. In the first phase, both the RMW and the vortex tilt decrease with time. In the second phase, the equivalent potential temperature in the lowest 1 km and the radius of maximum convergence (RMC) increase prior to the onset of RI. The Rossby number was also larger in the simulations (119) that experienced RI in the subsequent 24 h compared with the samples without RI. These findings are consistent with the study of Miyamoto and Takemi (2015), which showed that TC vortices with larger Rossby numbers were more likely to experience RI and, hence, to evolve into strong hurricanes (Fig. 4).

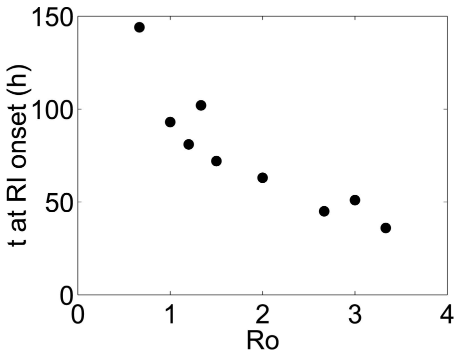

Fig. 4. Relationship between Rossby radius (Ro) and the time (t) of the onset of RI. Figure 20 of Miyamoto and Takemi (2015).

Using Weather Research and Forecasting (WRF) model ensemble simulations with different environmental vertical wind shear, SST, and ambient moisture conditions, Tao and Zhang (2014) found that the environmental shear could significantly affect the timing of TC intensification by influencing the spatial distribution of convection and subsequently changing the positive feedback between diabatic heating and the TC vortex primary circulation. In particular, the changes in the distribution and intensity of the diabatic heating were found to subsequently affect the secondary circulation strength and the vortex mean circulation. From idealized numerical experiments, Wang and Heng (2016) also evaluated the contribution of the near-surface high energy air in the eye region to TC intensification rate. Their results showed that when the surface entropy flux was turned off in the eye region, the equivalent potential temperature and convective available potential energy in the eye were largely suppressed while the IR of the simulated storm was reduced by about 30% during the RI phase. These results suggest that the near-surface high entropy air in the eye region can be crucial for initiating convection near the inner edge of the eyewall and facilitating eyewall contraction. This process leads to higher inner-core inertial stability, and thus, higher dynamical efficiency as the eyewall heating spins up the tangential winds near the RMW. All of this leads to a larger IR in the simulated TC.

Using five high-resolution ensembles based on the Advanced Research version of the WRF (ARW) model, Judt and Chen (2016) investigated the predictability of RI during Hurricane Earl (2010), which is considered as one of the best-observed hurricane RI cases to date. While environmental conditions control the maximum TC intensity and the likelihood of RI during the TC lifetime, both environmental and internal factors are found to contribute to uncertainty in RI timing. Complex interactions among environmental vertical wind shear, the mean vortex, and internal convective processes govern the TC intensification process and lead to diverse pathways to maturity. Although the likelihood of Earl undergoing RI seems to be predictable, the exact timing of RI has a stochastic component and low predictability. Despite uncertainty in the timing of RI, two dominant modes of RI emerged: members which undergo RI early in the storm lifecycle, and members which undergo RI later in the life cycle. In the early RI cases, a rapidly contracting RMW accompanies the development of the eyewall during RI. The late RI cases possess a well-developed eyewall prior to RI and form an upper-level warm core during the RI process. These differences indicate that RI is associated with distinct physical processes during particular stages of the TC life cycle.

Kowch and Emanuel (2015) analyzed frequency distributions of intensification and dissipation developed from synthetic open-ocean tropical cyclone data, and found that RI is part of a continuum of intensity change that shows no propensity toward a fat tail. This result suggests that TC intensification and dissipation are controlled by randomly distributed environmental and internal processes.

e) **Numerical Perspectives on RI**

This subsection reports new insights on RI from modeling studies. The relationship between deep convection including CBs and RI is a key aspect of this topic. Tang et al. (2018a) simulated Typhoon Mujigae (2015) using the ARW model and showed that the CBs play an important role in the formation of the warm cores in the middle and upper troposphere, respectively, which trigger and maintain RI. To focus on the roles of latent heating, Miller et al. (2015) used a WRF simulations of Hurricane Wilma (2005) to examine the impacts of changing latent heating rates on the RI. They found that simulated TCs experience substantially reduced IRs in experiments in which the latent heating is reduced. Simulations with greater latent heating rates generate more inner-core CBs during RI, with peak vertical motion in the eyewall occurring at higher altitudes. Li et al. (2016) simulated Typhoon Megi (2010) using the WRF model, which experienced both RI and gradual intensification processes during its lifetime. They showed that in small- or moderate-shear environments, the enhanced CBs release large amounts of latent heat in the upper troposphere, which enhances the upper-level warm core and leads to the intensification phase. During RI onset, strong convective cells concentrated in the eyewall downshear or left-of-shear. As Megi intensified rapidly, symmetric structures became well developed.

In WRF simulations of Typhoon Megi (2010), Lee and Wu (2018) found polygonal eyewall structure during the RI period, with high winds concentrated at each vertex of the polygonal eyewall. Furthermore, when conditions are conducive to TC intensification, the winds often amplify near each vertex of the polygonal eyewall, resulting in high inertial stability, more energy gain from enhanced local surface heat fluxes, higher tangential winds due to radial absolute angular momentum advection, greater supergradient winds, and a higher frequency of CBs located inside the RMW. Therefore, they suggested that the polygonal structure of the eyewall likely facilitates RI by amplifying the aforementioned features at each vertex, and enhancing their impact on the vortex-scale intensification.

Stern and Zhang (2016) examined the vertical aspects of the warm-core structure of Hurricane Earl (2010) on four different days, spanning periods of both RI and weakening. This study used a convection-permitting forecast, as well as high-altitude dropsondes. Results showed that during RI, strong warming occurs at all heights. Further, Chang and Wu (2017) explored the processes leading to the RI of Typhoon Megi (2010) in a sensitivity experiment that used a convection-permitting, full-physics ARW model and a different microphysical scheme. Their study revealed that the intermittent, active convection gradually strengthens the primary circulation, and that the development of a mid-level warm core tends to serve as a precursor to RI.

Another series of studies examined the relationship between RI and factors such as low-level convergence, surface fluxes, and vertical mixing. Through a WRF simulation of Typhoon Haikui (2012), Zhang et al. (2017e) showed that three factors play a key role in the RI process: 1) a remarkable increase in low-level moisture transport toward the inner core, 2) a favorable large-scale background field with low-level convergence, and 3) upper-level divergence. They also indicated that upper-level divergence could be used as an indicator for RI approximately six hours in advance. Zhang et al. (2017f) investigated Super Typhoon Rammasun (2014) in an ARW simulation and indicated that the storm’s intensification was closely related to the net energy gain rate, defined as the difference between the energy production due to surface entropy flux and the energy dissipation due to surface friction near the RMW. Liu et al. (2017) used the ARW model to study the RI of Hurricane Katrina (2005) before its subsequent weakening and landfall in the southern U.S. with the ARW model. During the RI period, modest differences (e.g., over 10 hPa) were seen in the simulated minimum sea-level pressure between two simulations with different boundary layer schemes. This suggests that improved representation of surface fluxes and vertical mixing in the boundary layer are essential for the accurate prediction of hurricane intensity changes. To explain why a hurricane experiences RI after the RMW contraction ceases, Qin et al. (2018) used the WRF model to examine a simulation of Hurricane Wilma (2005). When simulated RI is occurring but the RMW is nearly steady-state (no contraction), the local absolute angular momentum (AAM) tendencies in the eyewall are smaller in magnitude and narrower in width than those during the contracting RI stage. In addition, during the non-contracting stage, the AAM tendencies in the planetary boundary layer (PBL) increase with time following the time-dependent RMW, but during the contracting stage these tendencies decrease with time. These results suggest that intensification can be maintained during the non-contracting stage if the radial flux convergence of AAM overcompensates for the losses due to the vertical flux divergence of AAM at the RMW.

New insights regarding cloud microphysics have also been reported. Harnos and Nesbitt (2016a,b) investigated the initiation and maintenance of RI using two 1-km WRF simulations of the RI periods of hurricanes Ike (2008) and Earl (2010), under low and high wind shears, respectively. Although the intensification time series of each simulated storm is similar, the hydrometeor characteristics differ between the two cases, with Ike possessing less asymmetry and less vigorous convection than Earl. At least some of the diabatic heating remains within the RMW following eye development in each storm. The majority of the diabatic heating within the RMW of both cases occurs at subfreezing temperatures. This result indicates the importance of clouds associated with ice processes in these RI simulations. Further, they evaluated differences in the vertical velocity characteristics associated with various cloud populations for two simulated cases of RI under varying wind shears prior to the RI phase. In the simulated low-shear TC (Hurricane Ike), the top 1% of updraft magnitudes within the RMW occur at a height of 7 km, while in the simulated high-shear case (Hurricane Earl), the top 1% of updraft magnitudes occurred at 12 km.

Regarding the relationship between the TC atmospheric environment and RI, Chen and Gopalakrishnan (2015) investigated Hurricane Earl (2010) using the results of a forecast from the operational Hurricane WRF (HWRF) system and showed that the tilt was large at RI onset and decreased quickly once RI commenced. This result suggests that vertical alignment is the result, rather than the trigger, for RI. RI onset is associated with the development of upper-level warming in the eye, which results from upper-level storm-relative flow advecting the warm air caused by subsidence warming in the upshear-left region toward the low-level storm center. This scenario does not occur until persistent CBs are concentrated in the downshear-left quadrant. The temperature budget indicates that horizontal advection plays an important role in the development of upper-level warming in the early RI stage. Chen et al. (2018b) used ARW model simulations of Typhoon Vicente (2012) to investigate the key inner-core processes that effectively resist environmental vertical wind shear during RI onset. The convective precipitation shield (CPS) embedded in the downshear convergence zone plays a vital role in preconditioning the vortex before RI. The CPS induces a mesoscale positive vorticity band (PVB) characterized by vortical hot tower (HT) structures upstream and shallower structures (~4 km) downstream. Multiple mesovortices form successively along the PVB and are detached from the PVB at its downstream end, rotating cyclonically around the TC center (Fig. 5). The sufficient magnitude of the vorticity anomalies in the PVB facilitates the upscale growth of a mesovortex into a reformed inner vortex, which eventually replaces the parent TC vortex (i.e., downshear reformation), leading to RI onset. Tao and Zhang (2015) used WRF simulations to explore the effects of environmental shear on the dynamics and predictability of TCs. They showed that larger shear magnitudes resulted in less predictable TCs, especially at time of RI onset. This effect continues until the shear becomes too large for TC formation.

Regarding the effects of ocean coupling on RI, Kanada et al. (2017) investigated Typhoon Megi (2010) using the three-dimensional atmosphere–ocean coupled regional model, the Cloud Resolving Storm Simulator – Non-Hydrostatic Ocean model for the Earth Simulator (CReSS–NHOES). Because the warm sea increased near-surface water vapor and, hence, the convective available potential energy, the high SST in the eye region facilitated tall and intense updrafts inside the RMW and led to the start of RI. In contrast, high SST outside this radius induced local secondary updrafts that inhibited RI, even when the mean SST in the core region exceeded 29.0 degrees C. These secondary updrafts moved inward and eventually merged with the primary eyewall updrafts; the storm then intensified rapidly when the high SST appeared in the eye region. Thus, changes in the local SST pattern around the storm center strongly affect the RI process by modulating the radial structure of core convection. Wang and Wang (2014) also investigated Typhoon Megi (2010) in a simulation using the ARW model with both dynamical initialization and large-scale spectral nudging. They showed that the onset of

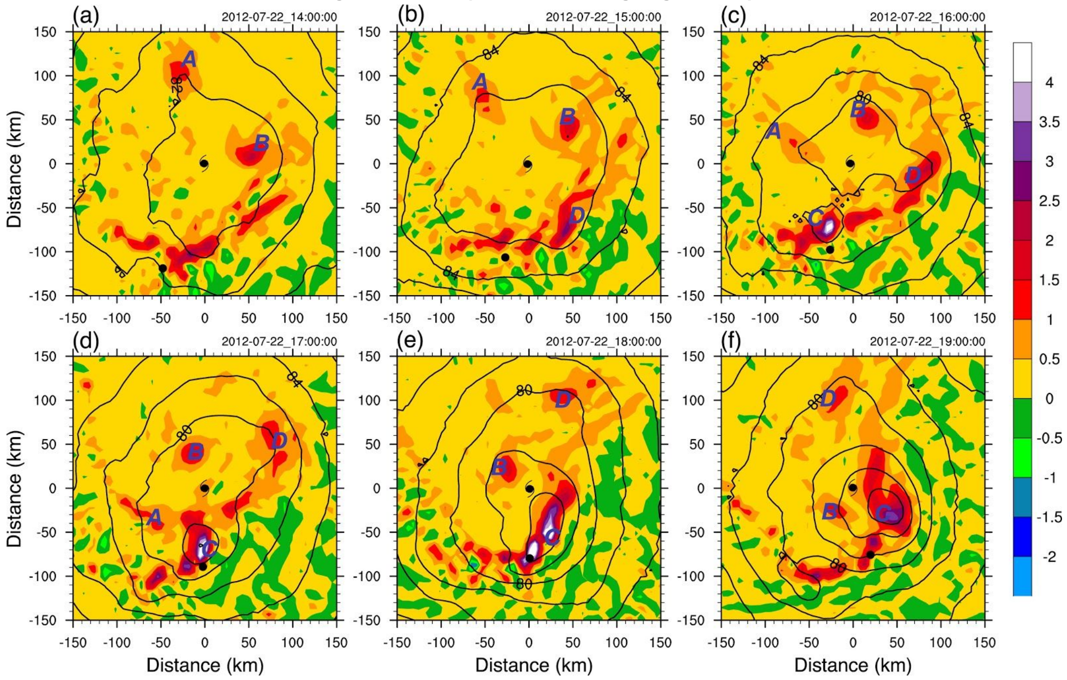

Fig 5. Hourly evolution of 900-hPa relative vorticity (shading; 10^{-3} s^{-1}) and geopotential height (contoured every 2 x 10^2 gpm) from (a) 1400 to (f) 1900 UTC 22 Jul 2012 for Typhoon Vicent (2012). The black hurricane symbol (dot) in each panel denotes the surface (500 hPa) TC center. Labels A–D denote different mesovortices. Note that mesovortex D is weak, loosely organized, and never dominates the vorticity asymmetries in 900 hPa, and thus its label D is an exception of chronological labeling. Figure 7 of Chen et al. (2018b).

RI was triggered by CBs that penetrate into the upper troposphere, leading to upper-tropospheric warming and the formation of the upper-level warm core. In turn, CBs with their roots inside of the eyewall in the boundary layer, were buoyantly triggered/supported by slantwise convective available potential energy (SCAPE) accumulated in the eye region. During RI, the convective areal coverage in the inner-core region increases, while decreases were seen in the updraft velocities in the upper troposphere and in the number of CBs. Ma et al. (2017) studied the impact of including a sea-spray scheme and a modified algorithm for momentum exchange on RI using the Australian Bureau of Meteorology's current operational TC model for TC Yasi (2011). The study showed that the revised model simulates a cooler and more moist region near the surface in the eyewall/eye region, and that this leads to an earlier RI evolution with stronger subsidence in the eye.The modified model simulation also features a stronger radial pulsating of the eye and eyewall convection on relatively short time scales. The enhancement of RI by the new scheme is characterized by eyewall ascent, radial convergence, and inertial stability inside the radius of azimuthal-mean maximum wind over low-to mid-levels, and by a ring-like radial distribution of relative vorticity above the boundary layer.

Regarding the reproducibility of TCs that rapidly intensified, Kanada and Wada (2015) tried to reproduce Typhoon Ida's (1958) extreme deepening (defined as a central pressure drop exceeding 90 hPa/24 h) using the JMA 2-km mesh nonhydrostatic mesoscale model (JMA-NHM). The combination of shallow-to-moderate convection and tall, upright CBs was found to be crucial to simulating the extreme RI. In a follow-up study, Kanada and Wada (2017) investigated 34 intense TCs with best-track minimum central pressures ≤ 900 hPa in the WNP. This study used a 20-km-mesh atmospheric general circulation model (AGCM20), which was subsequently downscaled via a 5-km-mesh regional atmospheric nonhydrostatic model (ANHM5). While most of the intense best-track TCs underwent RI and attained maximum intensities south of 25N, the AGCM20-simulated TCs tended to intensify longer and more gradually; only half of them underwent RI. Qin and Zhang (2018) conducted ultra-high resolution (finest horizontal mesh size of 333 m) WRF simulations of Hurricane Patricia (2015), the hurricane which broke intensification records both for peak intensity and 24-h change in intensity over the eastern Pacific basin. They revealed that Patricia's extraordinary development and its inner-core structures could be reasonably well simulated if ultra-high horizontal resolution, appropriate model physics, and realistic initial vortex intensity are incorporated. They concluded that the large-scale conditions (e.g., warm SST, weak vertical wind shear, and the moist intertropical convergence zone) and convective organization all played important roles in determining the predictability of Patricia's extraordinary RI and peak intensity.

A number of studies in this period examined the effectiveness of ensemble forecasts to elucidate key features of RI. Munsell et al. (2017) explored the dynamics and predictability of the intensification of Hurricane Edouard (2014) through a 60-member convection-permitting ensemble initialized with an ensemble Kalman filter for a WRF model that assimilated dropsondes collected during NASA's HS3 field program. Utilizing composite groups created according to the near-RI-onset times of the members, for increasing magnitudes of deep-layer shear, RI onset is increasingly delayed; intensification does not occur once a critical shear threshold is exceeded. Although the timing of intensification varies by as much as 48 h in the simulations, a decrease in shear is observed across the intensifying composite groups similar to that seen 6–12 h prior to RI. This decrease in shear is accompanied by a reduction in vortex tilt, as the precession and subsequent alignment process begin similar to that seen in the 24–48 h prior to RI. Leighton et al. (2018) also investigated Hurricane Edouard (2014) on the differences in both the TC inner-core structure and large-scale environment using ensemble forecasts from HWRF. They revealed that, for RI cases, as deep convection wrapped around from the downshear side of the storm to the upshear-left quadrant for RI members, vortex tilt and asymmetry reduce rapidly, and RI occurs. In contrast, for non-intensifying (NI) members, deep convection remains in the downshear/downshear-right quadrant, and storms do not intensify. The budget of tangential wind tendency reveals that in the RI members, the positive radial eddy vorticity flux significantly contributes to the spin-up of tangential wind in the middle and upper levels and also acts to reduce the tilt of the vortex (Fig. 6). In the NI members, the negative eddy vorticity flux spins down the tangential wind in the middle and upper levels and does not help the vortex become vertically aligned.

f) **New Developments in the Operational Prediction of RI**

This subsection reports new insights on the development or improvement of RI forecast schemes since IWTC-8. Zhang et al. (2017d) evaluated the impact of modifying the vertical eddy diffusivity (K-m) in HWRF's boundary layer parameterization on forecasts of TC RI. Results show that improvement in the vertical eddy diffusivity led to improved RI forecasts. HWRF forecasts with reduced K-m at RI onset possess a shallower boundary layer with stronger inflow, more unstable near-surface air outside the eyewall, stronger and deeper updrafts in regions farther inward from the RMW, and stronger boundary layer convergence closer to the storm center. Despite these structural differences, the mean storm intensity (as measured by the 10-m winds) is similar for the two groups (Fig. 7).

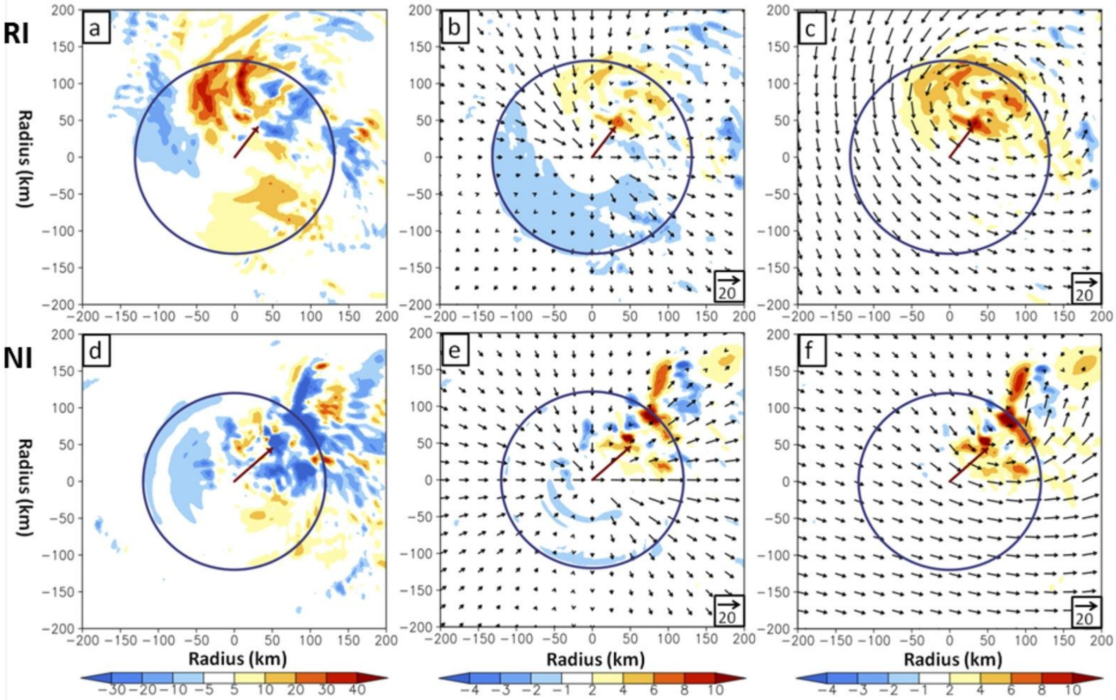

Fig 6. Horizontal cross sections of (a) eddy radial vorticity flux (m s^{-1} h^{-1}), (b) eddy radial component of storm-relative flow (vectors) and eddy vorticity (shading; 10^{-4} s^{-1}), (c) storm-relative flow (vectors) and vorticity (shading; 10^{-4} s^{-1}) averaged for RI members between 6 and 10 km and −3 and 0 h. (d)–(f) As in (a)–(c), respectively, but for the Non-intensifying (NI) members averaged between −7 and −4 h. Dark blue circles indicate the RMW and red arrows denotes the shear vector. Figure 10 of Leighton et al. (2018).

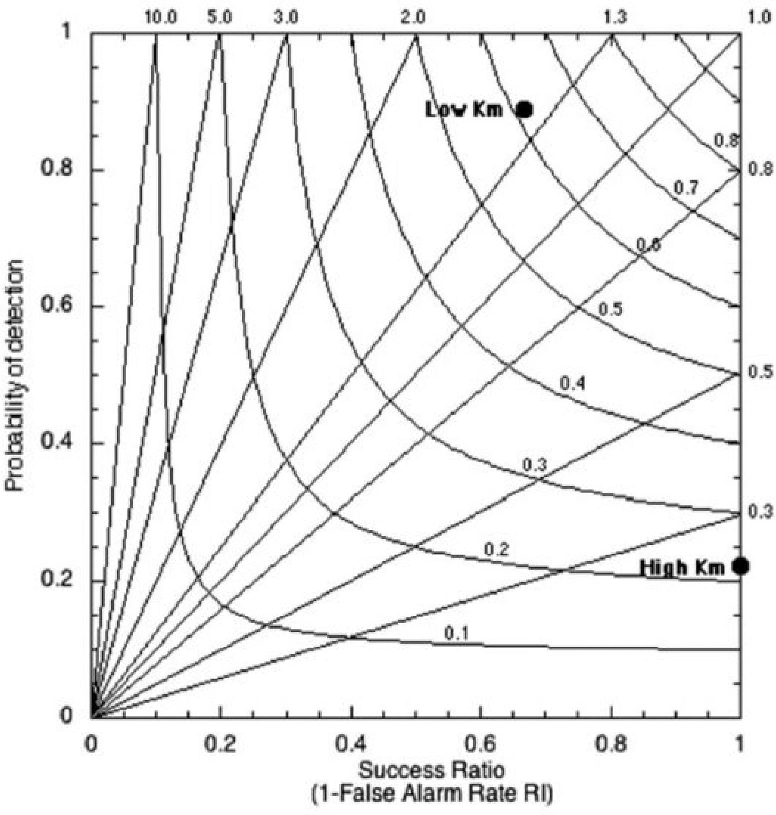

Fig. 7. RI verification using a the categorical performance diagram for the low-Km and high-Km groups. Note that a perfect forecast lies in the top right of the diagram when the probability of detection (POD) and success ratio (SR) approach unity. Figure 2 of Zhang et al. (2017d).

Shimada et al. (2017) investigated the relationship between both current intensity and degree of axisymmetry on a TC's future intensity change during the development and decay stages. These results, based on analysis of hourly Global Satellite Mapping of Precipitation (GSMaP) data (0.1° resolution) for 380 WNP TCs that occurred during 2000–2015, showed that the IR at the current time, and 6- and 12-h after the current time, are strongly related to both the current intensity and degree of axisymmetry during the development stage. When TCs start with a current central pressure (maximum sustained wind) between 945 and 995 hPa (85 and 40 kt, or 43.7 and 20.6 m/s, respectively), TCs with higher degree of axisymmetry experience a larger intensity change in the next 24 h, on average. For TCs starting with a current central pressure of 960–990 hPa, the mean value of the degree of axisymmetry is much higher for TCs experiencing RI than those for non-RI TCs. These results suggest that once a TC becomes axisymmetric, it tends to keep its axisymmetric structure and continue to intensify, so long as the environment remains favorable for intensification.

Zhuge et al. (2015) used TRMM data and the SHIPS development dataset to evaluate the potential for using inner-core HTs in operational RI forecasts for each of the TC-prone basins. The efficacy of using inner-core HTs to predict RI differed depending on the basin. For instance, the stand-alone HT-based RI prediction scheme showed little skill in the NA and eastern and central Pacific (ECP) basins, but yielded skill scores of >0.3 in the southern Indian Ocean (SI) and WNP basins. When HTs were used in conjunction with several storm and environmental parameters [previous 12-h intensity change, potential intensity (PI), percentage area from 50 to 200 km of cloud-top brightness temperatures lower than -10°C, and 850–200-hPa vertical shear magnitude with the vortex removed], the predictive skill score in the SI was 0.56. This is comparable to that of the SHIPS RII scheme, which is considered to be the most advanced RI prediction method. Rozoff et al. (2015) examined the probabilistic prediction of TC RI in the NA and eastern Pacific basins using a series of logistic regression models trained on environmental and infrared satellite-derived features. Results show that the inclusion of Microwave Imagery (MI)-based predictors yield more skillful RI models for a variety of RI and intensity thresholds. Compared with the baseline forecast skill of the non-MI-based RI models, the relative skill improvements from including MI-based predictors range from 10.6% to 44.9%. Grimes and Mercer (2015) also investigated the possibility to use large-scale processes as RI indicators within TC environments in the Atlantic basin. In the first phase of their study, the synoptic-scale variables that yielded the largest statistically significant differences between RI and non-RI TCs were identified through spatial analysis of NASA's Modern Era Retrospective-analysis for Research and Applications (MERRA) data from 1979 to 2009. A logistic regression and a support vector machine (SVM) classification algorithm were then used to diagnose the onset of RI at the 24-h lead time. The SVM model's skill, using synoptic-scale variables as predictors, was found to outperform the logistic regression model. The approach identified mid-level vorticity, pressure vertical velocity, 200–850-hPa vertical shear, low-level potential temperature, and specific humidity as the most significant predictors for diagnosing RI.

g) **Summary of Recent Findings on RI**

Despite extensive research on the RI topic over the past four years, many uncertainties remain regarding how to better simulate and predict the onset and continuation of RI. First, a better definition of RI is needed and should be applied to future studies. Most of the previous statistical studies used the 24-h case-based RI definition as defined by Kaplan and DeMaria (2003). As pointed out by Kieper and Jiang (2012) and Tao et al. (2017), RI usually happens as an *event,* which can last up to 78 h or even longer. About 76% of RI events lasted more than 24 h (Tao et al. 2017). The approach of treating any 24-h RI case as a single and independent event does not distinguish between the stages of an RI event, including at RI onset, during the middle of an RI event, and the ending period of an RI event. Failing to distinguish these different stages will cause challenges when studying the evolution of an RI event/storm. Second, it has been well recognized based on satellite observations that a high degree of axisymmetry of precipitation, convective, and thermodynamic parameters is associated with the subsequent RI (Kieper and Jiang 2012; Zagrodnik and Jiang 2014; Alvey et al. 2015; Tao and Jiang 2015; Zawislak et al. 2016; Tao et al. 2017; Xu et al. 2017; Shimada et al. 2017; Fischer et al. 2018; Jiang et al. 2018). On the other hand, case studies using aircraft observations and numerical simulations (Sanger et al. 2014; Stevenson et al. 2014, Susca–Lopata et al. 2015; Miller et al. 2015; Rogers et al. 2015; Rogers et al. 2016; Guimond et al. 2016; Li et al. 2016; Tang et al. 2018a) have recognized asymmetric CBs and HTs in the inner core as important factors contributing to the subsequent RI. In light of these findings, we recommend that future research directions focus on: a) studying RI as an event, b) improving understanding of the conditions and precursors to RI through symmetrical processes, and c) improving understanding of the conditions in which asymmetric CBs and HTs in the inner core may lead to RI precursors.

3.1.3 Eyewall Replacement Cycles (ERC)

a) **Introduction**

Satellite and in-situ observations demonstrate that concentric eyewall structures are common in intense tropical cyclones (TCs). These observations have shown that such structures are associated with pronounced changes in TC intensity and structure (Willoughby et al. 1982 and many studies afterwards). Observations also reveal that there are typically three distinct phases of intensity change associated with the secondary eyewall formation (SEF) and the subsequent ERC (Fig. 8). In phase I, intensification tends to slow near the onset of SEF. In Phase II, substantial weakening often occurs as the ERC progresses. In phase III, there is a likelihood of reintensification after the ERC completes, concurrent with a persistent contraction of the new primary eyewall (e.g., Sitkowski et al. 2011; Yang et al. 2013; Zhou and Wang 2013; Kossin and DeMaria 2016). At the time of the previous report for this subtopic (Stern et al. 2014), numerical models had started to be able to develop concentric eyewall structures, although ERCs were relatively rare in numerical simulations of TCs compared with the observed frequency. More recently, numerical models have demonstrated increased capabilities for generating concentric eyewalls and for predicting the associated intensity change.

This subsection synthesizes the peer-reviewed published literature of the past four years (2014–2018) to summarize the advancements in understanding that have been made of the TC intensity changes closely connected with the SEF and ERC. This synthesis includes an updated understanding of the climatology of intensity changes and the wind-pressure relationship during an ERC, observed ERCs with subtle intensity change, as well as the performance of (and uncertainty in) predicting ERC-associated intensity changes in state-of-the-art numerical models.

b) **Climatological ERC Model and Wind–Pressure Relationship during ERCs**

Noticing the disparity in intensity changes between the recon-anchored best-track data[2] and the SHIPS model[3] (DeMaria et al. 2005) (Fig. 9), Kossin and DeMaria (2016)

---

[2] The recon-anchored data herein are the NA best-track data (HURDAT2) during periods in which the hurricanes were actively sampled by aircraft reconnaissance.

developed a climatological model to reduce TC intensity change forecast errors in SHIPS during the weakening phase of ERCs (Phase II in Fig. 8). The weakening phase of an ERC event in observations is generally concurrent with either slow intensification, slow weakening, or a steady state intensity in SHIPS forecasts, suggesting that the weakening during an ERC is driven mostly by processes internal to the TC. Such weakening is distinct from the remainder of the weakening phase in the life cycle of TCs that occurs primarily due to the hostile external atmospheric conditions, less conducive oceanic conditions, or landfall.

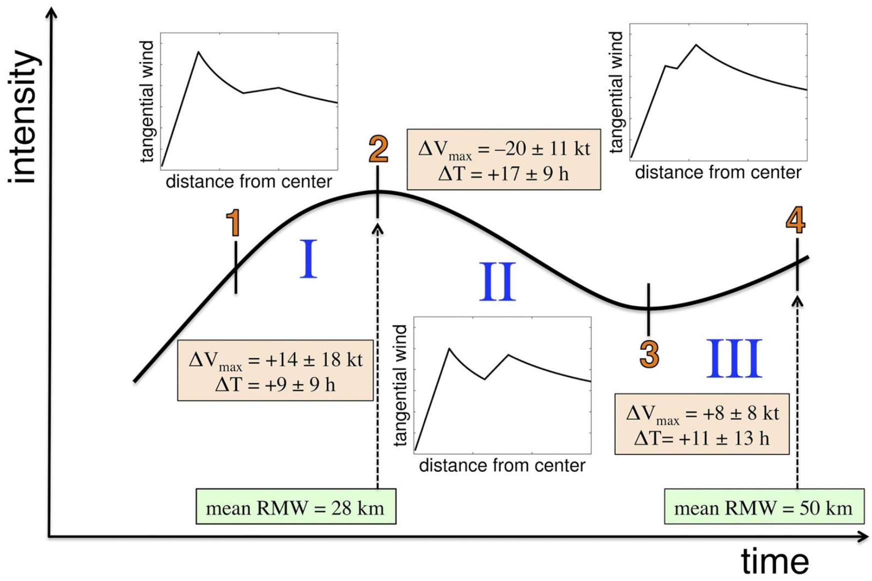

Fig 8. Schematic of the mean evolution of TC intensity during an ERC. The three inset figures illustrate typical radial profiles of flight-level tangential wind. From Sitkowski et al. (2011), Kossin and Sitkowski (2012), and Kossin (2015). Figure 9 of Kossin (2015).

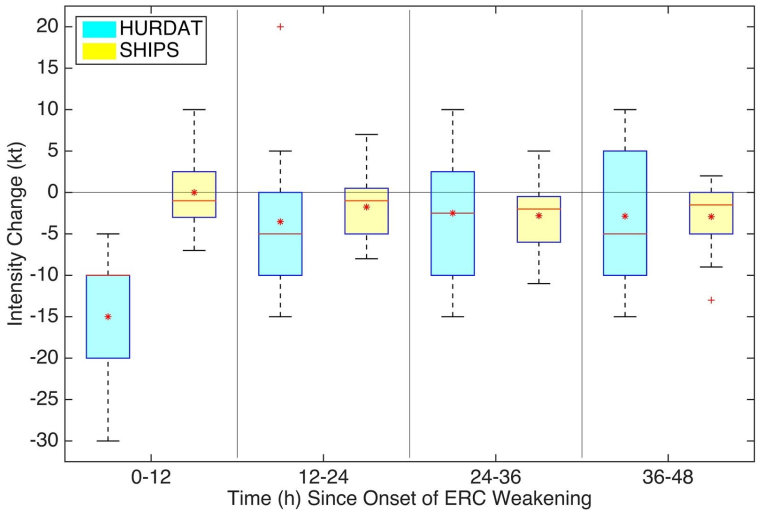

Fig 9. Comparison of 12-h intensity change in the recon-anchored best-track (HURDAT) versus SHIPS predictions following the onset of ERC weakening. Figure 2 of Kossin and DeMaria (2016).

This ERC climatology model, developed as a complement to SHIPS, is named E-SHIPS. The model was constructed based on 19 ERC events, in which aircraft reconnaissance data were intensively collected. Figure 10 demonstrates that E-SHIPS

[3] SHIPS is one of the primary guidance models that NOAA/NHC (National Oceanic and Atmospheric Administration/National Hurricane Center) uses for operational intensity forecasts.

manifests its best skill when applied at the onset of ERC weakening. Such an application is only feasible, however, when a forecaster has a high level of confidence, not only in the occurrence of an impending ERC, but also in the onset time of the associated weakening, since E-SHIPS substantially underestimates hurricane intensity when applied too early (e.g., 6-h prior to the onset of ERC weakening). A compromise approach, which is also a more realistic scenario, is to apply E-SHIPS at times when an ERC has begun and the TC is showing clear signs of weakening. When applied at 6 h after the onset of ERC weakening, E-SHIPS shows a significant reduction in errors of intensity predictions. For instance, the mean absolute errors were reduced more than 50% at 18-h lead-time. Due to this demonstrated success, E-SHIPS is being utilized by NOAA's NHC operations as a sub-algorithm of SHIPS.

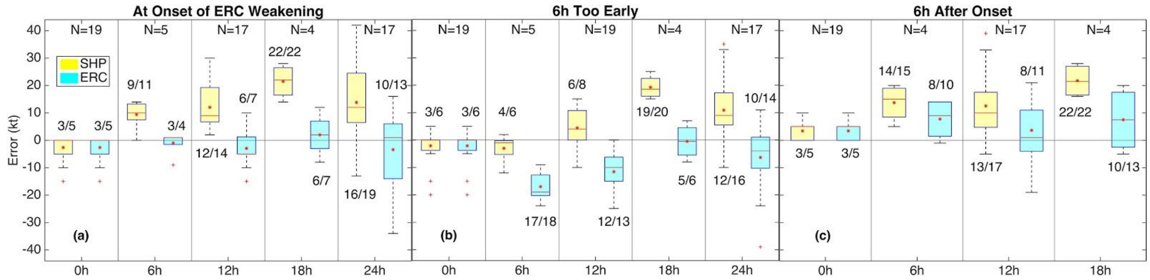

Fig 10. Error distributions for the ERC climatology model and SHIPS when the model is applied (a) at the onset of ERC weakening to 24 h after, (b) 6 h prior to the onset of weakening (too early), and (c) 6 h after the onset of weakening. Errors are relative to recon-anchored best-track values. Positive (negative) values denote where the model-predicted intensities are higher (lower) than the best-track data. Sample size, N, is shown for each forecast lead-time. The operational SHIPS data are available with 12-h resolution for pre-2005 storms, and with 6-h resolution out to 24-h lead-time and 12 h at longer lead times for 2005 and after. Mean absolute and root-mean-square errors are shown as numerical pairs above or below each boxplot (kt). Figure 4 of Kossin and DeMaria (2016).

Kossin (2015) showed that, during an ERC, the wind–pressure relationship (WPR) migrates away from the climatology used by the Dvorak technique, and toward a weaker maximum wind for a given minimum central pressure. The migration of the WPR during an ERC is quite different between hurricanes with intensities weaker and stronger than 100 kt (51.4 m/s). The weaker hurricanes usually get stronger when going through the three typical stages of ERC-associated intensity change (Fig. 8), while the stronger hurricanes tend to become weaker.[4] Compared with the Dvorak climatology during the three phases of ERC intensity change, weaker hurricanes experience a large drop in minimum central pressure for a given increase in maximum wind speed. Meanwhile, stronger hurricanes tend to experience a slight increase in minimum central pressure given an equivalent magnitude of wind speed reduction (Fig. 11). On average, the weaker (stronger) hurricanes intensify (weaken) by 8 (10) kt [4.1 (5.1) m/s], while their minimum central pressure decreases (increases) by 15 (2) hPa. The modified WPR can be applied to operational intensity forecast for hurricanes undergoing an ERC.

[4] Please note the intensity change herein is calculated by subtracting the mean intensity in Phase I from the mean intensity in Phase III (Figs. 1 and 4). The average of intensities at points 1 (3) and 2 (4) is used as a proxy for the mean intensity in Phase I (III) in Kossin (2015). In other words, this intensity change presents the total change through the periods of intensification, weakening, and reintensification.

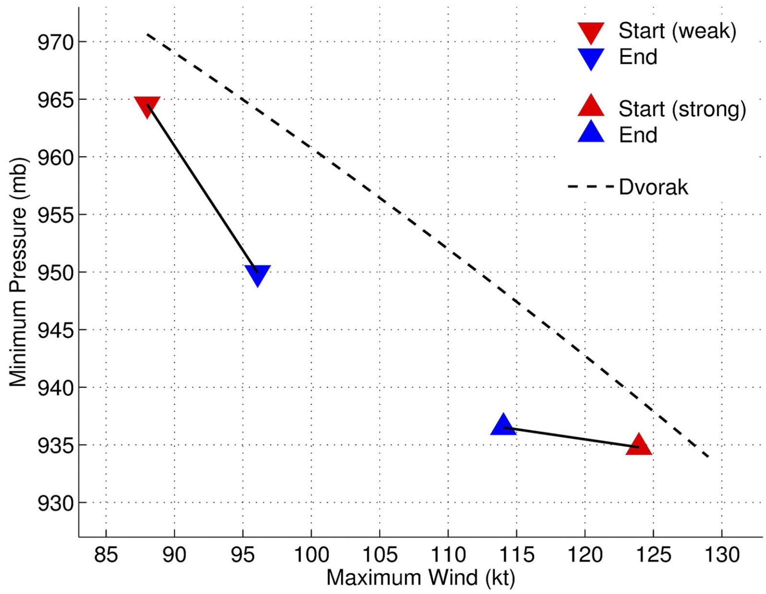

Fig 11. Mean WPR changes for TCs that begin an ERC as a weaker hurricane (V_{max} < 100 kt (51.4 m/s) and as a stronger hurricane (V_{max} > 100 kt (51.4 m/s)). The averages for the start and end are based, respectively, on values at points 1 and 2, and points 3 and 4 in Fig. 8. From Kossin (2015).

c) **ERCs with Subtle Intensity Change**

Satellite-based observational studies reveal that, statistically, typhoons with long duration concentric eyewalls (Yang et al. 2013), or with a wider moat (Zhou and Wang 2013), appear to maintain their intensity during the early ERC period, deviating from the mean behavior of all ERC cases. Supporting this finding, Tsujino et al. (2017) and Zhang and Perrie (2018) used radar observations of Typhoon Bolaven (2012) and Hurricane Ike (2008), respectively, and reported a lack of the typical intensity changes that might be expected during an ERC. Both studies identified the maintenance of the inner eyewall intensity and the nearly stationary radius of the outer eyewall as common factors. Using the CReSS model, Tsujino et al. (2017) reproduced the outer two eyewalls of the triple eyewalls and the associated intensity and structure evolution of Bolaven. They also carried out dynamical analyses to understand the responsible dynamical processes. Dougherty et al. (2018) reported on and studied the lack of intensity change associated with Hurricane Bonnie’s (1998) ERC (Fig. 12), which did not have a long-lived concentric eyewall structure. In this case, Bonnie’s intensity was largely maintained during the ERC (apart from a brief decrease), as the maximum wind speeds in the new concentric eyewall matched those in the old eyewall. After the ERC, the storm did not reintensify and the new eyewall underwent only limited contraction.

d) **Performance of and Uncertainty in Numerical Models**

Hazelton et al. (2018) evaluated TC forecasts in the 2-km resolution nested NOAA/Geophysical Fluid Dynamics Laboratory (GFDL) fvGFS (recently named as hfvGFS; finite-volume cubed-sphere dynamical core using the Global Forecast System (GFS) physical parameterizations) model covering most of the NA basin (hereafter, fvGFS-2km). They reported that an over-forecast of intensity during the ERC of Hurricane Earl (2010) was likely tied to an incorrect depiction of the secondary eyewall. In contrast, fvGFS-2km decently reproduced the weakening during the ERC in the forecast of Hurricane Matthew (2016) (Fig. 13). This weakening was attributed to the correct depiction of the SEF onset time and a satisfactory forecast of the ERC duration. The simulated ERC completed somewhat earlier than in the observed storm, resulting in a short-term (and unobserved) reintensification of the simulated storm after the ERC completed and before the environmental vertical wind shear became detrimental to intensification. The ability to generate a secondary eyewall and the subsequent ERC in the Matthew forecast demonstrates that the fvGFS model is capable of predicting at least some of the internal structural changes of ERCs, along with the associated intensity changes.

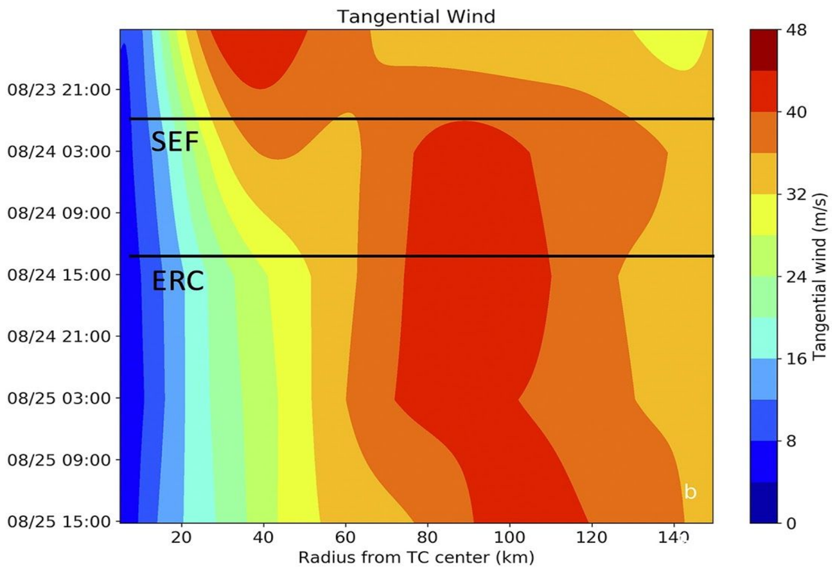

Fig. 12. Radius vs time Hovmöller of flight-level (700 hPa) tangential wind (m s^{-1}) from 1500 UTC 23 Aug to 1500 UTC 25 Aug. Black lines denote the times during which Bonnie's SEF and ERC occurred at 0000 UTC 24 Aug and 1200 UTC 24 Aug, respectively. Fig. 5b of Dougherty et al. (2018).

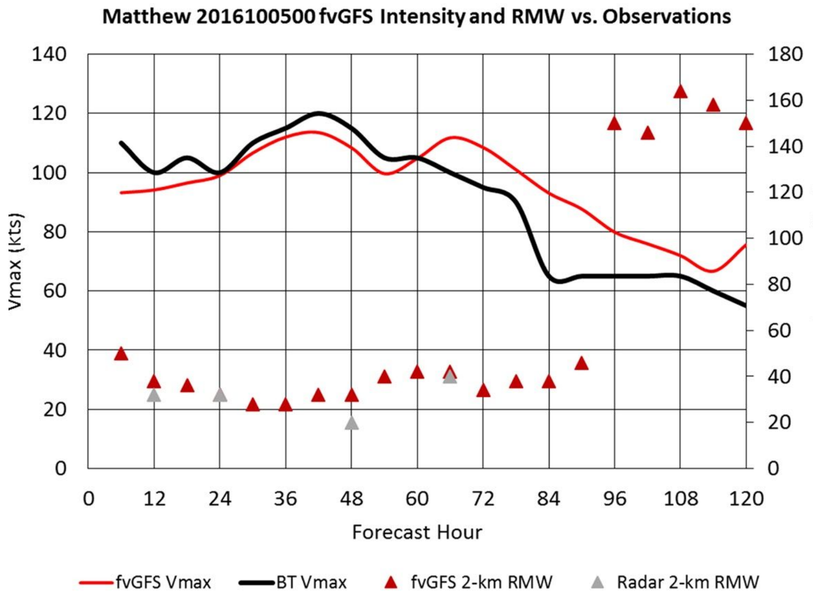

Fig 13. Maximum wind speed (kt) of Hurricane Matthew starting at 0000 UTC 5 Oct 2016 and ending at 0000 UTC 10 Oct 2016 from the NHC best-track (black) and the fvGFS forecast (red). The 2-km RMW from fvGFS forecasts and radar observations are shown by the red and gray triangles, respectively. Figure 13b of Hazelton et al. (2018).

Using the WRF-ARW model, Zhang et al. (2017a) carried out a set of 20 idealized, ensemble simulations in an environment of moderate vertical wind shear on two different computer clusters. Thirty-eight out of the 40 simulations produced at least one ERC, or an ERC-like [termed as "partial ERC" in Zhang et al. (2017a)] event, during the integration. This suggests that mild uncertainty exists concerning whether or not an SEF will occur in this given shear environment. These results show that the onset time of SEF, intensity and structure of the concentric eyewalls, and the ERC evolution are highly sensitive to small, unobservable, and random perturbations of the initial conditions. In most of these cases, the first ERC or ERC-like event takes place right after the end of the period of RI. The uncertainty in the onset time and duration of the RI period adds uncertainty to the ERC and, therefore, to the timing and amplitude of the associated intensity change (Fig. 14).

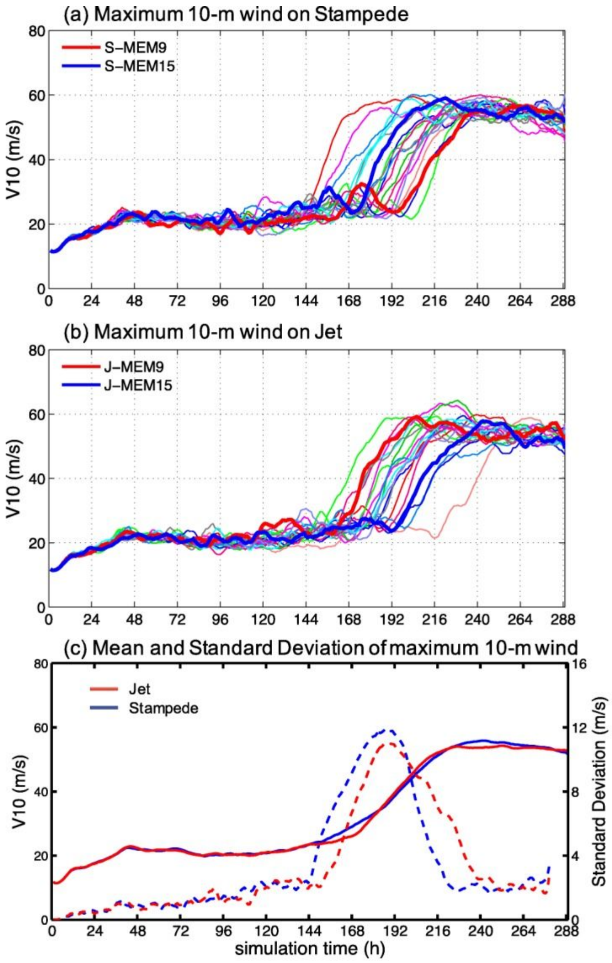

Fig 14. Evolution of maximum 10-m wind (m s^{-1}, running smoothed) on the (a) Stampede computer cluster and (b) Jet computer cluster. Lines with the same colors are the simulations with same initial conditions. (c) Comparison of the ensemble mean (solid line) and standard deviation (dash line) of 10-m wind for each ensemble. Figure 1 of Zhang et al. (2017a).

e) **Summary of Recent Findings on ERCs and TC Intensity Change**

The E-SHIP model and the migration of the wind-pressure relationship during ERCs both provide helpful guidance for intensity forecasts of hurricanes undergoing an ERC. It is unclear how well, or whether, the ERC climatology represents TCs in the WNP or other ocean basins where low-level inner-core aircraft data are rarely collected. Furthermore, uncertainty about the onset time of the SEF and ERC, variance in observed intensity changes, and variations in the documented durations for each phase (e.g., Sitkowski et al. 2011; Kossin and DeMaria 2016) are major sources of forecast errors in the simple ERC climatology model. The Microwave-based Probability of Eyewall Replacement Cycle (M-PERC) model[5], developed by the Cooperative Institute for Meteorological Satellite Studies (CIMSS), provides the probability of the onset of an ERC based on microwave-based predictors [CIMSS/Automated Rotational Center Hurricane Eye Retrieval (ARCHER); Wimmers and Velden 2016]. Details about this model are given in the Rapporteur Report for Topic 3.3: "Intensity guidance in operational perspectives".

While outer eyewall formation is no longer a rare event in state-of-the-art numerical models, it remains challenging to make accurate predictions of the occurrence and the details of an ERC event [e.g., the onset time of SEF and ERC; the location and contraction speed of the outer eyewall; the dissipation (intensification) rate of the inner (outer) eyewall; the duration, etc.]. SEF and ERC events have been suggested to be regulated by different factors and mechanisms, such as outer rainband heating (e.g., Rozoff et al. 2012; Zhu and Zhu 2014), which may be closely tied to environmental vertical wind shear (Fang and Zhang 2012; Didlake et al. 2018) and relative humidity (Hill and Lackmann 2009; Ge 2015); the storm intensity and structure (e.g., Kuo et al. 2008; Zhu and Zhu 2015; Ge et al. 2016; Guan and Ge 2018); boundary layer dynamics (e.g., Huang et al. 2012; Kepert 2013; Slocum et al. 2014; Abarca and Montgomery

[5] M-PERC model products are available at http://tropic.ssec.wisc.edu/real-time/archerOnline/web/index_erc.shtml.

2015; Kepert 2017); diurnal radiation cycles (Tang et al. 2017); and, the Wind-Induced Surface Heat Exchange (WISHE) mechanism (Cheng and Wu 2018). Uncertain representation of model physical processes (Zhu and Zhu 2015), uncertainty about the initial model conditions, and the chaotic nature of fluid dynamics (Zhang et al. 2017a) all add uncertainty to predictions of SEF and ERCs, and therefore, to intensity predictions during an ERC. Dynamical processes and factors affecting SEF and ERC are discussed in the Rapporteur Report for Topic 4.1: "The structure analysis and change: Secondary eyewall formation and expansion of the wind field".

3.1.4 Relation of Rainbands to Intensity Change

a) Introduction

Immediately outside the TC eyewall exists a region with a filamentation time less than the typical overturning time scale of individual convective clouds (Rozoff et al. 2006; Wang 2008; Li and Wang 2012a,b); this region is known as the rapid filamentation zone (RFZ). Inner rainbands are prominent in this zone because of straining deformation (Li and Wang 2012a,b; Moon and Nolan 2015a,b; Li et al. 2017). The TC outer core lies radially outside of the RFZ (approximately three times the RMW; Wang 2008; 2009), where outer spiral rainbands predominantly develop. Outer rainbands can be classified into two types: principal rainbands and distant rainbands (Houze 2010). Principal rainbands are stationary relative to the TC center and extend outward with a striking azimuthal wavenumber-1 signature. Distant rainbands are located farther from the center and contain more vigorous convective elements. Many studies confirm that the activity of spiral rainbands can significantly influence TC structure and intensity (Wang 2012; and cited references therein). This subsection discusses recent advancements in understanding on the role of rainbands in TC structure and intensity change.

b) Relationships Between Spiral Rainbands and TC Intensity Change

While the potential vorticity (PV) structure of TCs suggests that rainbands play a major role in size changes (Hill and Lackmann 2009), rainbands can also interact with the inner core of the TC to impact intensity. Kossin et al. (2000) show that eyewall–rainband interaction can arise from vortex Rossby wave interaction—a process that can result in the weakening of the primary eyewall. In attempts to unravel the relationship between spiral rainbands and intensification in observations, lightning activity has been used as a measure of convective activity/latent heat release in the outer-rainband region. Lightning activity—especially in the rainband regions—has been documented to be a potential indicator of TC intensity change. Xu et al. (2017) used global TRMM data to investigate TC lightning characteristics and their relationships with intensity change. The results demonstrated that TC total lightning flash density is maximized in the outer-rainband region and minimized in the inner-rainband region. Inner-core (outer rainband) lightning is generally negatively (positively) correlated to TC intensity change in the next 24 h (+24 h), with intensifying TCs having lower flash density than weakening and neutral TCs. This finding is consistent with the relationship found by DeMaria et al. (2012) and Stevenson et al. (2016) for Atlantic basin TCs, and a Hurricane Maria (2017) case study by Fierro et al. (2018) that leveraged preliminary Global Lightning Mapper data. However, DeMaria et al. (2012) did not find this relationship to hold true in the Eastern North Pacific basin [although Stevenson et al. (2016) did], and the discrepancies between various lightning studies still need to be addressed. Griffin (2017) examined tropical overshooting tops in longwave infrared imagery from geostationary satellites for rapidly intensifying and weakening TCs and confirmed the results of Xu et al. (2017). Griffin's study also showed that TRMM parameters of the convective depth and vertically integrated ice content in both the inner core and outer rainbands are both greater in intensifying TCs compared with TCs with a neutral intensity trend. Yang et al. (2018) examined the stratiform and convective characteristics of TCs in the WNP and found that the highest fraction of stratiform raining areas was located in the inner-band region; this promotes TC intensification. Didlake et al. (2018) found that increased rainband activity and organization occurred during the RI of Hurricane Earl (2010), consistent with Stevenson et al. (2014) and Yang et al. (2018). While a link has been found between rainband lightning activity and intensity change, the physical mechanisms behind this relationship need to be explored further.

c) Effects of Heating/Cooling in Rainbands on TC Intensity Change

Diabatic heating and cooling within the TC circulation have long been known to play a critical role in TC structure and intensity change (e.g., Malkus and Riehl 1960; Riehl and Malkus 1961; Yanai 1961; Möller and Shapiro 2002; Bui et al. 2009). Furthermore, diabatic heating and cooling in the various regions of a TC may play different roles in TC structure and intensity, and their associated changes (Eliassen 1951; Vigh and Schubert 2009; Pendergrass and Willoughby 2009; Wang 2009; Fudeyasu and Wang 2011; Rogers et al. 2013). Since the convection in TC rainbands is heterogeneous, the manner in which the rainband-associated diabatic heating and cooling affects TC structure and intensity change remains an unresolved issue in TC dynamics (Moon and Nolan 2010; Li et al. 2014a). Li et al. (2014a) revealed that the removal of heating (cooling) in the inner rainband region reduces (increases) storm intensity. This result is in a sharp contrast to the roles of diabatic heating and cooling in outer spiral rainbands, where an increase in heating (cooling) leads to a less intense (more intense) TC (Wang 2009).

Chen et al. (2018a) conducted a series of numerical sensitivity experiments to extend Li et al. (2014)'s study by evaluating the respective effects of convective and stratiform heating and cooling in the inner-rainband region on TC structure and intensity. They found that removing the convective heating within the inner-rainband region can effectively eliminate the inner-rainband activity and produce a moat-like zone outside the eyewall. Eyewall updrafts are significantly suppressed, the inner-core size is reduced, and the TC decays. When the convective heating in the inner-rainband region is increased by 50%, the storm first intensifies at a relatively slow rate, and then the TC inner-core size quickly expands outward. Hence, the conversion ratio of diabatic heating to kinetic energy can be effectively increased, which is responsible for RI. Removal of stratiform heating in the inner-rainband region leads to a slower intensification with a moderate final intensity. The decreased stratiform cooling elevates the equivalent potential temperature (θ_e) in the mid- to lower-troposphere and favors the formation of a thick, high-entropy boundary layer. As a result, the inward transport of high-entropy air in the boundary layer triggers RI. As the simulated storm intensifies further, the low-level θ_e outside the eyewall begins to decrease as a result of compensating subsidence, such that the simulated TC eventually terminates RI and then maintains a roughly steady state. The doubled stratiform cooling in the inner-rainband region is effective in eliminating TC RI because of the low-entropy air that prevails from the surface to the mid-troposphere during the early stage. If both the stratiform heating and cooling are removed, the structure and intensity changes bear close resemblance to the results in which the stratiform cooling was halved. Doubling both the stratiform heating and cooling generates the weakest storm.

Chan and Chan (2016) examined the sensitivity of the simulated TC intensity to microphysical schemes. They pointed out that, although the simulated TC track is not sensitive to the microphysical schemes, its intensity is significantly influenced by the choice of microphysical scheme. The simulated TC intensity is similar in the simulations using the WRF Single-Moment 5-class and WRF Single-Moment 6-class schemes, and is higher than those using the Ferrier scheme. The WRF Single-Moment 5-class and Single-Moment 6-class schemes generate more diabatic heating in rainbands than the Ferrier scheme. More diabatic heating could lead to larger upward motion, and hence result in higher upper-tropospheric divergence, lower-tropospheric convergence, and precipitation rates. This, consequently, leads to stronger inflow in the lower troposphere, enhances an inward transport of absolute angular momentum, and, thus, higher TC intensity.

Although the potential effects of diabatic processes associated with spiral rainbands on TC intensity changes have been examined with idealized numerical experiments, further observational evidence from real cases is needed to confirm the insights offered by these simulations.

d) **Role of Rainband Rainwater Evaporation in TC Intensity Change**

Li et al. (2015) revisited the effects of the evaporation of raindrops in different regions on TC structure and intensity by performing several sensitivity numerical experiments. Evaporation of raindrops in the outer-rainband region is shown to suppress the final intensity of a TC, whereas the effects of evaporation in the inner rainbands on TC intensity are very limited. The low-θ_e air in the boundary layer that results from evaporative cooling is transported radially inward and mixed into the eyewall region, reducing θ_e under the eyewall, and thus, reduces TC intensity. Evaporation in the inner rainbands hardly affects the activity of outer rainbands. Outer rainbands can still form when evaporation is switched off in the outer-core region. This result seems to suggest that the cold-pool dynamics associated with evaporation lead to the growth and/or sustenance of outer rainbands, rather than to their initiation. Li et al. (2015) also showed that excluding evaporation in inner rainbands has a very weak effect on the inner-core size of a storm. Evaporation in outer rainbands, however, generally limits the inner-core size.

e) **Radar Observations of TC Spiral Rainbands**

Yu et al. (2018) used long-term radar observations (2003–2015) to investigate a considerable number of outer rainbands from different TCs as they approached Taiwan island. Their study revealed that outer rainbands and squall lines frequently share similar structures. Outer rainbands with squall-line-like airflow patterns are common (~58%) and are generally characterized by convective precipitation and an obvious convergence zone between the band-relative rear-to-front flow and front-to-rear flow at low levels, with updrafts that tilt either frontward or rearward. The majority of non-squall-line airflow patterns are characterized by less convective precipitation and a deep layer of either front-to-rear flow (14%) or rear-to-front flow (16%) within the rainband.

Tang et al. (2018b) also showed that the mesoscale structure of the principal rainband shares some similarities with squall lines. They used airborne radar reflectivity fields and visible satellite images of Typhoon Hagupit (2008) to identify multiple quasi-linear subbands within the principal rainband. These subbands possessed upright and elevated updrafts and reflectivity cores. The flow pattern could be characterized as a hybrid structure, with some similarities to both inner and outer rainbands. The subbands contained a midlevel jet on the inner side of the reflectivity core that is likely accelerated by the heating of stratiform precipitation. They also contained a low-level jet that is attributed to the heating of convective precipitation (Fig. 15).

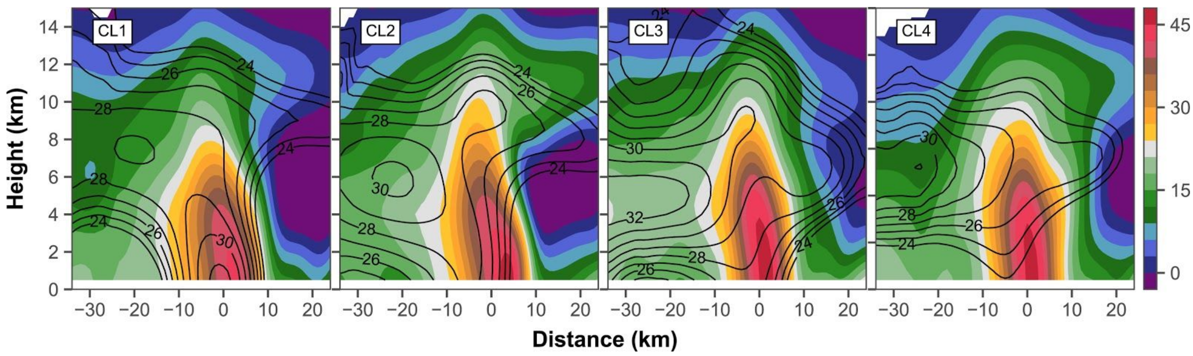

Fig 15. Tangential wind speed (contours) overlaid on the reflectivity (color) averaged along the subbands of the principal rainband from Typhoon Hagupit (2008). Only wind speeds greater than 24 m s^{-1} are shown. Figure 9 of Tang et al. (2018b).

Tang et al. (2018b) also found that that the subbands in Hagupit's principal rainband accumulate PV at lower levels. At midlevels, the significant horizontal advection of absolute angular momentum associated with the PV anomalies may act to intensify the TC. Compared to a previous analysis of a single subband (Tang et al. 2014), multiple passes from the aircraft document substantial variability in the strength of convection and estimated PV generation. This variability is attributed to variations in low-level shear and cold-pool interactions. In the 'optimal state' with the strongest upright convection, the low-level shear is approximately balanced by the cold pool, similar to the dynamics of a squall line. However, variations in the convective life-cycle and local environment of the principal rainband modulate the strength of the dynamical impacts pertaining to PV generation and absolute angular momentum advection. Low-level outflow associated with the secondary circulation of the subband may also hinder intensification by posing a barrier to the inflow.

The microphysical characteristics of TC rainbands may also affect intensity change. Brown et al. (2016) compared multiple microphysics parameterizations in WRF with polarimetric radar observations and found substantial differences in the probability distributions of simulated rain drop sizes and amounts. In aggregate, the schemes that produced the greatest rainfall accumulations resulted in the most intense simulated TCs. This suggests a link between total convective heating in the eyewall and rainbands, and intensity. That study did not partition the heating and microphysics contributed by the eyewall, inner rainbands, and outer rainbands, but another study (Wu et al. 2018) found that ice-phased microphysical processes above the melting level (including aggregation and riming) constitute the major pathway of rainfall production over land in the outer rainband. However, Wu et al. (2018) found that the microphysical processes were different from that of the inner rainband analyzed in Wang et al. (2016). The latter study documented a predominance of warm-rain processes in the inner rainband, which tends to concentrate heating at lower levels. In the intermediate region near the principal rainband, ice processes associated with stratiform rain may play a critical role in initiating a secondary eyewall; as discussed earlier in this report, this can have a profound influence on TC intensity (Didlake et al. 2018).

Radar observations suggest that microphysics, heating, and the dynamics of inner, principal, and outer rainbands have a complicated relationship, with no single factor dominating the influence on TC intensity. As viewed from either the PV generation or angular momentum advection frameworks, the overall effect of convective heating appears to be a spin-up the local low- and mid-level circulation. Mid-level jets associated with stratiform heating can also spin-up the local circulation through angular momentum advection above the frictional boundary layer. This local spin-up may have a positive influence on the overall outer core strength of the TC by increasing the total circulation. However, the local spin-up through rainband convective or stratiform heating may come at the expense of the eyewall intensity due to the interception and reduction of the low-level inflow at an outer radius. The past four years have seen extensive observational analysis on the dynamic and microphysical structure of rainbands. Such studies have shown that significant variability exists in 'snapshots' of rainband structure at different radii and at different stages of the convective life-cycle. This variability in the observed structures renders the determination of causal relationships between rainbands and intensity very difficult.

f) **Summary of the Role of Rainbands in TC Intensity Change**

Spiral rainbands comprise one of the major components of a TC, and their structural characteristics play significant roles in TC structure and intensity change. As such, rainbands have been examined by a number of observational and modeling studies over the past four years. Radar observations show that the finescale structures of outer rainbands frequently resemble squall lines. Additionally, these studies have concluded that ice-phased microphysical processes above the melting level dominate the major pathway of rainfall production in the overland outer rainband, in contrast to the predominance of warm-rain processes that occur in the inner rainband. Observations also indicate that the lightning flash density is maximized in the outer-rainband region and minimized in the inner-rainband region. Additionally, outer rainband lightning is found to be positively correlated to TC intensity change in the next 24 h. Idealized numerical simulations have demonstrated that convective heating in the inner rainband region generally promotes an increase to TC intensity; meanwhile, stratiform cooling in inner rainbands tends to hinder TC intensification. Evaporation of raindrops in the outer rainband region tends to suppress the final TC intensity, but the effects of evaporation in the inner rainbands are not significant. Although the physical link between spiral rainbands and TC intensity change has been established mainly through idealized numerical experiments, definitive observational evidence will be required to confirm these findings. The interactions between spiral rainband behavior (particularly microphysical processes within rainbands) and other TC components, and how these interactions affect TC intensity change, remain open issues (especially since rainbands are also strongly affected by the environment). Therefore, we recommend that specific, targeted observational and modeling investigations be undertaken to better understand interactions between spiral rainbands and their parent TCs and the specific mechanisms by which rainbands influence TC intensity.

3.1.5 Eyewall Instability and Inner-Core Mixing

a) **Introduction**

Mature tropical cyclones (TCs) tend to develop nonmonotonic PV profiles in the vicinity of the eyewall and, thereby, are susceptible to instabilities. For instance, the pronounced peak in the radial PV distribution may accommodate counter-propagating vortex Rossby (VR) waves with the ability to phase lock and induce mutual growth. This classic barotropic instability mechanism has been thoroughly investigated in the adiabatic two-dimensional (2D) nondivergent framework (where absolute vertical vorticity and PV are equivalent; e.g., Schubert et al. 1999) and is often assumed to be responsible for the generation of asymmetric features observed in real TCs (e.g., Reasor et al. 2000; Hendricks et al. 2012) as well as mixing induced within the inner core. Although this is one plausible explanation (for the origin of asymmetries), real TCs are essentially moist, three-dimensional (3D) continuously stratified vortices that possess distinct mean secondary circulations. As such, the applicability of simplified 2D arguments awaits rigorous comparison to more realistic theories and numerical simulations. This subsection summarizes advances in understanding eyewall instability and inner-core mixing processes over the last four years.

b) **Effect of Instability on TC Intensity Change in a Shallow Water (SW) System with Forced Mass Sink (2D case)**

As a first step towards understanding the effects of diabatic heating on inner-core instabilities, Hendricks et al. (2014) applied a mass sink (intended to parameterize moist convection) to a one-layer shallow water system. Depending on specifics of the parameterization, the impact of eyewall instability on TC intensity can exhibit either distinct similarities or differences when compared to the outcome of barotropic instability in the adiabatic 2D system. In particular, it was shown that when instabilities were triggered by a prescribed mass sink that has an annular shape[6] the onset of instability was marked by a decrease of the maximum velocity, while simultaneously deepening the central pressure deficit. This finding is consistent with the outcome from the unforced 2D case. On the other hand, when the forcing was designed to be proportional to the relative vorticity, the instability resulted in an overall intensification of the vortex (contrary to the unforced 2D case).

c) **Effect of Instability on TC Intensity Change in a SW System with Precipitation and Evaporation (2D case)**

The results of Hendricks et al. (2014) are interesting and potentially relevant. However, the fact that they largely rely on the characteristics of an ad hoc mass sink (the forcing) introduced in the SW system is a significant shortcoming. Lahaye and Zeitlin (2016) appear to have recognized this limitation and have presented results with a one-layer shallow water model augmented by adding a prognostic humidity equation, as well as self-consistent (but crude) parameterizations for precipitation and evaporation. In agreement with Hendricks et al. (2014), they found that the instability released within a moist precipitating simulation (that includes evaporation) results in intensification of the vortex. Perhaps one notable difference resides in the long-term impact of the instability on the vortex structure. In the case of Lahaye and Zeitlin (2016), the initial annular vortex relaxes into a monopolar structure, whereas in Hendricks et al. (2014) the annular vortex reforms after its initial breakdown.

d) **Effect of Instability on TC Intensity Change in 3D Cloud-Resolving Models**

The one-layer SW model is arguably a simple and useful tool that retains significant dynamical features of the primitive equations. Despite this, it can only describe an oversimplified version of the real atmosphere. A more complete evaluation of the impact of moist convection on inner-core instabilities requires the usage of 3D cloud-resolving models. Naylor and Schecter (2014) and Wu et al. (2016) applied this option in order to provide further insight. To elaborate, Naylor and Schecter (2014) quantitatively compared the instabilities in full-physics simulations to those in dry simulations where the vortices have the same azimuthal wind structure. Of interest, they found that moist convection has little impact on the initial exponential growth of inner-core asymmetries (similar growth rates of the asymmetries between moist and dry cases; Fig. 16). A detailed analysis of eddy kinetic energy reveals that the radial shear of mean angular

[6] It should be noted that not all cases with annular forcing presented in the paper resulted in an instability. For example, a broad and weak annular forcing may lead to a thick vortex ring that can remain stable.

velocity is a primary source in the budgets, whereas the production terms associated with the mean secondary circulation are relatively small. The secondary circulation only becomes important at later times in that it restores the vorticity annulus (in contrast with the dry simulations where the vortices relaxed into monopoles) and arrests the intensity change associated with horizontal PV mixing.[7] On the other hand, Wu et al. (2016) compared the vortex evolution in a number of simulations with variable convective heating.[8] In contrast to Naylor and Schecter (2014), their experiments appear to emphasize the significant role of the mean secondary circulation in maintaining the initial annular vortex structure. Note that both the results of Naylor and Schecter (2014) and Wu et al. (2016) are based on a relatively small sample of experiments and, thus, there is no firm reason to believe that they are general. For a more general picture, a 3D perturbation theory that incorporates both moisture and the vortex mean secondary circulation is needed. Fortunately, such a tool has been recently developed successfully by Schecter (2018) and awaits a thorough investigation.

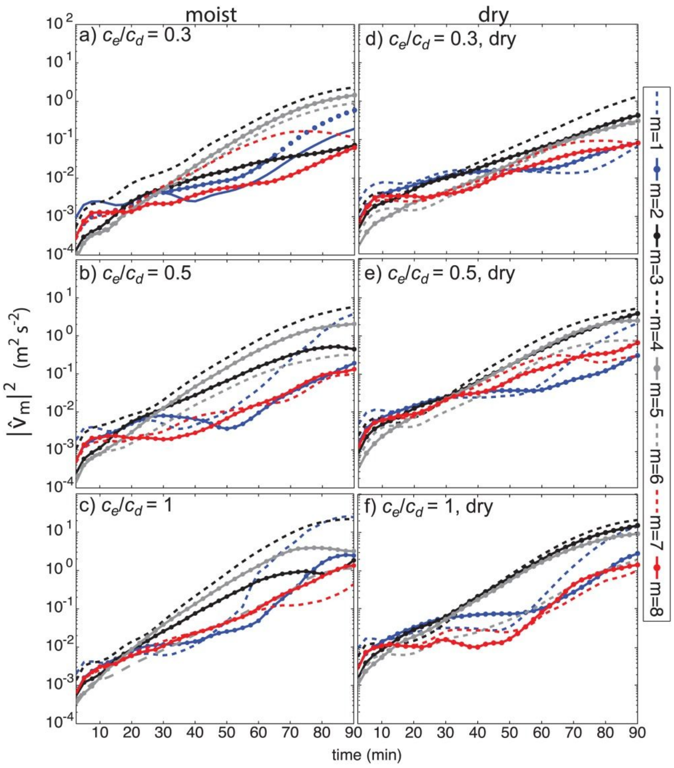

Fig 16. Time series of the squared amplitude of select components from the Fourier expansion of tangential velocity. Moist simulations are in the left plots, and dry simulations in the right. Here, it can be seen that before nonlinear saturation is apparent, the fastest growing modes have wave numbers ranging from 4 to 6 and e-folding times ranging from 15 to 20 min. The growth rates of the dominant modes are very similar between the moist simulations and their dry counterparts. Adapted from figure 4 of Naylor and Schecter (2014).

e) **Effect of Instability on TC Intensity Change due to Waves**

While the previous discussion focused on barotropic instability and subtler variants, this mechanism is not the only one supported within an annular vortex. Another instability mechanism involves a VR wave in the vortex core that spontaneously emits a frequency-matched spiral inertia gravity (IG) wave into the environment (e.g., Schecter and Montgomery 2004). The IG wave radiation is destabilizing because it's wave activity is negative. To conserve total wave activity, the positive component associated with the VR wave must grow. It is not always clear whether barotropic instability or

[7] Note that, in their study the simulations were initialized with quasi steady state vortices. By the end of the moist simulations, the maximum winds are approximately the same as in the initial conditions. On the other hand, the maximum winds in the dry simulations steadily decreased.
[8] In particular, the convective heating within a selected microphysics scheme was adjusted by a constant factor at each grid point in the domain.

radiation-driven instability should prevail (in the context of annular vortices). Menelaou et al. (2016) attempted to address this question with a comprehensive 3D linear stability analysis (applied to annular barotropic vortices whose basic state is in gradient and hydrostatic balance), and a suitably designed wave-activity diagnostic. The picture that emerges from their study suggests that increasing the Froude number (*Fr*) beyond unity tends to cause a transition (which can be abrupt or gradual depending on specifics) from nonradiative instabilities to radiation-driven instabilities[9] (Fig. 17). The essence of this figure can be captured following the relative importance of the term RAD (circle symbol), which represents the contribution to the growth rate from inertia-gravity wave radiation. From the left panel, it can be seen that the dominant eigenmode of this cyclone exhibits an abrupt transition at a critical Froude number. For $Fr < 1.5$, the magnitude of RAD is very small compared to that of other partial growth rates. As *Fr* increases beyond its critical value, *n* (which denotes the azimuthal wavenumber) changes from 4 to 2 and the status of RAD immediately elevates from negligible to dominant. On the other hand, from the right panel it can be seen that the prevailing instability of this cyclone gradually transitions from a nonradiative process to a radiation-driven affair as the Froude number becomes greater than 2. The transition is relatively smooth despite a sequence of abrupt drops in the azimuthal wavenumber from 5 to 4 to 3 to 2 followed by a jump to 3 and return to 2. Nevertheless, for certain case studies, it was further shown that the dominant modes of instability can also involve multiple mechanisms operating simultaneously[10] (e.g., radiative and barotropic instability).

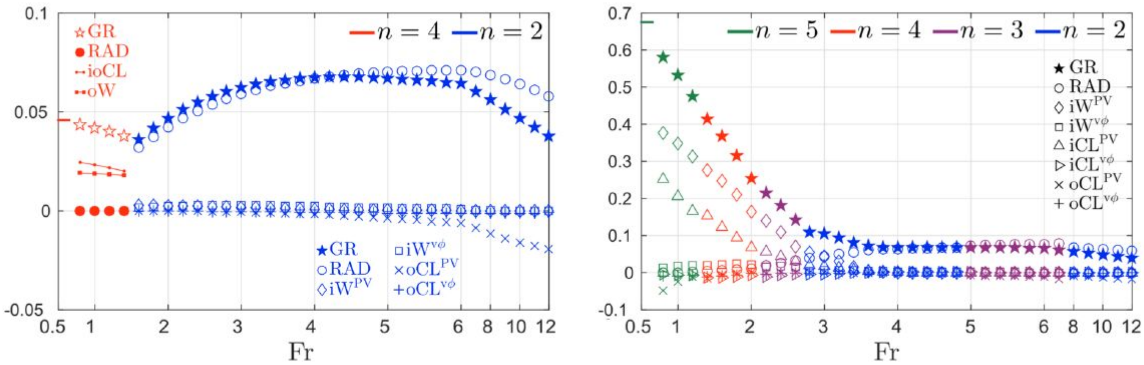

Fig 17. Froude number, Fr, dependence of the generic instability of an annular cyclone with (left) thin annulus and a shallow central vorticity hole, or (right) thin annulus and a deep central vorticity hole. Growth rate (GR; star symbol) and partial growth rates (remaining symbols) scaled to the basic state angular velocity. The partial growth rates are calculated from suitable angular pseudo-momentum budgets. See text for more details. Adapted from figure 8 of Menelaou et al. (2016).

While it is important to understand the time scale and spatial structure of the dominant inner-core instability, it may be more important to understand its consequences on TC structure and intensity. Although the linear stability analysis of Menelaou et al. (2016) revealed that the VR–IG wave instability may become relevant in the parameter regime of a major TC, it says nothing about its long-term (and nonlinear) effects. Menelaou and Yau (2018) attempted to further elucidate this using a conventional 3D

[9] Here, the analysis excludes moisture and is applied to annular vortices without a peripheral vorticity skirt. Adding parameterized eyewall moisture or an outer vorticity skirt can switch the order of dominance between nonradiative and radiation-driven modes of instability.
[10] Note that for a multi-mechanistic mode, assessing the role of each mechanism in destabilizing the vortex requires special care and can lead to inconsistencies without the right diagnostic (Schecter and Menelaou 2017).

primitive equation nonlinear model initialized with dry non-convective annular TC-like vortices. At first, their study verified that spontaneous radiative imbalance can indeed be the dominant destabilizing mechanism even within a nonlinear model. After destabilization, they demonstrated that its long-term nonlinear effects can lead to the formation of mesovortices, vortex merger, and mixing processes that can relax the initial annular vortex into one with a monotonic distribution (similar to the long-term outcome of classical barotropic instability; Fig. 18).

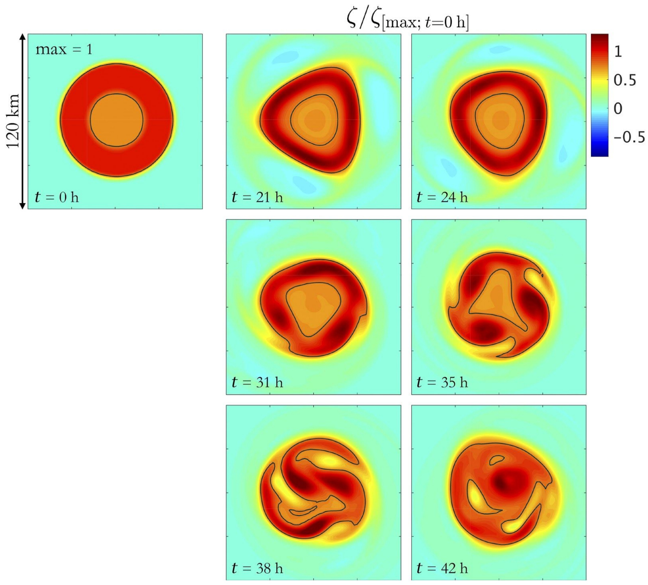

Fig 18. Long-term nonlinear evolution of spontaneous radiative imbalance excited in an annular cyclone perturbed by an initial n = 3 thermal pulse. (top left) Horizontal cross section of normalized relative vorticity $\zeta=\zeta_{[max;t=0\ h]}$ at initial time t = 0 h. (center and right column) Normalized relative vorticity vs time. The cross sections are taken at a selected vertical level. The normalization factor $\zeta_{[max;t=0\ h]}$ is the initial maximum value of the relative vorticity. Figure 11 of Menelaou and Yau (2018).

e) **Summary of the Role of Instability and Mixing Processes on TC Intensity Change**

Recent work has extended numerical analyses of inner core instability processes from 2D barotropic frameworks to more realistic 3D frameworks that include moisture and parameterized mass sinks. Whereas, barotropic instability in a 2D framework leads to deepening of the pressure deficit but a decrease in intensity, results from simulations in more realistic frameworks show that instability processes may cause intensification under certain assumptions [cf Lee and Wu (2018), as discussed in subsection 3.1.2e]. Considerable uncertainty remains as to whether the secondary circulation prevents relaxation of the vortex to a monopole (or how quickly it might restore the vortex back to an annular state) and as to the effects of moist convective processes on instability. Additional studies examined other types of instabilities caused by spontaneous IG radiation from VR waves. More work is needed to understand the long-term and nonlinear effects of VR-IG instability. Because the PV structure is critical in understanding the vortex state (annular vs. monopole) during instability mixing events, future research should consider observational strategies to better assess the PV structure of TCs.

3.1.6 Relationship between Surface Fluxes and Intensity Change

a) **Introduction**

Latent heat energy is critical to drive TCs. Many studies have shown that sea-surface fluxes play an essential role in providing latent heat to the TC core where the energy is converted into kinetic energy (e.g., Raymond and Herman 2012). It is also well understood that the surface friction dissipates the kinetic energy of TC (e.g., Ekman 1905; Haurwitz 1935, 1936). Consequently, TCs are largely controlled by surface enthalpy and momentum fluxes as can be shown through potential intensity theory (e.g., Kleinschmidt 1951). While the community has long recognized the importance of surface fluxes in TC intensity changes, recent literature from the past four years (2014–2018) continues to provide new understandings of this topic.

b) The Role of Surface Fluxes in TC Intensity Change

Since surface fluxes are parameterized through bulk aerodynamic formulae in most numerical and theoretical models, the effects of air–sea exchange coefficients on TC intensity and structure have remained a vital area of investigation. Despite knowing the critical importance of the surface drag coefficient, obtaining accurate measurements of this quantity at the higher wind speeds found in intense TCs remains problematic (e.g., Vickery et al. 2000; Powell et al. 2003; Bell and Montgomery 2008; Powell et al 2009; Bell et al. 2012; Rastigejev and Suslov 2014). Soloviev et al. (2017) studied the impact of wind-speed dependence of the surface drag coefficient on TC intensification. They found that the drag coefficient has a local minimum at approximately 60 m s^{-1}, and that the resulting negative slope of the drag coefficient between 35 and 60 m s^{-1} contributes positively to TC intensification; meanwhile, the positive slope above 60 m s^{-1} favors weakening (Fig. 19).

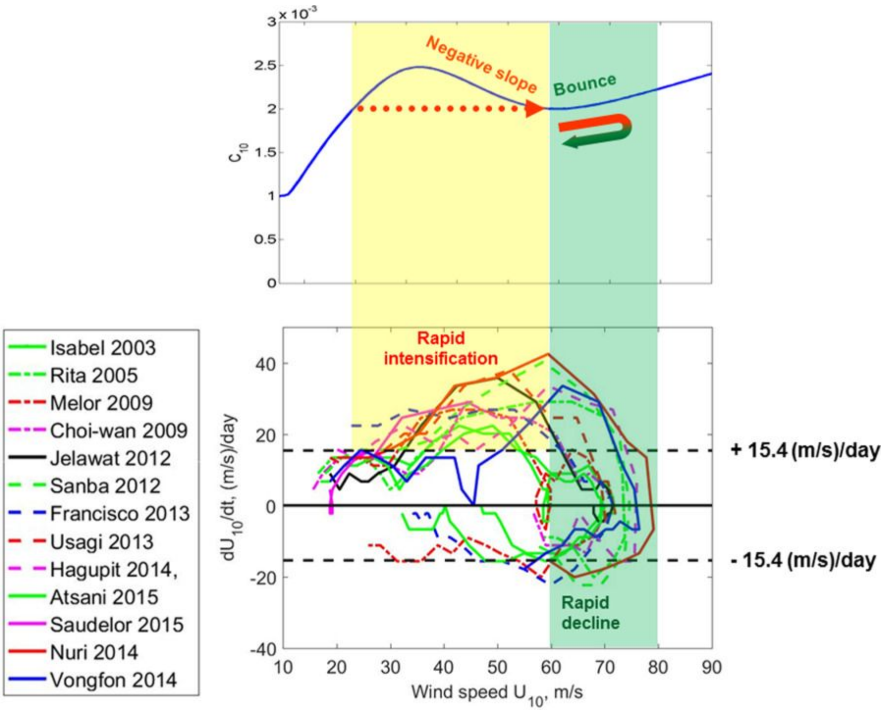

Fig 19. (Top) Wind-speed dependence of surface drag coefficient. (Bottom) Observed rate of change in wind speed 10-m level at as a function of wind speed. Figure 7 of Soloviev et al. (2017).

Kwon and Kim (2017) demonstrated that a change in the momentum coefficient with wind speed affects the radial distribution of angular momentum (i.e., the size of TC), which changes the TC intensity. Using dropsondes from aircraft flights, in situ observations, and satellite data for Hurricane Earl, Jaimes et al. (2015) showed that the bulk enthalpy fluxes are controlled by the thermodynamic disequilibrium between the sea surface and the near-surface air, not by the wind speed. Ma et al. (2017) examined the impacts of revised parameterization of sea-surface fluxes including processes associated with sea spray on TCs, and showed that sea spray processes result in cooling and moistening of the near-surface air in the eyewall and eye regions; this increases the thermodynamic disequilibrium and enhances the surfaces fluxes, favoring RI. When the exchange coefficients are treated stochastically in an ensemble modeling framework, the standard deviation of TC intensity forecasts decreases (Torn 2016). Meanwhile, when the ocean conditions are treated stochastically, the standard deviation of the intensity forecasts is greater. An increase in the drag coefficient results in a narrower radius and a lower height of maximum tangential wind (Coronel et al. 2016). Green and Zhang (2014) investigated the impacts of four parameters proposed to control the wind-speed dependence of exchange coefficients: two are multiplicative factors, while the other two control the coefficient at high wind speeds. They found that the impact of the multiplicative parameter for the drag coefficient on the WPR is larger than that for the enthalpy coefficient. The coefficients also affect the simulated warm-core structure and precipitation (Ming and Zhang 2016). Li et al. (2014b) showed that including the nonbreaking wave-induced mixing in the parameterization, which is caused by surface wave stirring, results in better forecasts of TC intensity. Zhang et al. (2017b) showed that incorporation of effects of sea spray increases the maximum cooling of SST in the right-hand side of Typhoon Rammasun (2002).

c) **Measuring and Parameterizing Surface Fluxes**

Measuring the surface fluxes under strong wind conditions is a challenging topic. Potter et al. (2015) succeeded in making the first-ever direct measurements of sea-surface momentum fluxes during the Impact of Typhoons on the Ocean in the Pacific (ITOP) campaign. Their analysis shows evidence of a rolloff at wind speeds faster than 22 m s^{-1}. Mueller and Veron (2014) formulated a simple model developed from Lagrangian stochastic simulations. Their results show that the spray-mediated fluxes may be sensitive to the size distribution of the drops. Parameterizations of the surface exchange coefficients have been developed by several studies. Zweers et al. (2015) developed a parameterization incorporating effects of sea spray, which has a wind-speed dependence consistent with observations; they showed that a model using this parameterization can reasonably simulate TC intensity. Andreas et al. (2015) developed a physics-based bulk algorithm for the air–sea surface flux with spray-mediated transfer as well as the interfacial process by molecular motion. As their algorithm is physics-based, it can be extended to hurricane winds. Liu et al. (2017) investigated the sensitivity of simulated Hurricane Katrina (2005) to boundary layer schemes. They showed that the Mellor–Yamada–Janjic scheme results in stronger surface fluxes and vertical mixing, which enhances air-sea interaction. The measurement of surface fluxes under fast-wind conditions is still difficult and needs to be conducted in the future.

The effects of surface fluxes on intensity and structure of TCs have been investigated by several studies. Wada (2015a) showed that the RI of Typhoon Man-yi is associated with a mesovortex inside the RMW, which is attributed to barotropic-convective instability induced by relatively high SST and steep gradients of sea-level pressure and tangential wind. Wada (2015b) showed that the minimum value of tropical cyclone heat potential (TCHP) for intensification in the WNP is low (40–60 kJ cm^{-2}) around 5–10°N, west of 120°E and east of 140°E, whereas it is high (80–100 kJ cm^{-2}) around 15–20°N. Ma et al. (2015) examined the relative roles of thermal and moisture effects by considering the sea-spray effects and showed that TC intensity is sensitive to latent heat flux, not total enthalpy flux. Xu (2015) showed that overland latent heat fluxes intensified Typhoon Haitang when it was near Taiwan island, while the sensible heat fluxes from the land weakened it. Chen et al. (2017) revealed that—compared to a case with fixed cold-wake SST—the decrease in TC intensity due to a cold wake is delayed when air-sea interaction is allowed in the simulation. This delayed weakening of the TC is attributed to a "wake jet" that transports moist air inward (Fig. 20).

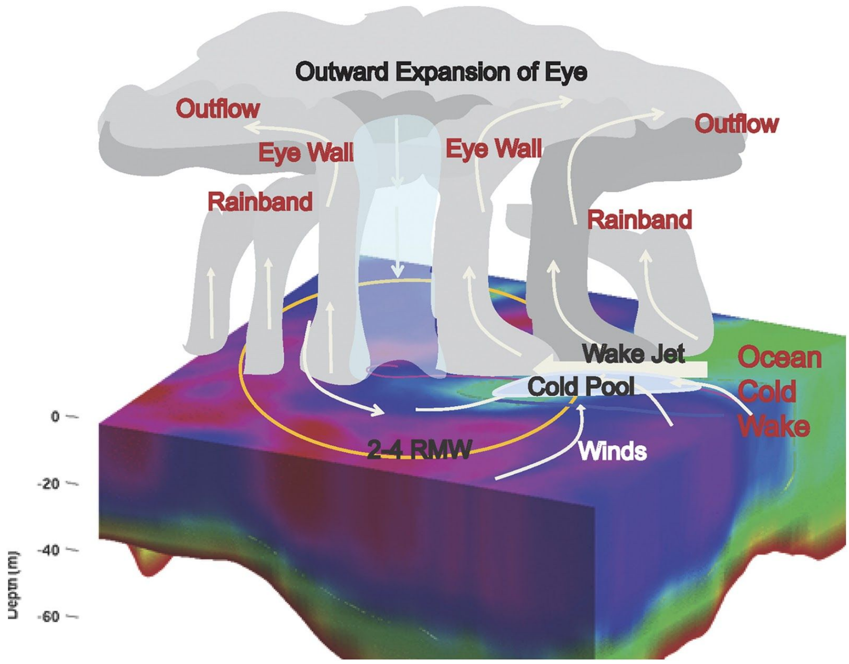

Fig 20. Conceptual model of the physical processes associated with the atmospheric response in a translating TC from right to left with a trailing ocean cold wake (green) with an atmospheric cold pool (light blue). Figure 13 of Chen et al. (2017).

d) **Potential Intensity and Surface Fluxes**

As surface fluxes play a dominant role in the PI theory (e.g., Kleinschmidt 1951), some researchers have studied PI theory by focusing on the fluxes. Based on observational data, Kowaleski and Evans (2015) showed remarkable differences in observed surface fluxes compared with fluxes calculated from PI theory, especially around the RMW. Strazzo et al. (2015) analyzed TCs generated by two global climate models and showed that the sensitivity of PI to SST is not statistically different from that of observed maximum intensity or limiting intensity. Chavas (2017) developed a simple theory of TC ventilation and showed that capping the surface flux reduces the PI and amplifies the detrimental effect of ventilation. Miyamoto et al. (2017) developed an analytical model of PI that incorporates the TC-induced sea-surface cooling (Fig. 21). They derived a nondimensional parameter that represents the degree of ocean cooling, which depends on TC intensity, size, translation speed, and ocean stratification.

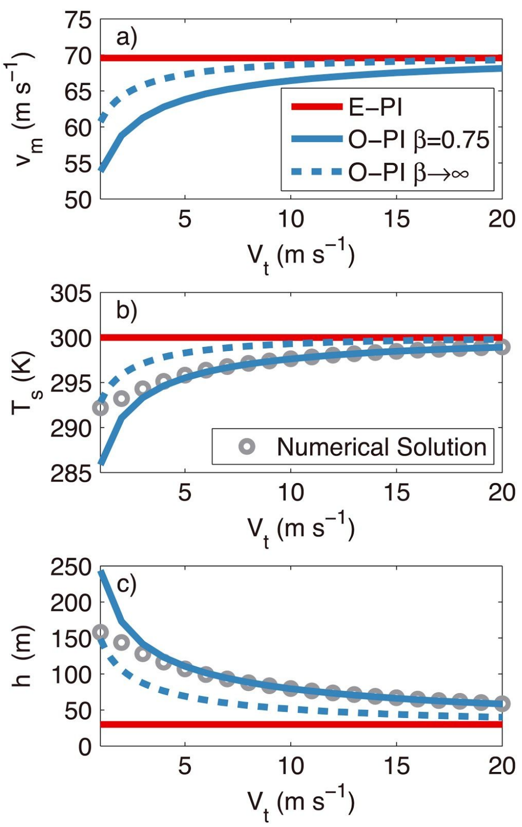

Fig 21. (a) TC intensity, (b) SST, and (c) mixed-layer depth as a function of translation speed of TC. The red and blue lines represents Emanuel's PI and PI incorporating ocean cooling. The circles show numerical simulations using an ocean model. Figure 2 of Miyamoto et al. (2017).

Many studies have examined the impacts of surface fluxes on the TC boundary layer since this region is directly affected by such fluxes. Lee and Chen (2014a,b) showed that the boundary layer is stable above the TC-induced cold wake in the right-rear quadrant, which suppresses rainbands and enhances inflow in the boundary layer (Fig. 22). Analyzing an integrated energy equation that encloses all of the TC Carnot legs, Kieu (2015) found that the dissipative heating in the boundary layer is inherently included in the energy budget in PI theory. Based on observations by the Global Positioning System dropsonde, Zhang et al. (2017c) showed the importance of the surface-flux induced boundary layer recovery in regulating the low-level thermodynamic field of TC. Zhu et al. (2016) showed that including TC-induced SST cooling may decrease the instability in the boundary layer to below the criterion required for the generation of roll vortices; in this scenario vortices can not form. In contrast, when TC-induced cooling is not considered, the criterion is satisfied and roll vortices can form. The effects of roll vortices on TC intensity and structure are not yet understood and hence further studies are needed.

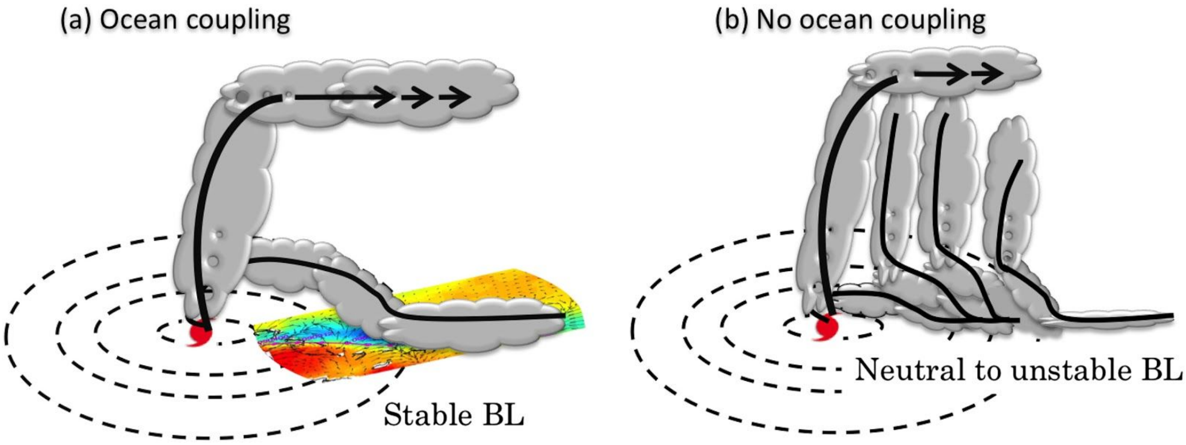

Fig 22. Schematic of boundary-layer flow in (a) a coupled model and (b) an uncoupled model. Figure 15 of Lee and Chen (2014a).

e) **Sea-Surface Temperature Response**

A number of studies have shown that the radial distributions of surface fluxes play an important role in determining the intensity and size of TCs. To the degree that these surface fluxes depend on SST, which is a function of the ocean's response to the TC-induced mixing and upwelling, the TC intensity depends on the time-evolving radial distributions of SSTs in a complicated fashion that depends on the disequilibrium of the air-sea interface. Sun et al. (2014) showed that the enhancing SSTs within the range of 1.5–2.0 times the RMW contributes to an increase in TC intensity and a decrease in inner-core size, while enhancing the SSTs outside works in an opposite manner. Kanada et al. (2017) showed that high SST inside the RMW increases CAPE and is more likely to produce strong convective updrafts, which can lead to RI. In contrast, high SSTs outside the RMW induces secondary updrafts that inhibit RI. Zhang et al. (2017b) investigated the energetics at the ocean surface and showed that the surface flux is approximately balanced with energy dissipation inside 2.3 times the RMW. Ma et al. (2015) examined the sensitivity of TC size to surface sensible heat flux and found that TC size shrinks by over 20% when the heat flux is removed. The adiabatic cooling associated with radial inflow is largely balanced with the heat flux. Zhao and Chan (2017) examined the relationship between SST cooling and the subsequent change in TC size. In their coupled simulations, an initially small TC retains its small size throughout its life cycle, whereas the initially large TCs (Fig. 23) become more intense due to higher enthalpy fluxes in the inner core region.

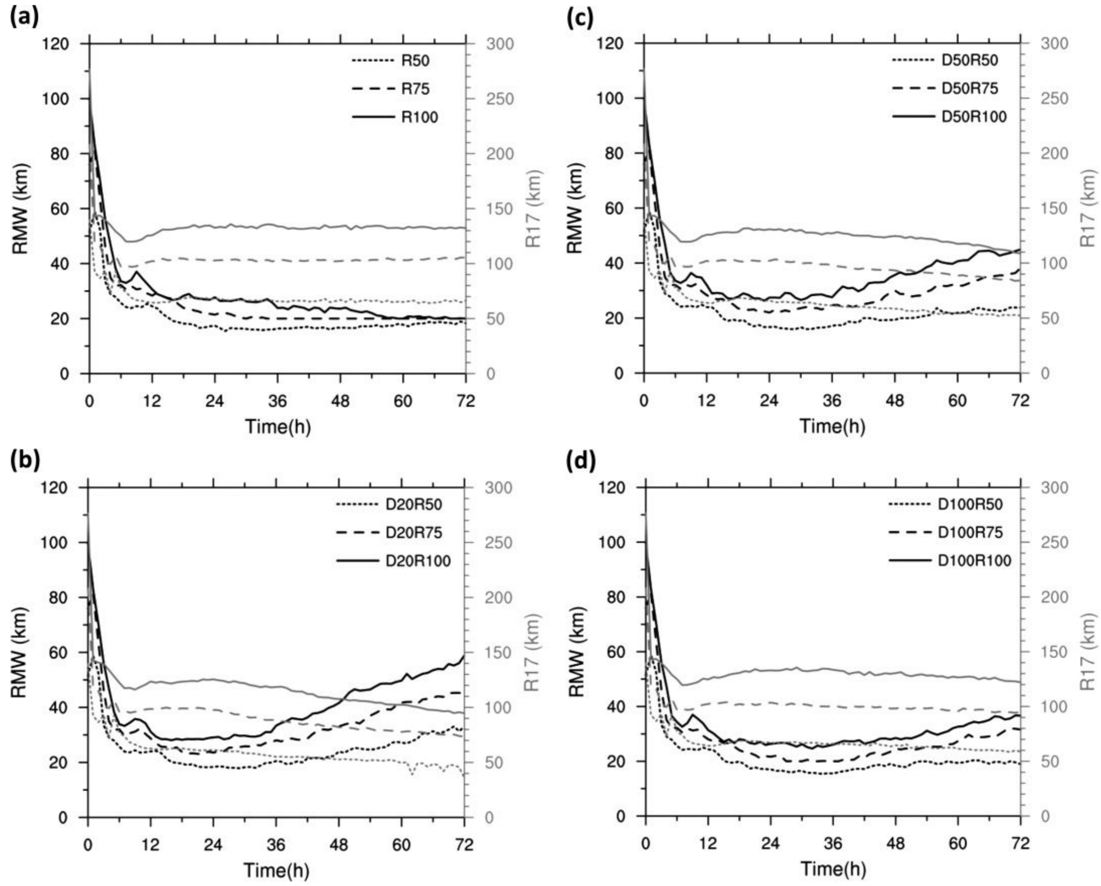

Fig 23. Time series of RMW in (a) uncoupled simulations, (b) simulations with 20-m mixed-layer depth, (c) with 50-m depth, and (d) with 100-m depth. The initial RMW is denoted as the digit with R. Figure 5 of Zhao and Chan (2017).

Several other studies have examined the TC-induced cooling. Potter et al. (2017) analyzed observational data in the Philippine Sea in 2010 and showed that the decrease in mixed layer temperature is well predicted by the TC's translation speed and wind speed. They attributed 12–47% of the mixed layer heat loss to enthalpy fluxes, which is much greater than previous reports. Wei et al. (2017) used a machine learning technique to propose a parameterization of TC-induced SST cooling. This machine-learning-based parameterization performs better at predicting the SST cooling than a method based on linear regression. Jullien et al. (2014) conducted a multidecadal, coupled regional simulation in the South Pacific. They showed that anticyclonic ocean eddies have the effect of insulating against storm-induced upwelling and mixing. This tends to reduce the SST cooling. In contrast, cyclonic eddies promote stronger SST cooling. Lai et al. (2015) showed that the TC-induced SST cooling differs between coastal areas and the open sea. Seroka et al. (2016, 2017) illustrated the importance of representing the coastal regions by examining the effect of the Mid-Atlantic Bight on the intensity of Hurricane Irene (2011) and Tropical Storm Barry (2007).

f) **Summary of the Role of Surface Fluxes and TC Intensity Change**

The role of surface fluxes in TC intensity change continues to be a critical research topic. Advances in both modeling and observing surface fluxes have improved our understanding of the relationships between TC intensification and the drag and enthalpy coefficients. New physics-based parameterization have been developed which incorporate the effects of sea spray and interfacial effects (Andreas et al. 2015; Soloviev et al. 2017). In particular, the wind-speed dependence of the drag coefficient that results from sea spray effects appears to produce a local minimum near 60 m s^{-1}; this may explain, in part, why TCs rapidly intensify from 35–60 m s^{-1}, but weaken soon after reaching high intensity (Soloviev et al. 2017). Also, recent work has shown that bulk enthalpy fluxes are controlled by the thermodynamic disequilibrium between the sea surface and the near-surface air, not by the wind speed (Jaimes et al. 2015), and that sea spray processes can increase the thermodynamic disequilibrium favoring enhanced fluxes and RI (Ma et al. 2017). Additionally, TC intensity has been found to be sensitive to latent heat fluxes, but not total enthalpy fluxes (Ma et al. 2015). Models which incorporate the effects of sea spray can reasonably simulate TC intensity (Zweers et al. 2015), and models which include the mixing produced by nonbreaking waves can improve TC intensity forecasts (Li et al. 2014b).

Progress has also been made with regard to understanding of the role of surface fluxes on potential intensity and the impact of the SST response of the ocean. Dissipative heating in the boundary layer is found to be inherently included in the energy budget of PI theory (Kieu 2015). A number of studies have shown that the radial distributions of surface fluxes play an important role in determining the intensity and size of TCs (Sun et al. 2014; Lee and Chen 2014a,b; Kanada et al. 2017; Zhao and Chan 2017). Analysis of the energetics at the ocean surface shows that the surface flux is approximately balanced with energy dissipation inside 2.3 times the RMW (Zhang et al. 2017b). TC-induced cooling may also decrease the instability in the boundary layer to the point where roll vortices do not form (Zhu et al. 2016), however the overall effect of roll vortices on TC intensity change is not yet known.

Despite considerable progress over the last four years, considerable uncertainties still remain as to the wind-speed dependence of the surface drag and enthalpy coefficients. Observations of surface fluxes in high wind conditions remains a pressing need. Additional efforts are also needed to transition recent research advancements into operations.

3.1.7 Mechanisms of Tropical Cyclone Intensification

a) **Introduction**

The challenge of understanding the mechanisms by which TCs intensify has captivated the research community for much of the past half century. Scores of papers have been written proposing (or discussing) the various intensification mechanisms. Because of the difficulty in applying observational evidence to definitively answering the deep questions on intensification mechanisms, much of the research to date has utilized theories and numerical simulations. The incompleteness of theoretical approaches, limited observational sampling, and the imperfections of models have resulted in considerable epistemic uncertainty, leaving much room for debate. With this in mind, we enter this section realizing that terminology can be vital. For instance, referring to a description of one or more intensification mechanisms as a *paradigm* may have the implicit connotation (whether intended or not), that the theoretical or conceptual description being put forward is *the dominant paradigm* (that is, that the view is already widely accepted or broadly held by the community) and that competing ideas are 'wrong'. In reality, it is likely that a number of different intensification mechanisms are operating in concert with each other. A better word to describe the theoretical or conceptual description of a collection of intensification mechanisms would be *framework*. A more holistic view, then, is to realize that while previous frameworks may have been incomplete, recent frameworks largely expand on and refine previous frameworks. Understanding the relative contributions of each mechanism to the overall intensification of the TC should be a key goal, although this aspect has often been given lesser attention in studies. In this introduction, we do not attempt to review all variants of the intensification frameworks that have been proposed, but to provide context for the following discussion, we briefly review several of the key historical frameworks. For more thorough reviews of historical intensification frameworks, we refer the reader to the cogent discussions of Montgomery and Smith (2014) and Montgomery (2016).

The first main intensification framework was proposed separately, but nearly simultaneously, by Charney and Eliassen (1964) and Ooyama (1964), who posited that TC development and subsequent intensification involved a collaborative interaction between convection and the larger vortex scale. In this view, the combined effects of convective updrafts lead to the development of a secondary circulation that results in the import of angular momentum and moisture into the vortex. The associated influx moisture has the effect of invigorating the convection, while the import of angular momentum results in a spin-up of the vortex circulation. It was further hypothesized that these two effects result in an instability feedback loop, with stronger convection leading to more spin-up and vice versa. This collaborative effect was termed Convective Instability of the Second Kind (CISK), and was studied in a quasi-geostrophic balance model. CISK was criticized, in part, because it was a linear model (it used geostrophic balance).

Ooyama (1982) proposed a refinement to the CISK idea by adding gradient wind balance to the theory. As Montgomery (2016) points out, this theory, termed the "cooperative intensification theory for tropical cyclones", had its roots in Ooyama's (1969) paper, which studied TC intensification in an axisymmetric, balanced vortex in a stably-stratified atmosphere. The addition of gradient wind balance and recognition of the role of differential latent heating from the organized convection made this a nonlinear theory, but the basic idea is similar to CISK. For the purposes of this review, recent advancements to this intensification mechanism are covered below in subsection b) "Balanced Symmetrical Intensification Mechanism".

The next major development occurred with Emanuel (1986), who recognized the critical role of air-sea latent and sensible heat fluxes in both the development and maintenance of TCs. In this view, the intensification of a TC can be viewed as a finite amplitude air-sea interaction instability. Later, Emanuel (1991) coined the term wind-induced surface heat exchange (WISHE), with Yano and Emanuel (1991) providing further explanation: 'The acronym WISHE is intended to replace and unify the terms "air-sea interaction" used by E87 [Emanuel 1987] and "evaporation-wind feedback" used by Neelin et al. (1987).' Subsequently, this framework has gone on to receive widespread recognition as a plausible explanation for the growth of hurricanes. The major limitations of the original WISHE theory are the assumption of axisymmetry and quasi-balance. The original WISHE theory has undergone revisions in recent years. Emanuel (2012) modified the theory to account for small-scale turbulence in the outflow layer, which sets the thermal stratification there, affecting both the maximum intensity and intensification rate. Zhang and Emanuel (2016) capped the wind speed used in the surface enthalpy flux calculation, and derived a new maximum potential intensity (MPI) formula. Recent discussion on this intensification mechanism is covered below in subsection c).

This synthesis summarizes 40 papers that have been written since 2014 either on, or are related to, intensification mechanisms. In addition to advanced ideas on the historical intensification mechanisms, we also cover papers from a recently-proposed boundary-layer spin-up mechanism (subsection d) and the attempt to combine several key intensification mechanisms into a unified framework called the "rotating-convection" framework (subsection e). A summary follows, along with a recommendation on a possible path to resolve some of the long-standing debates.

b) **Balanced Symmetrical Intensification Mechanism**

The Eliassen (1951) vortex model has provided numerous insights into the response of balanced, rotating dynamics to forcing, especially in the context of TCs. The balanced response to diabatic heating in a vortex with radially and vertically varying static stability, inertial stability, and baroclinicity reminiscent of observed tropical cyclones has assisted in providing a mechanism for intensification, RI, warm-core structures, and eyewall replacement (e.g., Shapiro and Willoughby 1982; Schubert and Hack 1982; Vigh and Schubert 2009; Sitkowski et al. 2012; Musgrave et al. 2012). With respect to intensification and maintenance of observed TCs, recent in situ aircraft and tail Doppler radar and ground-based lightning network TC studies (e.g., Rogers et al. 2013, 2015, 2016; Martinez et al. 2017, Stevenson et al. 2018; Dougherty et al. 2018) have found ties between observations and the theoretical results that link TC intensification to the location of diabatic heating in relation to the high inertial stability region.

However, criticisms of the balanced, symmetric dynamics lie in the extent to which the conceptual ideas that arise from the balanced vortex model can be applied quantitatively to real TCs or in comparisons against numerical simulations (e.g., Smith et al. 2018). In addition to asymmetric arguments, the criticisms primarily focus on the inability of the balanced, symmetric model's diabatic forcing to dynamically evolve in time with the vortex from one balanced state to the next as well as the framework's inability to adequately link the unbalanced dynamics of the boundary layer to the overlying fluid. Solutions of the inviscid, balanced vortex model miss the coupling between the boundary layer Ekman pumping and eyewall convection (e.g., Raymond and Herman 2012).

While time-dependent, analytic solutions of the Eliassen (1951) balanced vortex model that allow diabatic heating to evolve have not been found, Schubert et al. (2016) offer a new perspective on balanced, symmetric intensification through using wave-vortex theory (Salmon 2014). By developing a forced, balanced axisymmetric model from the theory, Schubert et al. (2016) illustrate the dry, dynamical processes involved with the incubation time (Ooyama 1969) of a TC prior to spin up. The authors also show that there is not a one-to-one relationship between absolute angular momentum surfaces and the RMW during intensification in that the contraction of the RMW can cease prior to reaching peak intensity (Stern et al. 2015) and absolute angular momentum surfaces can continue to shift inward (Smith and Montgomery 2015). Even though this framework offers new insight into balanced, symmetric intensification, it is important to know that the small Froude number (*Fr*) restriction imposed by a wave-vortex theory may limit the model's applicability to a stratified fluid.

Despite advances in balanced, symmetric dynamics with respect to TC intensification, the development of analytical solutions that connect the unbalanced boundary layer dynamics to the diabatic forcing in the free atmosphere of a TC continues to remain elusive.

c) **WISHE Intensification Mechanism**

Under the WISHE intensification mechanism, an axisymmetric TC intensifies through a self-induced positive feedback between the tangential wind field and the wind-speed dependent surface moist entropy flux (Fig. 24; Emanuel 1997, 2004, 2012; Montgomery et al. 2009; Montgomery and Smith 2014). In recent studies, the viewpoint of WISHE as the dominant intensification mechanism has been reviewed and investigated.

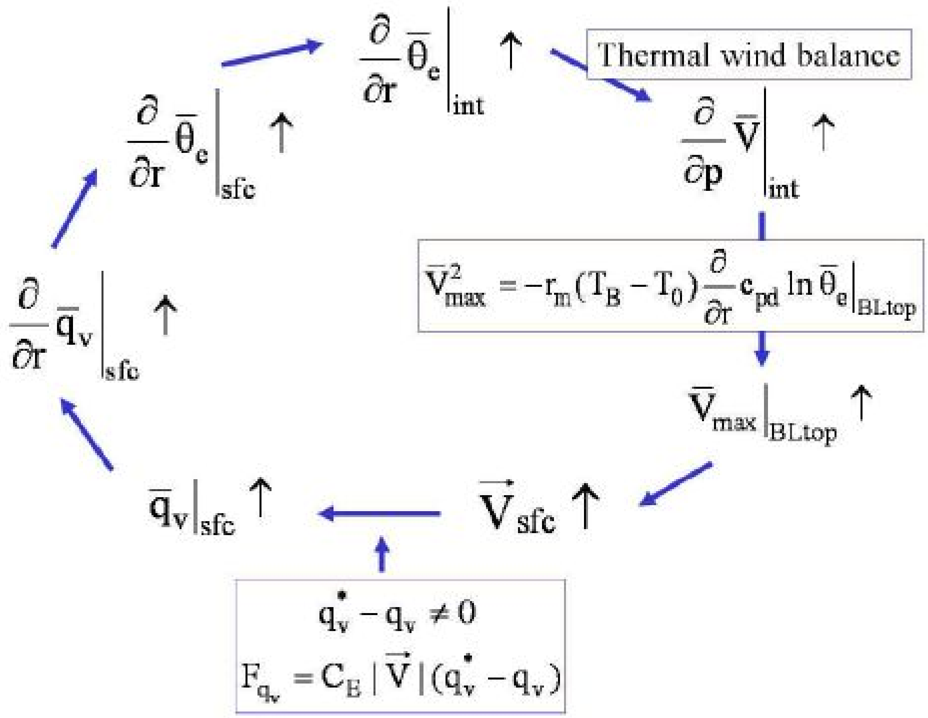

Fig. 24. Schematic of the evaporation-wind intensification mechanism. See the paper for a detailed discussion of this figure. Figure 6 in Montgomery and Smith (2014).

Montgomery et al. (2015) found "contradictory definitions of WISHE as well as ambiguous and generally incomplete descriptions of the putative intensification mechanism" in the literatures, and examined "shortcomings in the linkages proposed by others between these fluxes and other elements of the intensification process". For instance, The COMET Program (Chapter 8, 2013) failed to mention the wind speed-dependent heat flux in the WISHE feedback mechanism. The study also reiterates the important role of surface moisture fluxes in intensification but showed that the wind-speed dependence of surface fluxes is not necessary for intensity change (figure 1 in Montgomery et al. 2015) and that TC intensification can proceed even without evaporative downdrafts (also shown in Montgomery et al. 2009), as opposed to that in Emanuel (1997). This is also the case for tropical depression intensification in which spin up follows even with wind-independent heat fluxes (Murthy and Boos 2018). Lee and Frisius (2018), using simple and complex TC models, found a "positive relationship between the radial CAPE gradient and the intensification rate which disagrees with the basic assumption of WISHE model."

Zhang and Emanuel (2016), on the other hand, redefined WISHE by proposing a tendency equation for the peak wind speed in an idealized, balanced, axisymmetric TC model (Eqns. 5 and 8 in the paper, Eqn. 17 in Emanuel 2012) to quantify the feedback of cyclone winds at the RMW on the surface fluxes. Their analytical solution (Eqn. 10 and fig. 1a in the paper) and numerical simulations with capped surface enthalpy fluxes (figs 4 and 5 in the paper) show that wind-induced surface enthalpy flux affects the rate of intensification, even though it is not a necessary condition for intensification of TCs in general. They also reiterated that "some other process or processes must work to bring the system to such a state that WISHE could conceivably lead to further amplification" that is, "once a mesoscale column of nearly saturated air is established, WISHE can begin to amplify the disturbance" (Emanuel 1989, 2012). The results in Chavas (2017) further verify the importance of WISHE on the intensity dynamics of real-world TCs but also noted the non-necessity of the WISHE mechanism to intensification. However, and as pointed out by Montgomery et al. (2014), the revised tendency equation in the new WISHE mechanism introduces an additional term that describes a control of "ring-like eddy structures encircling the vortex axis" on TC intensification. "In reality, real turbulent mixing occurs locally in azimuth and the axisymmetric assumption is highly questionable" as shown in Persing et al. (2013). With the inclusion of non-gradient wind effects above the boundary layer in Emanuel's WISHE formulation, the IR found in a nonhydrostatic numerical model was reproduced (Peng et al., 2018).

d) Boundary Layer Spin-Up Mechanism

The boundary layer spin-up mechanism is a component of the rotating-convection framework (described below in subsection e) which provides an explanation for the occurrence of the maximum tangential wind speed in the boundary layer. It is important to note that the boundary layer spin-up mechanism requires the classical mechanism to operate (in contrast to what was purported in Smith et al. 2009, statements which have since been corrected in subsequent papers). Also, this mechanism does not propose a separate explanation for a positive tendency of the maximum wind speed above the boundary layer.

Observations (e.g. Kepert 2006a,b; Bell and Montgomery 2008; Zhang et al. 2011; Sanger et al. 2014; Montgomery et al. 2014) as well as numerical model simulations (e.g. Zhang et al. 2001; Smith et al. 2009; Persing et al. 2013) show that the maximum tangential wind in a mature TC occurs in the frictional boundary layer, typically a few hundred meters above the surface. An explanation for this finding was proposed by Smith and Vogl (2008) and Smith et al. (2009). This so-called boundary-layer spin-up mechanism, may be understood as follows. In the boundary layer, air parcels converge comparatively rapidly because, unlike the flow above the layer, which is in approximate gradient wind balance, the flow is subgradient (i.e. the sum of the centrifugal force and Coriolis force acting on an air parcel is less than the inward-directed pressure gradient. As the air parcels spiral cyclonically inward in the boundary layer, they lose some of their absolute angular momentum M to the surface because of the opposing frictional torque. The tangential wind component v is related to M by the formula $v = \frac{M}{r} + \frac{1}{2}fr$, where r is the radius and f is the Coriolis parameter. Thus, v may increase significantly as r decreases if the fractional rate of loss of M is appreciably less than the relative rate of decrease of the air parcel's radius. In such circumstances, the increase in v may be large enough for v to exceed its local (gradient) value (say v_g) at the top of the boundary layer.

Since the rate of loss of M per unit radial distance decreases with the number of spirals the air parcel makes for a given radial displacement, the rate is a monotonically decreasing function of the inflow speed. However, the loss rate increases monotonically as the surface drag and, thus, the frictional torque increase. If v does exceed v_g at some radius, the agradient force (the sum of the centrifugal, Coriolis, and pressure gradient forces) acting on an air parcel is positive and we say that the flow there is supergradient. If this happens, the agradient force combines with the radial frictional force to produce a rapid deceleration of inward-moving air parcels, whereupon the flow turns upward. As air parcels are expelled vertically from the boundary layer, they carry their tangential momentum with them and the positive agradient force drives them outward while approximately conserving their M. As a result, v decreases as the air parcels adjust toward a new state of gradient balance above the boundary layer.

Whether or not v does actually exceed v_g at some inner radii can be ascertained only by doing a nonlinear boundary layer calculation or a full vortex simulation, although the foregoing considerations show this to be a plausible possibility. In fact, both simulations and observations of intensifying and mature TCs show regions of supergradient flow as the air decelerates radially in the boundary layer and turns upward into the eyewall (Bao et al. 2012; Smith et al. 2009; Montgomery et al. 2014). Recent papers emphasizing the role of the boundary layer spin-up mechanism are Montgomery and Smith (2014), Smith and Montgomery (2016a,b), Smith et al. (2017), and Kilroy et al. (2017b).

There has been recent debate on the importance of the boundary layer spin-up mechanism in the overall intensification of a TC (Heng and Wang 2016a; Heng et al. 2017; Smith and Montgomery 2016a; Montgomery and Smith 2018; Heng and Wang 2016b; Heng et al. 2018). The essence of the debate is twofold: 1) whether the boundary layer spin-up mechanism contributes significantly to the intensification of a TC or if it is just a fast adjustment processes to surface friction (Heng and Wang 2016a,b; Smith and Montgomery 2016a); and 2) whether the secondary circulation in a TC simulated in a full-physics model can be captured by the quasi-balanced symmetrical vortex dynamics (the linear Sawyer-Eliassen equation). Heng and Wang (2016a,b) considered that the boundary layer spin-up mechanism proposed by Smith et al. (2009) explains the formation of supergradient wind, a process that has been well-studied previously in the literature (e.g, Kepert 2001; Kepert and Wang 2001), and that the formation of supergradient wind (namely the boundary layer spin-up mechanism of Smith et al. 2009) is a fast adjustment process that could not be a major mechanism of TC intensification. Nevertheless, if the boundary layer spin-up mechanism articulated above is only attempted to explain the formation mechanism of supergradient wind in the TC boundary layer, the debate would be irrelevant and should not be a major issue at all.

Although the second issue is partly related to the first issue, the crux of the matter lies in the treatment of the numerical solution of the Sawyer-Eliassen equation. In order to obtain a converging solution, it is necessary to assure the ellipticity of the equation. The solution is also sensitive to vertical resolution, and in particular, in the frictional boundary layer where the vertical gradient of flow is extremely large. Heng et al. (2017, 2018) showed that the solution based on the linear Sawyer-Eliassen equation could largely capture the secondary circulation in a TC simulated in a full-physics model, even in the boundary layer where the flow is largely unbalanced. This is in sharp contrast to the earlier results in Bui et al. (2009). Heng et al. (2018) clarified that although the balanced symmetrical vortex dynamics still underestimate the inflow in the frictional boundary layer to some extent, the underestimation does not affect the overall azimuthal mean tangential wind budget. That means that the quasi-balanced symmetrical vortex dynamics can largely explain the intensification of a TC. They also emphasized that the unbalanced boundary layer dynamics is key to TC intensification, mainly through modifying the strength and radial location of eyewall updaft and thus diabatic heating (see also Kepert 2017), but not in the way of the boundary layer spin-up mechanism articulated by Smith et al. (2009).

Thus, the key point of contention of recent debates is not on whether the unbalanced boundary layer dynamics are important to TC intensification, but on how the unbalanced boundary layer dynamics do so—whether this occurs through the spin-up of supergradient wind—or through its modification of the strength and radial location of eyewall updraft and thus diabatic heating. Therefore, future observational and numerical studies need to investigate the manner in which boundary layer dynamics contributes to eyewall updaft/convection.

e) **Rotating-Convection Intensification Framework**

Recent theoretical work has led to the development of a new framework for understanding both tropical cyclogenesis and TC intensification, the so-called rotating-convection framework. Reviews of this framework and its relationship to previous theories of TC behaviour are provided by Montgomery and Smith (2014, 2017), Smith and Montgomery (2016c), and Smith et al. (2017). In essence, the new description constitutes an overarching framework for interpreting the complex vortex-convective phenomenology in simulated and observed TCs. It is important to point out that this framework includes and generalizes the classical mechanism of Ooyama (1964, 1969, 1982) and the boundary layer spin-up mechanism (Smith and Vogl 2008; Smith et al. 2009; Montgomery and Smith 2014; Smith and Montgomery 2016a,b; Smith et al. 2017; and Kilroy et al. 2017b). The rotating-convection framework explicitly recognizes the presence of localized, rotating deep convection whose vorticity is amplified greatly over that of the broad-scale vortex circulation by vortex-tube stretching and tilting processes. The framework includes an azimuthally averaged description of storm behaviour that takes into account the effect of locally asymmetric (or eddy) processes. The framework can be framed in terms of absolute angular momentum or absolute vorticity.

From a vorticity perspective, an important mechanism for the intensification of an existing vortical circulation is the inward flux of absolute vorticity into the vortex in the lower troposphere brought about by inflow produced there by the collective effects of deep convection. This is, in essence, the classical mechanism for intensification articulated by Ooyama (1969), and is reviewed in detail in section 4 of Montgomery and Smith (2017). In an angular momentum framework, this mechanism is equivalent to the radial convergence of absolute angular momentum, which, in axisymmetric flow and in the absence of friction, is approximately materially conserved.

The rotating-convection framework has been used to interpret the dynamics in tropical cyclogenesis idealized numerical model calculations (Kilroy et al. 2016, 2017a,b, 2018; Kilroy and Smith 2017). Kilroy et al. (2017a) showed that there is no intrinsic difference between the dynamics of tropical genesis and intensification. The mechanism has been used also to interpret the development of tropical lows over land (Smith et al. 2015; Kilroy et al. 2016, 2017c; Tang et al. 2016) from a vorticity perspective using data provided by ECMWF analyses.

f) **Summary of TC Intensification Mechanisms**

Publications in the time period (2014–2018) covered in this synthesis focused largely on developments in three major intensification mechanisms: (i) balanced symmetrical intensification mechanism, (ii) wind-induced surface heat exchange (WISHE), and (iii) boundary layer spin-up mechanism,. Additionally, a new *rotating-convection framework* has emerged, which combines several of these intensification mechanisms, along with previous historical ideas, into the new framework that recognizes that several intensification mechanisms act together in concert. The recent review papers

(Montgomery and Smith 2014; Montgomery 2016; Smith and Montgomery 2016c[11]; Montgomery and Smith 2017) have been quite beneficial in discussing some of the overarching similarities and distinctions between these mechanisms and their roles in various historical and recently-posited intensification frameworks. We recommend that future research continue this more holistic approach, especially focusing on methods to determine the relative contributions of these mechanisms to overall TC intensification, as well as to investigate whether there are complementary or competing interactions between the mechanisms. In particular, the role of the boundary layer dynamics in contributing to eyewall updrafts and convection needs to be investigated in future observational and numerical studies. To make more rapid progress, it is possible that more organized and coordinated efforts are needed. One path forward would be for scientists of competing theories and frameworks to team up together in a larger collaborative effort to resolve some of these long-standing debates. We recommend that funding agencies recognize this potential approach and design funding calls specifically toward this purpose. We further recommend that the WMO sponsor an international workshop in the near future to bring leading researchers together to review in more detail the issues involved in the controversy on intensification mechanisms and to develop a strategy for future international research collaboration to resolve these issues.

3.1.8 New and Emerging Research Topics

a) Introduction

Several new topics on internal influences on TC intensity change have emerged in recent years. In this section, we discuss some of the more prominent recent ideas, including: (i) the role of vortex structure on TC intensification rate, (ii) the maximum potential intensification rate (MPIR) of TCs, and (iii) the role of upper level outflow on TC intensity change.

b) Role of Vortex Structure on TC Intensification Rate

Carrasco et al. (2014) compared the RMW and AR34 of TCs that underwent RI versus those that slowly intensified or were steady state over a 24-h period for NA TCs during 1990–2010. They found that the intensity change was negatively correlated with both RMW and AR34. Xu and Wang (2015) examined the dependence of TC IR on SST, storm initial intensity (maximum sustained surface wind speed V_{max}), and storm size, in terms of the RMW parameter from the Automated Tropical Cyclone Forecast (ATCF) system b-decks[12] for NA TCs. They found that, for NA TCs during 1988–2014, the TC IR depends strongly on storm intensity, the RMW, the average radius of gale-force wind, and the outer-core wind skirt parameter DR34 (= AR34 - RMW). Xu and Wang (2015) showed that TC IR increases with increasing storm intensity when TC V_{max} was below about 70 to 80 kt (or 36.1 to 41.2 m/s), but decreases with increasing intensity afterwards (Fig. 25a), and that TC IR is negatively correlated with the RMW, AR34, and DR34 (Fig. 25b,c,d).

[11] Smith and Montgomery (2016) is a review published in *Weather* that was written for the educated lay person, including forecasters.

[12] It is important to note that the RMW parameter is not a "best-tracked" quantity in HURDAT2 or the ATCF b-decks. That is, it does not undergo the post-season analysis that other best-tracked parameters like track and intensity undergo. For more discussion on this issue, see Vigh et al. (2012) and the accompanying supplement.

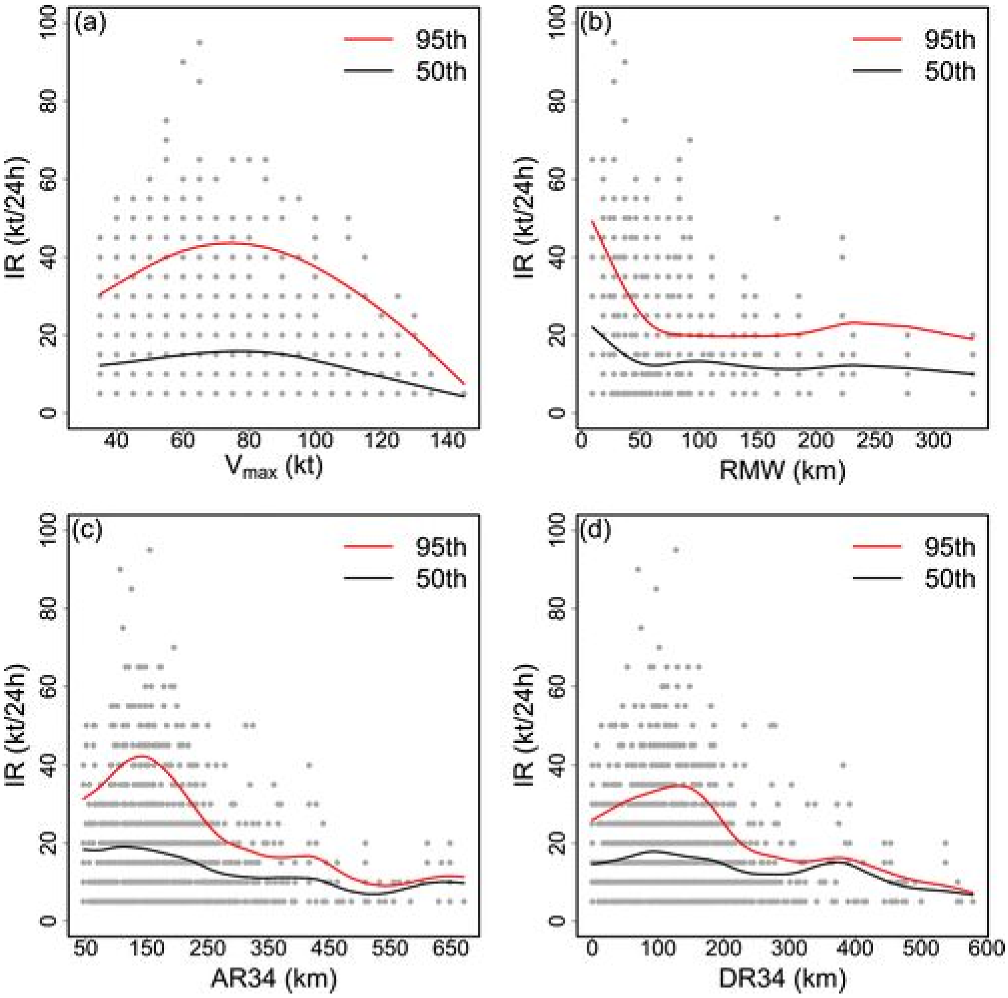

Fig 25. Scatter plots of subsequent 24-h IR vs. (a) storm intensity, (b) RMW, (c) AR34, and (d) DR34 in the NA from 1988 to 2012. Red and black curves are the 95th and 50th %-iles of IR for given storm intensity in (a) and size parameters in (b)–(d), respectively. Figure 1 of Xu and Wang (2015).

Xu and Wang (2015) also found that RI can only happen in a relatively narrow range of the parameter space that includes the storm intensity, and both the RMW and AR34 (or DR34). More recently, Xu and Wang (2018a) extended the statistical analysis of NA TCs to WNP TCs during 1982–2015. Overall, similar to that in the NA, TC IR is positively (negatively) correlated with storm intensity when V_{max} is below (above) 70 kt (36 m/s), and the TC IR is negatively correlated with the RMW. RI occurs only in a relatively narrow range of parameter space in storm intensity and both inner- and outer-core sizes, with the highest IR appearing for V_{max} = 80 kt (41.2 m/s) [compared with 70 kt (36 m/s) for the NA], RMW ≦ 40 km, AR34 = 150 km, and DR34 = 100 km. The highest frequency of occurrence of intensifying TCs occurs for V_{max} ~ 40–60 kt (20.6–30.9 m/s), RMW ~ 20–60 km, AR34 = 200 km, and DR34 = 120 km.

To improve the representation of TC structure and its relationship to TC intensity and intensification, Guo and Tan (2017) proposed a new concept of TC ‘fullness’ to quantitatively measure the storm wind structure. The TC fullness is defined as the ratio of the extent of the outer-core wind skirt to the outer-core size of the TC. They found that TC intensity is more strongly correlated with fullness than with other measures comprising just a single size parameter, and rapidly increasing fullness favors the intensification of a TC. However, how the new parameter is connected to the dynamical characteristics of the TC vortex still needs to be more thoroughly understood.

The dependence the TC's IR on its initial structure has been numerically studied based on ensemble simulations using an axisymmetric model (CM1) by Xu and Wang (2018b). The results show that a TC with an initially larger RMW, or with a slower radial decay of tangential wind outside the RMW, possesses lower inertial stability inside the RMW (or relatively higher inertial stability outside the RMW), and develops more active convection in the outer core region and weaker boundary-layer inflow. Such TCs experience a lower IR during the primary intensification stage, suggesting one possible explanation for the observed dependence of TC IR on TC size and structure.

Wang and Heng (2016) used idealized ensemble numerical simulations to evaluate the contributions of the near-surface high energy air in the TC eye to IR. They found that the near-surface high energy air in the eye contributes about 42% to the IR of a simulated TC, which is in sharp contrast to the 3-4% that such air contributes to the MPI. This was found to occur not through the enhancement of CBs in the eyewall, as had been previously hypothesized, but through initiation of convection near the inner edge of the eyewall. This new convection facilitates eyewall contraction and leads to higher inner-core inertial stability, and thus higher dynamical efficiency of eyewall heating in spinning up the tangential winds near the RMW. Since the near-surface high energy air in the TC eye is also determined by the surface wind distribution inside the RMW, the finding also strongly suggests that the inner core wind structure of the initial TC vortex is a key determinant of the future IR, in particular for those storms with relatively large eye size.

Although both SST and the initial storm intensity have been included in some operational statistical intensity prediction schemes (e.g., SHIPS; DeMaria et al. 2005; Kaplan et al. 2015), storm size parameters have not been considered in RI schemes (e.g., Rozoff et al. 2015). This might be partly due to the lack of a systematic analysis of the dependency of TC IR on storm structure and size based on observations, and partly due to the lack of accurate measurements of storm size and structure parameters from observations. Note that although the RMW is currently estimated routinely in various ocean basins, the shape parameter for the radial tangential wind profile is not routinely provided in real time in any ocean basin. Nevertheless, results from Xu and Wang (2018b), together with those of Carrasco et al. (2014), Xu and Wang (2015), and Xu and Wang (2018a), strongly suggest that it is important to consider TC size parameters in statistical intensity prediction schemes, and to accurately represent the initial TC structure in numerical prediction models in order to achieve improved TC intensity forecasts (e.g., Kaplan et al. 2015; Bender et al. 2017).

c) **Maximum Potential Intensification Rate (MPIR)**

Since TC intensification and maintenance are controlled by similar physical processes, a natural extension of the MPI concept is the maximum potential intensification rate (MPIR), introduced by Xu et al. (2016). Based on the best track data of NA TCs (Landsea and Franklin 2013), they showed that SST exerts a strong control, not only the MPI, but also on the MPIR, with the latter reflecting the upper bound of IR that a TC can reach given favorable environmental conditions. They constructed an empirical relationship between the MPIR and SST for TCs over the NA based on the best track TC data and observed SSTs during 1988–2014. Similar to the empirical relationship between MPI and SST, the empirically fitted MPIR increases with increasing SST, with a more rapidly increasing trend when SST is higher than 27℃ in the NA (Fig. 26).

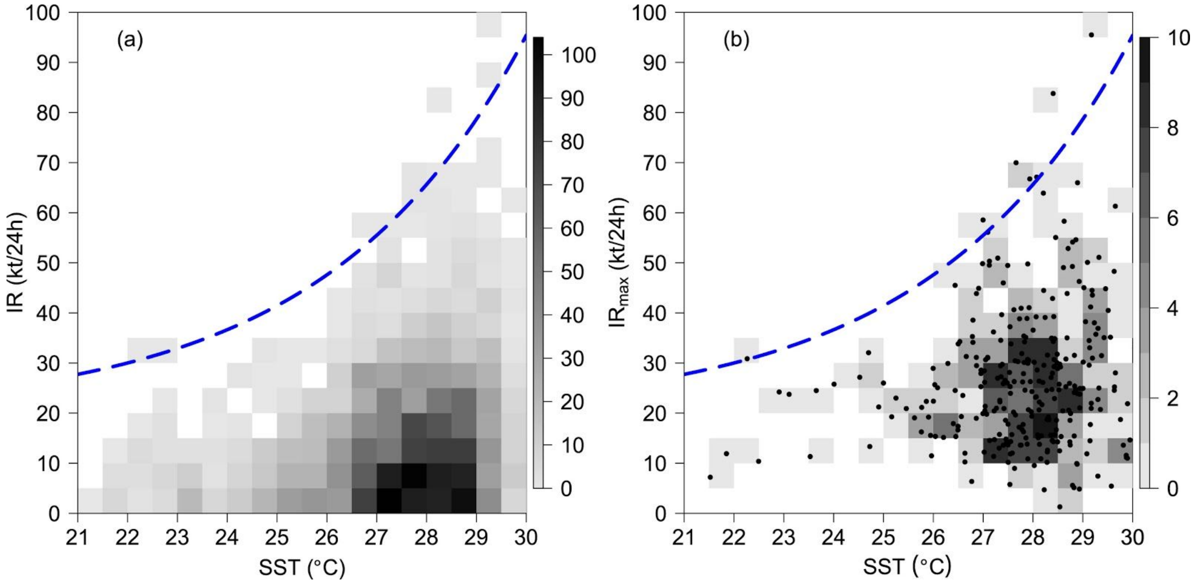

Fig. 26. (a) IR frequency (kt day^{-1}) and (b) lifetime maximum IR (IR_{max}, kt day^{-1}) versus SST (°C) for NA TCs (1988-2014). Also plotted in (b) is the scatter diagram of IR_{max} (dots). Both panels include the empirically fitted MPIR (dashed blue, kt day^{-1}). Figure 3 of Xu et al. (2016).

More recently, Xu and Wang (2018a) also constructed an empirical relationship between the MPIR and SST for WNP TCs. The SST-determined MPIR shows a linear increasing trend of MPIR with increasing SST (for SSTs larger than 26℃). This is roughly consistent with the trend in the same SST range in the NA, although the MPIR–SST relationship in the NA is expressed as an exponential function of SST with a sharp increase when SST is greater than 27℃ (Xu et al. 2016). The empirically fitted MPIR is higher (lower) over SSTs above (below) 28℃ over the WNP than over the NA, which is shown to be related to the weaker (stronger) environmental vertical wind shear (VWS) in regions with higher (lower) SSTs over the WNP than over the NA. Such differences are consistent with the different spatial distributions in the climatological SST and VWS. Results also show that only 10% (5.5%) of intensifying TC cases reached 40% (50%) of their MPIR and about 24% (15%) of TCs' lifetime maximum IR (IR_{max}) reached 50% (60%) of their MPIR, and only 6% reached 80% of their MPIR. Almost all TCs reached their lifetime IR_{max} while experiencing moderate VWS of around 6–10 m s^{-1}. This was especially true for TCs with large IR_{max}, consistent with the well-understood fact that large VWS is generally unfavorable for TC intensification.

The preference of the lifetime IR_{max} to occur in moderate VWS is interesting and as yet, remains unanswered. It could be due to the fact that most TCs reached their lifetime IR_{max} after they reached relatively strong intensity [e.g., over 70 kt (36 m/s)], and thus are able to effectively resist the detrimental effect of moderate VWS. Another possible explanation could be due to the fact that moderate deep-layer VWS is common in the tropics where SST is high (Wang et al. 2015; Finocchio and Majumdar 2017). As a result, SST could dominate VWS in controlling the TC IR under the condition of moderate VWS. Nevertheless, the results provide observational evidence for the existence of the MPIR for TCs, and this suggests that it should be possible to develop a theoretical MPIR. On the other hand, although SST is one of the most important parameters for TC intensification, the relationship between SST and TC IR varies considerably from basin to basin, with SST explaining less than 4% of the variance in TC IRs in the NA, 12% in the WNP, and 23% in the eastern Pacific. Several factors are shown to be responsible for these inter-basin differences. This variation can be explained as smaller horizontal SST gradients in the NA, and SST tends to vary out of phase with VWS and outflow temperature in the WNP (Balaguru et al. 2015; Foltz et.al 2018).

Note that the intensity dependence of IR in observations (Fig. 26a) could be partially contributed by the dependence of IR on SST. Therefore, in a more recent study, Xu and Wang (2018a) discussed the frequency distribution of all intensifying TC cases and also TC cases in specified SST ranges for the intensity dependence of IR for WNP (Fig. 27, a similar result can be obtained for NA TCs, not shown). It confirms that the intensity dependence of IR does not result from the dependence of IR on SST. Furthermore, higher SST corresponds to higher IR and also higher MPIR, which also shifts toward the higher TC intensity side. For the SST above 27°C, the MPIR is the largest for TCs with V_{max} around 60 to 70 knots, which is similar to that observed for NA TCs (Fig. 25a). Note that in these previous studies, emphases have been on the top 95th percentiles because the studies have attempted to reveal the intrinsic IR with minimum negative effects from strong external influences as discussed below. The recent results thus strongly suggest that the intensity dependence of TC IR and the dependence of MPIR on SST are both determined primarily by internal dynamics. However, neither of them can be inferred from the current IR theory.

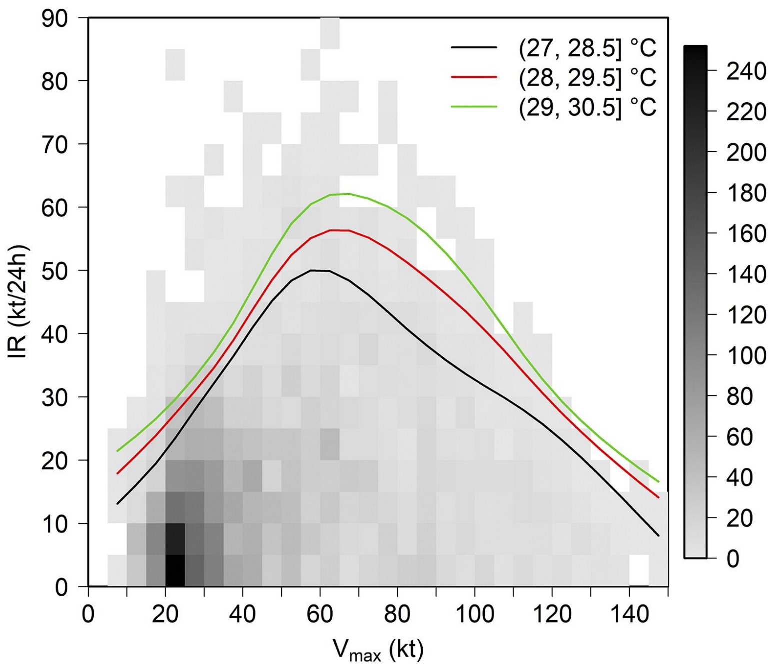

Fig 27. Frequency of TC IRs (kt day^{-1}) against TC intensity (V_{max}, knot) for the WNP TCs (1982-2015). The fitted 95th percentiles as a function of SST for three 1.5℃ intervals of SST starting at 27, 28, and 29℃ are shown as black, red, and green curves, respectively. Note that for the SST ranges given in the legend, "(" means "greater than", "]" means "less than or equal to". Figure 6 of Xu and Wang (2018a).

The empirical MPIR was shown to increase with the SST under the TC, or equivalently, to increase with the MPI of the TC itself, because the MPI is largely determined by SST. Xu et al. (2016) also found that the empirical MPIR depends roughly linearly on the MPI computed from observations. However, the existing IR theory predicts the MPIR as a function of the square of MPI at V_{max} = 0 (Emanuel 2012; Ozawa and Shimokawa 2015). This means that current IR (and MPIR) theory does not adequately reproduce the dependence of the MPIR on TC MPI and TC intensity in observations. The discrepancy in the MPIR dependence on storm intensity between the current theory and observations suggests that some dynamical processes key to TC intensification could be missing in the current theory, or that some assumptions are too restrictive and not suitable for the early intensification stage for which the theory was developed. Motivated by the observed dependence of TC MPIR on storm intensity and MPI, Wang et al. (2016) introduced an energetically-based MPIR theory (unpublished conference presentation). They used the MPI model of Emanuel (2012), and as in Ozawa and Shimokawa (2015), but instead of focusing on the steady-state maximum intensity for which power generation and power dissipation are equal, they examined the unsteady period of intensification when power generation exceeds dissipation (Fig. 28). From this approach, an energy gain rate is obtained, from which the MPIR is found. The new ingredient of their MPIR theory is the introduction of a dynamical efficiency of the Carnot heat engine, which is parameterized as a function of the inner-core inertial stability of the TC based on the best track TC data instead of the constant 70% value used in Ozawa and Shimokawa (2015). Since the energetically-based MPIR theory does not include any detailed dynamics, it is likely that an alternative MPIR theory could be further developed, which could provide useful for the upper bound of TC intensity forecasts. Considerable further research is needed in this area.

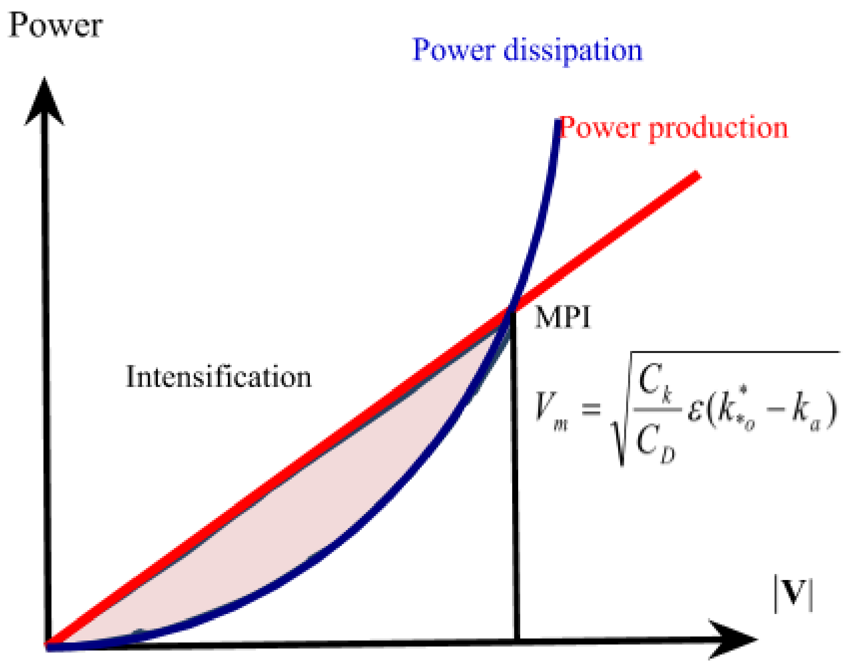

Fig 28. Schematic showing power dissipation (blue curve) and power generation (red curve) as functions of 10-m sustained wind speed in a typical TC. The pink shaded area indicates the power available for the TC to intensify up to its MPI (modified from Wang 2012, 2015).

d) **Role of TC Outflow on Intensity Change**

In recent years, there has been a renewed interest in the role of outflow on TC intensity change. The TC's deep convective mass flux, which is processed through the inner-core region, is then exhausted to the environment at upper tropospheric levels through asymmetric outflow jets. Such jets exist because the TC outflow follows the path of least resistance, which tends to be regions of weak inertial stability (Rappin et al. 2011). Often, either (or both) an equatorward and a poleward jet may exist at some point in the TC life cycle. The linkage of the internally-forced TC outflow with the environment through these jets, and their role in intensity change, has been a subject of recent interest, building on earlier work (e.g., Merrill 1988a,b). Field campaigns have occurred in recent years, obtaining new unique measurements of the upper levels over the TC. The 2012−2014 HS3 (Braun et al. 2016) used an unmanned Global Hawk (GH) aircraft to take long-duration measurements of the outflow and below using both *in-situ* and remote measurements. The TCI (Doyle et al. 2017) used a manned WB-57 aircraft with a new dropwindsonde system to measure the critical outflow region at high horizontal and vertical resolution. Building on HS3, the National Oceanic and Atmospheric Administration (NOAA) Sensing hazards with operational unmanned technology (SHOUT) field campaign was conducted in 2015−2016 using the GH to obtain measurements through the troposphere from the outflow layer to the surface.

The mechanism by which TCs undergo internal intensity change through outflow dynamics is currently not well understood. As evidence of the potential importance of outflow in intensity change, Emanuel (2012)'s modification of WISHE hypothesized that small-scale turbulence in the outflow region can set the outflow temperature and thermal stratification, and thus affect maximum potential intensity and intensity change. Recently, there has been renewed debate on the active versus passive outflow scenarios (Komaromi and Doyle 2018). In the passive scenario, the outflow is a slave to the underlying vortex, and does not feed back to the vortex to affect the intensity change. In the active scenario, upper level forcing can enhance TC outflow, and through secondary circulation changes, affect the intensity change of the low-level vortex. Recent results from idealized modeling suggest that radiative forcing in the outflow may play an important role in TC intensity change (Navarro and Hakim 2016; Navarro et al. 2017). It is expected that as a result of the recent field campaigns described above, new research on understanding the role of outflow on TC intensity change will be obtained in the future.

e) Summary of Emerging Research Topics

Three new emerging topics on internal influences on TC intensity change were discussed. The first topic emphasizes the critical role of vortex structure on the subsequent IR. In particular, the highest IRs are observed to occur in a relatively narrow subrange of the parameter space [i.e., V_{max} ~ 40–60 kt (20.6–30.9 m/s), RMW ~ 20–60 km, AR34 = 200 km, and DR34 = 120 km]. Results strongly suggest that it is important to consider TC size parameters in statistical intensity prediction schemes, and to accurately represent the initial TC structure in numerical prediction models in order to achieve improved TC intensity forecasts. The second topic seeks to understand the factors setting the upper bound on the IR (the MPIR) using observational and theoretical approaches based on energetics. The TC intensity, SST, and MPI all appear to be important, but the current theory is inadequate to fully explain the MPIRs of observed TCs. The final topic emphasizes the possible role of TC outflow on the IR, and whether active or passive outflow is a dominant factor. In closing this subsection, we recommend that substantial future research further investigate the broad theoretical and numerical basis for ideas such as the MPIR of TCs and the relationship between vortex structure (including the outflow) and IR.

3.1.9 Overall Summary and Conclusions

This report summarizes approximately 177 peer-reviewed publications during the 2014–2018 period to assess progress in understanding of internal influences on TC intensity change. The subject of internal influences on intensity change covers a wide range of dynamical and physical aspects, ranging from the role of rainbands, shallow convection, CBs, ERCs to aspects of inner core instability and mixing, and surface fluxes. This report also includes special sections on RI and intensification mechanisms, as well as several new topics that have recently emerged, such as the role of TC outflow, the role of vortex structure on a TC's IR, and a new theory for what sets the fastest rate at which TCs may intensify. A brief overview of the developments in each of these areas is now given.

The issue of RI has been a considerable focus of researchers in the past few years, with 60 publications touching on this topic. One aspect that has recently received more appreciation is on how the definition of RI impacts the framing of the study. While many statistical studies have used a case-based definition [e.g., a 30 kt (15.4 m/s) increase in intensity in 24 h], it has recently been recognized that RI is an *event* which can last up to 78 h or longer. Thus, it is important to study the various stages of an RI event to learn more about what types of structures and dynamical processes are involved in initiating, sustaining, and terminating RI in TCs. Recent work has bolstered earlier findings that increased and widespread shallow convection around the storm center is a first indication of RI and can be used as a predictor for the onset of RI. A common theme among many observational satellite-based studies is that a high degree of axisymmetry is associated with the subsequent RI, however other case studies using aircraft observations and numerical simulations have recognized asymmetric pathways to RI, with inner core CBs and HTs recognized as important factors. Recent studies using lightning data have resulted in new understanding through detailed analysis of the radial and azimuthal distribution and movement of CBs before and during RI. Despite extensive research on the RI topic, many uncertainties remain regarding how to better simulate and predict the onset and continuation of RI.

SEFs and ERCs have long been recognized as important modulators of TC intensity change. By 2014, observational studies had established the basic climatological understanding of ERC influences on intensity change. Since 2014, the climatological understanding of ERCs has been updated to provide additional details on the wind-pressure-relationship, recognizing distinctly different behaviors between less intense and more intense TCs. This improved climatological knowledge has recently been applied to operational forecasting via the E-SHIPS statistical model. New studies have also increased understanding of non-canonical ERC events, such as those in which there are only subtle intensity changes. The increasing capability of numerical models to simulate ERCs, both in idealized and operational settings, has lead to new appreciation of the dynamical processes and associated uncertainties with respect to: the onset time of SEF and ERC, the location and contraction speed of the outer eyewall, the dissipation (intensification) rate of the inner (outer) eyewall, and the duration of ERC events. While accurate deterministic predictions of the impact of ERCs remain elusive, the improved understanding that has resulted from these various lines of investigation is leading to more accurate intensity forecasts through techniques such as E-SHIPS.

Spiral rainbands comprise a major portion of the TC and their structural characteristics play significant roles in TC structure and intensity change. Recent observational work has found that outer rainband lightning is positively correlated with subsequent 24-h TC intensity change. Idealized numerical simulations have demonstrated that convective heating in the inner rainband region generally promotes intensification, while stratiform cooling in inner rainbands tends to hinder TC intensification. Evaporation of raindrops in the outer rainband region tends to suppress the final TC intensity, but these effects are not significant in inner rainbands. Despite these advances, considerable uncertainties still remain in the understanding of the interactions between spiral rainband behavior (particularly microphysical processes within rainbands) and other TC components, and how these interactions affect TC intensity change.

Recent work has extended numerical analyses of inner core instability processes from 2D barotropic frameworks to more realistic 3D frameworks that include moisture and parameterized mass sinks. Whereas, barotropic instability in a 2D framework leads to deepening of the pressure deficit but a decrease in intensity, results from simulations in more realistic frameworks show that instability processes may cause intensification under certain assumptions. Considerable uncertainty remains as to whether the secondary circulation prevents relaxation of the vortex to a monopole (or how quickly it might restore the vortex back to an annular state) and as to the effects of moist convective processes on instability. Additional studies examined other types of instabilities caused by spontaneous IG radiation fromi VR waves. More work is needed to understand the longer-term and nonlinear effects of VR-IG instability on the vortex evolution. Because the PV structure is critical in understanding the vortex state (annular vs. monopole) during instability mixing events, future research should consider observational strategies to better assess the PV structure of TCs.

Surface fluxes play an essential role in providing latent heat to the TC core where energy is converted into kinetic energy, as well as in dissipating kinetic energy through friction. As a result, TCs are largely controlled by surface enthalpy and momentum fluxes. Advances in both modeling and observing surface fluxes have improved our understanding of the relationships between TC intensification and the drag and enthalpy coefficients, as well with the SST response. In particular, recent work suggests that the wind-speed dependence of the drag coefficient, with a minimum near 60 m s^{-1}, may partially explain why many TCs intensify rapidly between 35 and 60 m s^{-1}, but tend to weaken soon after reaching Category 5 intensity. Despite progress over the last four years, considerable uncertainties still remain and the research advancements still need to be transitioned to operations.

The mechanisms by which TCs intensify has been a hotly debated area of research. From the first descriptions of TC intensification frameworks more than 60 years ago, the community has seen various major frameworks arise, such as the CISK framework (involving cooperation between convection and the vortex scale), the WISHE mechanism (wind-induced surface heat exchange), the balanced, symmetric mechanism, and most recently, the rotating convection framework (rotating small-scale convection in conjunction with boundary layer spin-up). Many of these frameworks have built upon previous frameworks, adding refinements or descriptions of new intensification mechanisms that operate in conjunction with previously-described mechanisms. Nevertheless, vigorous debate is still occurring as to the suitability of using balanced frameworks to understand intensification, whether or not WISHE is an essential part of TC intensification, and the exact role of the boundary layer in TC spin-up. Despite more than 40 additional studies on intensification mechanisms in this period, very considerably uncertainty remains.

This report also covered three new emerging topics on internal influences on TC intensity change. The first topic emphasizes the critical role of vortex structure on the subsequent IR. Through analyzing past observed TCs, as well as numerical simulations, the phase space of IR dependence on initial intensity, SST, RMW, and size was explored. These results showed that the fastest IRs occurred in a relatively narrow subrange of the parameter phase space at relatively low initial intensities and small to modest vortex scales [i.e., V_{max} ~ 40–60 kt (20.6–30.9 m/s), RMW ~ 20–60 km, AR34 = 200 km, and DR34 = 120 km]. This finding has motivated development of new ideas on the factors that set the upper bound on the IR (the MPIR) from an energetics perspective. The third topic emphasizes the possible role of TC outflow on the IR, and whether active or passive outflow is a dominant factor.

In conclusion, significant advances in understanding of internal influences on TC intensity change have been made over the past four years. With several notable exceptions, these advances have been largely incremental, and have been spurred by new observations, more sophisticated numerical simulation approaches, and through new lines of theoretical development. Below, we offer recommendations for new research directions and strategies that might be undertaken to make even more rapid progress in the coming years.

3.1.10 Recommendations

A number of recommendations have been made by the WG, as follows:

1. *We recommend that future research directions focus on: a) studying RI as an event (rather than a 24-h case-based RI definition), b) improving understanding of the conditions and precursors to RI through symmetrical processes, and c) reconciling seemingly conflicting findings on the conditions and processes in which asymmetric inner-core CBs and HTs may lead to RI precursors.*
2. *Continued advancements and diagnostics and testing activities are needed in NWP models to improve the accuracy of SEF and ERC event timing and the associated intensity changes. We recommend that such efforts incorporate non-standard evaluation metrics beyond track, intensity, and wind structure, such as the explicit prediction of eyewall and secondary eyewall structure.*
3. *We recommend that specific, targeted observational and modeling investigations be undertaken to better understand interactions between spiral rainbands and their parent TCs and the specific mechanisms by which rainbands influence TC intensity.*
4. *Because the PV structure is critical in understanding the vortex state (annular vs. monopole) during instability mixing events, we recommend that future research consider observational strategies to better assess the PV structure of TCs. We also recommend that structure databases include observable markers of mixing processes (eyewall mesovortices and polygonal or elliptical eyewall structures as seen in satellite imagery and radar imagery). In general, researchers would benefit from mesoscale analyses of well-observed cases.*
5. *Advances in both modeling and observing surface fluxes have improved our understanding of the relationships between TC intensification and the drag and enthalpy coefficients, as well as the SST response, however considerable uncertainties still remain. We recommend that new observational platforms be devised and routinely deployed to continue advancing understanding of surface fluxes, and that the resulting knowledge be transitioned to operations.*
6. *Much recent work has been undertaken on intensification mechanisms, however considerable knowledge gaps remain as to the role of different mechanisms. In particular, the role of the boundary layer dynamics in contributing to eyewall updrafts and convection, as well as in supergradient spin-up, needs to be investigated in future studies based on observations and numerical simulations. To speed up progress in reconciling current debates, we recommend that scientists with competing theories and frameworks team up together in a larger collaborative effort to resolve long-standing debates. We recommend that funding agencies recognize this potential approach and design funding calls specifically toward this purpose.*
7. *We further recommend that WMO sponsor an international workshop in the near future to bring leading researchers together to review in more detail the issues involved in the controversy on intensification mechanisms and to develop a strategy for future international research collaboration to resolve these issues.*
8. *In light of substantial new lines of investigation on the role of vortex structure, outflow, and other environmental influences on the IR of TCs, we recommend that substantial future research further investigate the broad theoretical and numerical basis for ideas such as the MPIR of TCs and the relationship between vortex structure (including the outflow) and IR.*
9. *With the finding that the TC IR depends critically on the structure of the vortex, we further recommend that statistical-dynamical intensity prediction schemes*

consider TC size parameters and that significant efforts continue to be made to ensure that numerical prediction models represent the initial TC structure as accurately as possible.

Primary contributors to each section:

This report would not have been possible without the diligent work and substantial contributions of the WG members. Following is a list of the primary contributors to each main section of the report. For each section, WG members are listed in author-order by the degree to which they contributed to writing and editing.

3.1.2 Rapid Intensification
Haiyan Jiang (Team Lead)
Ryo Oyama
Olivier Bousquet
Jonathan Vigh (assistance)

3.1.3 Eyewall Replacement Cycles
Yi-Hsuan Huang (Team Lead)
Kristen L. Corbosiero
Jonathan Vigh (assistance)
Jeff Kepert

3.1.4 Relation of Rainbands to Intensity Change
Qingqing Li (Team Lead)
Kristen L. Corbosiero
Michael Bell
Jonathan Vigh (assistance)
Christopher Slocum

3.1.5 Eyewall Instability and Inner-Core Mixing
Konstantinos Menelaou (Team Lead)
Jonathan Vigh (assistance)

3.1.6 Relationship between Surface Fluxes and Intensity Change
Yoshiaki Miyamoto (Team Lead)
Christopher Slocum
Jeff Kepert
Jonathan Vigh (assistance)

3.1.7 Mechanisms of Tropical Cyclone Intensification
Roger Smith
Christopher Slocum
Rochelle Coronel
Eric Hendricks
Jonathan Vigh (Team Lead)

3.1.8 New and Emerging Research Topics
Yuqing Wang
Jing Xu
Eric Hendricks
Jonathan Vigh (Team Lead)

Acknowledgments:

We are grateful to Chun-Chi (Maggie) Lien (National Taiwan University) for creating the list of 3417 papers that have published on tropical cyclones since 2014. We also thank her for sharing a detailed explanation of the technique that was used to create this list.

Acronyms used in the report:

AAM – Absolute angular momentum
AGM – Atmospheric general circulation model
AMV – Atmospheric Motion Vector
ANHM – Atmospheric Nonhydrostatic Model
ARCHER – Automated Rotational Center Hurricane Eye Retrieval
AR34 – Average 34-kt wind radius
ARW – Advanced Research WRF
ATCF – Automated Tropical Cyclone Forecast (ATCF) system
CAPE – Convective available potential energy
CB – Convective burst
CIMSS – Cooperative Institute for Meteorological Satellite Studies
CISK – Conditional instability of the second kind
CM1 – Cloud-resolving Model 1
CPS – Convective precipitation shield
CReSS-NHOES – Cloud Resolving Storm Simulator-Non-Hydrostatic Ocean model for the Earth Simulator
DR34 – outer-core wind skirt parameter (DR34 = AR34 - RMW)
EBT – Extended best track
ECP – Eastern and Central Pacific
ERC – Eyewall replacement cycle
GFS – Global Forecast System
GH – Global Hawk
GSMaP – Global Satellite Mapping of Precipitation
HURDAT2 – Hurricane database
HS3 – Hurricanes and Severe Storms Sentinel
HT – Hot tower
HWRF – Hurricane Weather Research and Forecasting
IG – Inertia-gravity
IR – Intensification rate
ITOP – Impact of Typhoons on the Ocean
IWTC – International Workshop on Tropical Cyclones
JMA – Japan Meteorological Agency
JTWC – Joint Typhoon Warning Center
MAE – Mean absolute error
MERRA – Modern Era Retrospective-analysis for Research and Applications
MI – Microwave imagery
M-PERC – Microwave-Based Probability of Eyewall Replacement Cycle
MPI – Maximum potential intensity
MPIR – Maximum potential intensification rate
NHC – National Hurricane Center
NHM – Nonhydrostatic model
NI – Non-intensifying
NIO – North Indian Ocean
NA – North Atlantic

NASA – National Aeronautics and Space Administration
NOAA – National Oceanic and Atmospheric Administration
OHC – Ocean heat content
ONR – Office of Naval Research
PBL – Planetary boundary layer
PI – Potential intensity
POD – Probability of detection
PR – Precipitation radar
PV – Potential vorticity
PVB – Positive vorticity band
RI – Rapid intensification
RMC – Radius of maximum convergence
RMW – Radius of maximum winds
RSME – Root mean squared error
RW – Rapid weakening
ROCI – Radius of outermost closed isobar
SCAPE – Slantwise convective available potential energy
SEF – Secondary eyewall formation
SHIPS – Statistical Hurricane Intensity Prediction System
S-RMW – Steady-state radius of maximum winds
SHOUT – Sensing Hazards with Operational Unmanned Technology
SST – Sea surface temperature
SVM – Support vector machine
SW – Shallow water
SWIO – Southwest Indian Ocean
TC – Tropical cyclone
TCHP – Tropical cyclone heat potential
TCI – Tropical Cyclone Intensity
TIL – Tropopause inversion layer
TRMM – Tropical Rainfall Measurement Mission
VMAX – Maximum sustained wind near surface
VR – Vortex Rossby
VRW – Vortex Rossby wave
VWS – Vertical wind shear
WG – Working Group
WISHE – Wind Induced Surface Heat Exchange
WMO – World Meteorological Organization
WNP – Western North Pacific
WPR – Wind pressure relationship
WRF – Weather Research and Forecasting
WWLLN – World Wide Lightning Location Network

References:

Abarca, S. F., and M. T. Montgomery, 2015: Are eyewall replacement cycles governed largely by axisymmetric balance dynamics? *J. Atmos. Sci.*, **72**, 82–87, doi:10.1175/JAS-D-14-0151.1.

Alvey III, G., J. Zawislak, and E. J. Zipser, 2015: Precipitation properties observed during tropical cyclone intensity change. *Mon. Wea. Rev.*, **143**, 4476–4492, doi:10.1175/MWR-D-15-0065.1.

Andreas, E. L., L. Mahrt, and D. Vickers, 2015: An improved bulk air-sea surface flux algorithm, including spray-mediated transfer. *Q. J. R. Meteorol. Soc.*, **141**, 642-654, doi:10.1002/qj.2424.

Balaguru, K., G. R. Foltz, L. R. Leung, E. D'Asaro, K. A. Emanuel, H. Liu, and S. E. Zedler, 2015: Dynamic Potential Intensity: An improved representation of the ocean's impact on tropical cyclones. *Geophys. Res. Lett.,* **42**, 6739–6746, doi:10.1002/2015GL064822.

Bao, J., G.Gopalakrishnan, S. G. Michelson, and M. T. Montgomery, 2012: Impact of physics representations in the HWRFX on simulated hurricane structure and pressure–wind relationships. *Mon. Wea. Rev.*, **140**, 3278–3299, doi:10.1175/MWR-D-11-00332.1.

Bell, M. M. and M. T. Montgomery, 2008: Observed structure, evolution, and potential intensity of category 5 Hurricane Isabel (2003) from 12 to 14 September. *Mon. Wea. Rev.,* **136,** 2023-2046, 10.1175/2007MWR1858.1.

Bell, M. M., M. T. Montgomery, and W.-C. Lee, 2012: An axisymmetric view of concentric eyewall evolution in Hurricane Rita (2005). *J. Atmos. Sci.,* **40,** 2414-2432, 10.1175/JAS-D-11-0167.1.

Bender, M. A., T. P. Marchok, C. R. Sampson, J. A. Knaff, and M. J. Morin, 2017: Impact of storm size on prediction of storm track and intensity usi ng the 2016 operational GFDL hurricane model. *Wea. Forecasting*, **32**, 1491–1508 , doi:10.1175/WAF-D-16-0220.1

Bovalo, C., C. Barthe, N. Yu, and N. Begue, 2014: Lightning activity within tropical cyclones in the South West Indian Ocean. *J. Geophys. Res.-Atmos.*, **11**9, doi:10.1002/2014JD021651.

Braun, S. A., P. A. Newman, and G. M. Heymsfield, 2016: NASA' Hurricane and Severe Storm Sentinel (HS3) Investigation. *Bull. Amer. Meteorol. Soc.*, **97**, 2085–2102, doi:10.1175/BAMS-D-15-00186.1.

Brown, B. R., M. M. Bell, and A. Frambach, 2016: Validation of simulated hurricane drop size distributions using polarimetric radar. *Geophys. Res. Lett.*, **43**, doi:10.1002/2015GL067278.

Bui, H. H., R. K. Smith, M. T. Montgomery, and J. Y. Peng, 2009: Balanced and unbalanced aspects of tropical cyclone intensification. *Q. J. Roy. Meteor. Soc.*, **135**, 1715–1731, doi: 10.1002/qj.502.

Carrasco, C. A., C. W. Landsea, and Y. L. Lin, 2014: The influence of tropical cyclone size on its intensification. *Wea. Forecasting*, **29**, 582–590, doi:10.1175/WAF-D-13-00092.1.

Chan, K. T. F., and J. C. L. Chan: 2016: Sensitivity of the simulation of tropical cyclone size to microphysics schemes. *Adv. Atmos. Sci.*, **33**, 1024–1035, doi:10.1007/s00376-016-5183-2.

Chang, C.-C., and C.-C. Wu, 2017: On the processes leading to the rapid intensification of Typhoon Megi (2010). *J. Atmos. Sci.*, **74**, 1169–1200, doi:10.1175/JAS-D-16-0075.1.

Charney, J.G. and A. Eliassen, 1964: On the Growth of the Hurricane Depression. *J. Atmos. Sci.*, **21**, 68–75, doi:10.1175/1520-0469(1964)021<0068:OTGOTH>2.0.CO;2.

The COMET Program (2013), Introduction to Tropical Meteorology, 2nd ed., Chap 8: Tropical Cyclones, Univ. Corp. for Atmos. Res., Boulder, Colo. [Available at http://www.meted.ucar.edu/training_module.php?id5868.]

Chavas, D. R., 2017: A simple derivation of tropical cyclone ventilation theory and its application to capped surface entropy fluxes. *J. Atmos. Sci.*, **74**, 2989-2996, doi:10.1175/JAS-D-17-0061.1.

Chen, G., C.-C. Wu, and Y.-H. Huang, 2018a: The role of near-core convective and stratiform heating/cooling in tropical cyclone structure and intensity. *J. Atmos. Sci.,* **75**, 297–326, doi:10.1175/JAS-D-17-0122.1.

Chen, H., and S. G. Gopalakrishnan, 2015: A study on the asymmetric rapid intensification of Hurricane Earl (2010) using the HWRF system. *J. Atmos. Sci.*, **72**, 531–550, doi:10.1175/JAS-D-14-0097.1.

Chen, S., R. L. Elsberry, and P. A. Harr, 2017: Modeling interaction of a tropical cyclone with its cold wake. *J. Atmos. Sci.*, **74**, 3981-4001, doi:10.1175/JAS-D-16-0246.1.
Chen, X.-M., Y. Wang, and K. Zhao, 2015: Synoptic flow patterns and large-scale characteristics associated with rapidly intensifying tropical cyclones in South China Sea. *Mon. Wea. Rev.*, **143**, 64–87, doi:10.1175/MWR-D-13-00338.1.
Chen, X., Y. Wang, J. Fang, and M. Xue, 2018b: A numerical study on rapid intensification of Typhoon Vicente (2012) in the South China Sea. Part II: Roles of inner-core processes. *J. Atmos. Sci.*, **75**, 235–255, doi:10.1175/JAS-D-17-0129.1.
Cheng, C.-J., and C.-C. Wu, 2018: The role of WISHE in secondary eyewall formation. *J. Atmos. Sci.*, **75**, 3823–3841, doi:10.1175/JAS-D-17-0236.1.
Coronel, R., M. Sawada, and T. Iwasaki, 2016: Impacts of surface drag coefficient and planetary boundary layer schemes on the structure and energetics of Typhoon Megi (2010) during Intensification. *J. Meteorol. Soc. Japan*, **94**, 55-73, doi:10.2151/jmsj.2016-004.
DeMaria, M., M. Mainelli, L. K. Shay, J. A. Knaff, and J. Kaplan, 2005: Further improvements to the Statistical Hurricane Intensity Prediction Scheme (SHIPS). *Wea. Forecasting*, **20**, 531–543, doi:10.1175/WAF862.1.
DeMaria, M., R. T. DeMaria, J. A. Knaff, and D. Molenar, 2012: Tropical cyclone lightning and rapid intensity change. *Mon. Wea. Rev.,* **140**, 1828–1842, doi: 10.1175/MWR-D-11-00236.1.
Didlake, A. C., P. D. Reasor, R. F. Rogers, and W.-C. Lee, 2018: Dynamics of the transition from spiral rainbands to a secondary eyewall in Hurricane Earl (2010). *J. Atmos. Sci.*, **75**, 2909–2929, doi:10.1175/JAS-D-17-0348.1.
Dougherty, E. M., J. Molinari, R. F. Rogers, J. A. Zhang, and J. P. Kossin, 2018: Hurricane Bonnie (1998): Maintaining intensity during high vertical wind shear and an eyewall replacement cycle. *Mon. Wea. Rev.*, **146**, 3383–3399, doi:10.1175/MWR-D-18-0030.1.
Doyle, J. D., J. R. Moskaitis, J. W. Feldmeier, R. J. Ferek, M. Beaubien, M. M. Bell, D. L. Cecil, R. L. Creasey, P. Duran, R. L. Elsberry, W. A. Komaromi, J. Molinari, D. R. Ryglicki, D. P. Stern, C. S. Velden, X. Wang, T. Allen, B. S. Barrett, P. G. Black, J. P. Dunion, K. A. Emanuel, P. A. Harr, L. Harrison, E. A. Hendricks, D. Herndon, W. Q. Jeffries, S. J. Majumdar, J. A. Moore, Z. Pu, R. F. Rogers, E. R. Sanabia, G. J. Tripoli, and D. Zhang, 2017: A view of tropical cyclones from above: The Tropical Cyclone Intensity Experiment. *Bull. Amer. Meteor. Soc.*, **98**, 2113–2134, doi:10.1175/BAMS-D-16-0055.1.
Duran, P., and J. Molinari, 2018: Dramatic inner-core tropopause variability during the rapid intensification of Hurricane Patricia (2015). *Mon. Weather Rev.*, **146**, 119–134, doi:10.1175/MWR-D-17-0218.1.
Eliassen, A, 1951: Slow thermally or frictionally controlled meridional circulation in a circular vortex. *Astrophys. Norv.*, **5**, 19–60.
Ekman, V. W., 1905: On the influence of the Earth's rotation on ocean-currents. *Arch. Math. Astron.Phys.*, **2**, 1-52.
Emanuel, K.A., 1986: An air-sea interaction theory for tropical cyclones. Part I: Steady-state maintenance. *J. Atmos. Sci.*, **43**, 585–605, doi:10.1175/1520-0469(1986)043<0585:AASITF>2.0.CO;2.
Emanuel, K. A., 1989: The finite-amplitude nature of tropical cyclogenesis. *J. Atmos. Sci.*, **46**, 3431–3456, doi:10.1175/1520-0469(1989)046,3431:TFANOT.2.0.CO;2.
Emanuel, K. A., 1991: The theory of hurricanes. *Ann. Rev. Fluid Mech.*, **23**, 179-196.
Emanuel, K. A., 1997: Some aspects of hurricane inner-core dynamics and energetics. *J. Atmos. Sci.*, **54**, 1014–1026, doi:10.1175/1520-0469(1997)054<1014:SAOHIC>2.0.CO;2.
Emanuel K. A., 2004: Tropical cyclone energetics and structure, atmospheric turbulence and mesoscale meteorology, E. Fedorovich, R. Rotunno and B. Stevens, eds., Cambridge University Press, 280 pp.

Emanuel, K. A., 2012: Self-stratification of tropical cyclone outflow. Part II: Implications for storm intensification. *J. Atmos. Sci.*, **69**, 988–996, doi:10.1175/JAS-D-11-0177.1.
Fang, J., and F. Zhang, 2012: Effect of beta shear on simulated tropical cyclones. *Mon. Wea. Rev.*, **140**, 3327–3346, doi:10.1175/MWR-D-10-05021.1.
Fierro, A. O., S. N. Stevenson, and R. M. Rabin, 2018: Evolution of GLM-observed total lightning in Hurricane Maria (2017) during the period of maximum intensity. *Mon. Wea. Rev.* **146**, 1641–1666, doi:10.1175/MWR-D-18-0066.1.
Finocchio, P. M. and S. J. Majumdar, 2017: A statistical perspective on wind profiles and vertical wind shear in tropical cyclone environments of the Northern Hemisphere. *Mon. Wea. Rev.*, **145**, 361–378, doi:10.1175/MWR-D-16-0221.1
Fischer, M. S., B. H. Tang, K. L. Corbosiero, and C. M. Rozoff, 2018: Normalized convective characteristics of tropical cyclone rapid intensification events in the North Atlantic and eastern North Pacific. *Mon. Wea. Rev.*, **146**, 1133–1155, doi:10.1175/MWR-D-17-0239.1.
Foltz, G. R., K. Balaguru, and S. Hagos, 2018: Interbasin differences in the relationship between SST and tropical cyclone Intensification. *Mon. Wea. Rev.*, **146**, 853–870, doi:10.1175/MWR-D-17-0155.1.
Fudeyasu, H., and Y. Wang, 2011: Balanced contribution to the intensification of a tropical cyclone simulated in TCM4: Outer-core spinup process. *J. Atmos. Sci.*, **68**, 430–449, doi:10.1175/2010JAS3523.1.
Gao, S., S. N. Zhai, B. Q. Chen, and T. Li, 2017: Water budget and intensity change of tropical cyclones over the western North Pacific. *Mon. Weather Rev.*, **145**, 3009–3023, doi:10.1175/MWR-D-17-0033.1.
Ge, X., 2015: Impacts of environmental humidity on concentric eyewall structure. *Atmos. Sci. Lett.*, **16**, 273–278, doi:10.1002/asl2.553.
Ge, X., L. Guan, and S. Zhou, 2016: Impacts of initial structure of tropical cyclones on secondary eyewall formation. *Atmos. Sci. Lett.*, **17**, 569-574, doi:10.1002/asl.707.
Green, B. W. and F. Q. Zhang, 2014: Sensitivity of tropical cyclone simulations to parametric uncertainties in air-sea fluxes and implications for parameter estimation. *Mon. Weather Rev.*, **142**, 2290-2308, doi:10.1175/MWR-D-13-00208.1.
Griffin, S. M., 2017: Climatology of tropical overshooting tops in North Atlantic tropical cyclones. *J. Appl. Meteorol. Climatol.,* **56**, 1783–1796, doi:10.1175/JAMC-D-16-0413.1.
Grimes, A., and A. Mercer, 2015: Synoptic-scale precursors to tropical cyclone rapid intensification in the Atlantic Basin. *Adv. Meteorology,* 814043, 16 pp, doi:10.1155/2015/814043.
Guan, L., and X. Ge, 2018: How does tropical cyclone size affect the onset timing of secondary eyewall formation? *J. Meteorol. Res.*, **32**, 124–134, doi:10.1007/s13351-018-7023-z.
Guimond, S. R., G. M. Heymsfield, P. D. Reasor, and A. C. Didlake Jr, 2016: The rapid intensification of Hurricane Karl (2010): New remote sensing observations of convective bursts from the Global Hawk platform. *J. Atmos. Sci.*, **73**, 3617–3639, doi:10.1175/JAS-D-16-0026.1.
Guo, X., and Z.-M. Tan (2017), Tropical cyclone fullness: A new concept for interpreting storm intensity, *Geophys. Res. Lett.*, **44**, 4324–4331, doi:10.1002/2017GL073680.
Harnos, D., and S. W. Nesbitt, 2016: Passive microwave quantification of tropical cyclone inner-core cloud populations relative to subsequent intensity change. *Mon. Weather Rev.*, **144**, 4461–4482, doi:10.1175/MWR-D-15-0090.1.

Harnos, D. S., and S. W. Nesbitt, 2016a: Varied pathways for simulated tropical cyclone rapid intensification. Part I: Precipitation and environment. *Q. J. Roy. Meteor. Soc.*, **142**, 1816–1831, doi:10.1002/qj.2780.
Harnos, D. S., and S. W. Nesbitt, 2016b: Varied pathways for simulated tropical cyclone rapid intensification. Part II: Vertical motion and cloud populations. *Q. J. Roy. Meteor. Soc.,* **142**, 1832–1846, 10.1002/qj.2778.
Haurwitz, B., 1935: On the change of the wind with elevation under the influence of viscosity in curved air currents. *Gerlands Beitr. Geophys.*, **45**, 243-267.
Haurwitz, B., 1936: Supplementary to: On the change of the wind with elevation under the influence of viscosity in curved air currents. *Gerlands Beitr. Geophys.*, **47**, 203-205.
Hazelton, A. T., L. Harris, and S.-J. Lin, 2018: Evaluation of tropical cyclone structure forecasts in a high-resolution version of the multiscale GFDL fvGFS model. *Wea. Forecasting*, **33**, 419–442, doi:10.1175/WAF-D-17-0140.1.
Hendricks, E. A., M. S. Peng, B. Fu, and T. Li, 2010: Quantifying environmental control on tropical cyclone intensity change. *Mon. Wea. Rev.*, **138**, 293–344, doi:10.1175/2009MWR3185.1.
Hendricks, E. A., B. D. McNoldy, and W. H. Schubert, 2012: Observed inner-core structural variability in hurricane Dolly (2008). *Mon. Wea. Rev.*, **140**, 4066–4077, doi:10.1175/MWR-D-12-00018.1.
Hendricks, E. A., and W. H. Schubert, Y.-H. Chen, H.-C. Kuo, and M. S. Peng, 2014: Hurricane eyewall evolution in a forced shallow-water model. *J. Atmos. Sci.*, **71**, 1623–1643, doi:10.1175/JAS-D-13-0303.1.
Heng, J., and Y. Wang, 2016a: Nonlinear response of a tropical cyclone vortex to prescribed eyewall heating with and without surface friction in TCM4: Implications for tropical cyclone intensification. *J. Atmos. Sci.*, **73**, 1315–1333, doi:10.1175/JAS-D-15-0164.1.
Heng, J., and Y. Wang, 2016b: Reply to "Comments on 'Nonlinear response of a tropical cyclone vortex to prescribed eyewall heating with and without surface friction in TCM4: Implications for tropical cyclone intensification.' " *J. Atmos. Sci.*, **73**, 5105–5109, doi:10.1175/JAS-D-16-0262.1.
Heng, J., Y. Wang, and W. Zhou, 2017: Revisiting the balanced and unbalanced aspects of tropical cyclone intensification. *J. Atmos. Sci.*, **74**, 2575–2591, doi:10.1175/JAS-D-17-0046.1.
Heng, J., Y. Wang, and W. Zou, 2018: Reply to "Comments on 'Revisiting the Balanced and Unbalanced Aspects of Tropical Cyclone Intensification' ". *J. Atmos. Sci.* **75**, 2497–2505, doi:10.1175/JAS-D-18-0020.1.
Hill, K. A., and G. M. Lackmann, 2009: Influence of environmental humidity on tropical cyclone size. *Mon. Wea. Rev.*, **137**, 3294–3315, doi:10.1175/2009MWR2679.1.
Houze, R. A., 2010: Clouds in tropical cyclones. *Mon. Wea. Rev.,* **138**, 293–344, doi:10.1175/2009MWR2989a.1.
Huang, Y.-H., M. T. Montgomery, and C.-C. Wu, 2012: Concentric eyewall formation in Typhoon Sinlaku (2008). Part II: Axisymmetric dynamical processes. *J. Atmos. Sci.*, **69**, 662–674, doi:10.1175/JAS-D-11-0114.1.
Jaimes, B., Shay, L.K., and E. W. Uhlhorn, 2015: Enthalpy and Momentum Fluxes during Hurricane Earl Relative to Underlying Ocean Features. *Mon. Weather Rev.*, **143**, 111-131, doi:10.1175/MWR-D-13-00277.1.
Jiang, H., 2012: The relationship between tropical cyclone rapid intensification and the strength of inner-core convection. *Mon. Wea. Rev*., **140**, 1164–1176, doi:10.1175/MWR-D-11-00134.1.
Jiang, H., and E. M. Ramirez, 2013: Necessary conditions for tropical cyclone rapid intensification as derived from 11 years of TRMM data. *J. Climate*, **26**, 6459–6470, doi:10.1175/JCLI-D-12-00432.1.

Jiang, H., J. P. Zagrodnik, C. Tao, and E. J. Zipser 2018: Classifying precipitation types in tropical cyclones using the NRL 37 GHz color product. *J. Geophys. Res.*, **123**, 5509–5524, doi:10.1029/2018JD028324.
Judt, F., and S. S. Chen, 2016: Predictability and dynamics of tropical cyclone rapid intensification deduced from high-resolution stochastic ensembles. *Mon. Wea. Rev.*, **144**, 4395–4420, doi:10.1175/MWR-D-15-0413.1.
Jullien, S. P. Marchesiello, C. E. Menkes, J. Lefevre, N. C. Jourdain, G. Samson, and M. Lengaigne, 2014: Ocean feedback to tropical cyclones: climatology and processes. *Clim. Dyn.*, **43**, 2831-2854, doi:10.1007/s00382-014-2096-6.
Kanada, S., and A. Wada, 2015: Numerical study on the extremely rapid intensification of an intense tropical cyclone: Typhoon Ida (1958). *J. Atmos. Sci.*, **72**, 4194–4217, doi:10.1175/JAS-D-14-0247.1.
Kanada, S, S. Tsujino, H. Aiki, M. K. Yoshioka, Y. Miyazawa, K. Tsuboki, and I. Takayabu, 2017: Impacts of SST patterns on rapid intensification of Typhoon Megi (2010). *J. Geophys. Res.-Atmos.*, **122**, 13245-13262, doi:10.1002/2017JD027252.
Kanada, S., and A. Wada, 2017: Different climatological characteristics, inner-core structures, and intensification processes of simulated intense tropical cyclones between 20-km global and 5-km regional models. *J. Climate*, **30**, 1583–1603, doi:10.1175/JCLI-D-16-0093.1.
Kaplan, J., and M. DeMaria, 2003: Large-scale characteristics of rapidly intensifying tropical cyclones in the North Atlantic basin. *Wea. Forecasting*, **18**, 1093–1108, doi:10.1175/1520-0434(2003) 018<1093:LCORIT>2.0.CO; 2.
Kaplan, J., M. DeMaria, and J. Knaff, 2010: A revised tropical cyclone rapid intensification index for the Atlantic and Eastern North Pacific basins. *Wea. Forecasting*, **25**, 220–241, doi:10.1175/2009WAF2222280.1.
Kaplan, J, C. M. Rozoff, M. DeMaria, C. R. Sampson, J. P. Kossin, C. S. Velden, J. J. Cione, J. P. Dunion, J. A. Knaff, J. A. Zhang, J. F. Dostalek, J. D. Hawkins; T. F. Lee; J. E. Solbrig, 2015: Evaluating environmental impacts on tropical cyclone rapid intensification predictability utilizing statistical models. *Wea. Forecasting*, **30**, 1374–1396, doi:10.1175/WAF-D-15-0032.1.
Kepert, J. D., 2001: The dynamics of boundary layer jets within the tropical cyclone core. Part I: Linear theory. *J. Atmos. Sci.*, **58**, 2469-2484, doi:10.1175/1520-0469(2001)058<2569:TDOBLJ>2.0.CO;2.
Kepert, J. D., and Y. Wang, 2001: The dynamics of boundary layer jets within the tropical cyclone core. Part I: Nonlinear enhancement. J. Atmos. Sci., 58, 2485-2501, doi:10.1175/1520-0469(2001)058<2485:TDOBJ>2.0.CO.2.
Kepert, J. D., 2006a: Observed boundary layer wind structure and balance in the hurricane core. Part I: Hurricane Georges. *J. Atmos. Sci.*, **63**, 2169–2193, doi:10.1175/JAS3745.1.
Kepert, J. D., 2006b: Observed boundary layer wind structure and balance in the hurricane core. Part II: Hurricane Mitch. *J. Atmos. Sci.*, **63**, 2194–2211, doi:10.1175/JAS3746.1.
Kepert, J. D., 2013: How does the boundary layer contribute to eyewall replacement cycles in axisymmetric tropical cyclones? *J. Atmos. Sci.*, **70**, 2808–2830, doi:10.1175/JAS-D-13-046.1.
Kepert, J. D., 2017: Time and space scales in the tropical cyclone boundary layer, and the location of the eyewall updraft. *J. Atmos. Sci.*, **74**, 3305–3323, doi:10.1175/JAS-D-17-0077.1.
Kieper, M., and H. Jiang, 2012: Predicting tropical cyclone rapid intensification using the 37-GHz ring pattern identified from passive microwave measurements. *Geophys. Res. Lett.*, **39**, L13804, doi:10.1029/2012GL052115.
Kieu, C., 2015: Revisiting dissipative heating in tropical cyclone maximum potential intensity. *Q. J. R. Meteorol. Soc.*, **141**, 2497-2504, doi:10.1002/qj.2534.

Kilroy, G. and R. K. Smith, 2017: The effects of initial vortex size on hurricane genesis and intensification. *Q. J. Roy. Meteor. Soc.*, **143**, 2832-2845, doi:10.1002/qj.3134.

Kilroy G., Smith R. K., M. T. Montgomery, B. Lynch and C. Earl-Spurr, 2016: A case study of a monsoon low that intensified over land as seen in the ECMWF analyses. *Q. J. Roy. Meteor. Soc.*, **142**, 2244-2255, doi:10.1002/qj.2814.

Kilroy, G., R. K. Smith and M. T. Montgomery, 2017a: A unified view of tropical cyclogenesis and intensification. *Q. J. Roy. Meteor. Soc.*, **143**, 450-462, doi:10.1002/qj.2934.

Kilroy, G., M. T. Montgomery and R. K. Smith, 2017b: The role of boundary layer friction on tropical cyclogenesis and intensification. *Q. J. Roy. Meteor. Soc.*, **143**, 2524-2536, doi:10.1002/qj.3104.

Kilroy, G., R. K. Smith and M. T. Montgomery, 2017c: Tropical low formation and intensification over land as seen in ECMWF analyses. *Q. J. Roy. Meteor. Soc.*, **143**, 772-784, doi:10.1002/qj.2963.

Kilroy, G., R. K. Smith and M. T. Montgomery, 2018: The role of heating and cooling associated with ice processes on tropical cyclogenesis and intensification. *Q. J. Roy. Meteor. Soc.*, **144**, 99-114, doi:10.1002/qj.3187.

Kleinschmidt, E., 1951: Grundlagem einer theorie der tropischen zyklonen. *Arch. Met. Geophys. Bioklimatol.,* **4a**, 57-72.

Komaromi, W. A., and J. D. Doyle, 2018: On the dynamics of tropical cyclone and trough interactions. J. Atmos. Sci., 75, 2687-2709. doi:10.1175/JAS-D-17-0272.1

Kossin, J. P., W. H. Schubert, and M. T. Montgomery, 2000: Unstable interactions between a hurricane's primary eyewall and a secondary ring of enhanced vorticity. *J. Atmos. Sci.* **57**, 3893–3917, doi:10.1175/1520-0469(2001)058<3893: UIBAHS >2.0.CO;2.

Kossin, J. P., and M. Sitkowski, 2012: Predicting hurricane intensity and structure changes associated with eyewall replacement cycles. *Wea. Forecasting*, **27**, 484–488, doi:10.1175/WAF-D-11-00106.1.

Kossin, J. P., 2015: Hurricane wind–pressure relationship and eyewall replacement cycles. *Wea. Forecasting*, **30**, 177–181, doi:10.1175/WAF-D-14-00121.1.

Kossin, J. P., and M. DeMaria, 2016: Reducing operational hurricane intensity forecast errors during eyewall replacement cycles. *Wea. Forecasting*, **31**, 601–608, doi:10.1175/WAF-D-15-0123.1.

Kowaleski, A. M. and J. L. Evans, 2015: Thermodynamic observations and flux calculations of the tropical cyclone surface layer within the context of potential intensity. *Weather Forecasting*, **30**, 1303-1320, doi:10.1175/WAF-D-14-00162.1.

Kowch, R., and K. Emanuel, 2015: Are special processes at work in the rapid intensification of tropical cyclones? *Mon. Wea. Rev.*, **143**, 878–882, doi:10.1175/MWR-D-14-00360.1.

Kuo, H.-C., W. H. Schubert, C.-L. Tsai, and Y.-F. Kuo, 2008: Vortex interactions and barotropic aspects of concentric eyewall formation. *Mon. Wea. Rev.*, **136**, 5183-5198. doi:10.1175/2008MWR2378.1.

Kwon, Y. C. and T. Kim, 2017: Impact of air-sea exchange coefficients on the structure and intensity of tropical cyclones. *Terr. Atmos. Ocean. Sci.*, **28**, 345-356, doi:10.3319/TAO.2016.11.16.01.

Lahaye, N. and V. Zeitlin, 2016: Understanding instabilities of tropical cyclones and their evolution with a moist convective rotating shallow-water model. *J. Atmos. Sci.*, **73**, 505–523, doi:10.1175/JAS-D-15-0115.1.

Lai, Q. Z., L. G. Wu, and C. L. She, 2015: Sea surface temperature response to Typhoon Morakot (2009) and its influence. *J. Trop. Meteorol.,* **21**, 111-120.

Landsea, C. W. and J. L. Franklin, 2013: Atlantic Hurricane Database uncertainty and presentation of a new database format. *Mon. Wea. Rev.*, **141**, 3576–3592, doi:10.1175/MWR-D-12-00254.1.

Lee, C.-Y. and S. S. Chen, 2014a: Stable boundary layer and its impact on tropical cyclone structure in a coupled atmosphere–ocean Model. *Mon. Wea. Rev.*, **142**, 1927–1944, doi:10.1175/MWR-D-13-00122.1.
Lee, C.-Y. and S. S. Chen, 2014b: Corrigendum (vol. 142, p. 1939, 2014). *Mon. Weather Rev.*, **142**, 4890-4890, doi:10.1175/MWR-D-14-00315.1.
Lee, J.-D., and C.-C. Wu, 2018: The role of polygonal eyewalls in rapid intensification of Typhoon Megi (2010). *J. Atmos. Sci.*, doi:10.1175/JAS-D-18-0100.1 (in press).
Lee M., and T. Frisius, 2018: On the role of convective available potential energy (CAPE) in tropical cyclone intensification. *Tellus A*, **70**, 1433433, doi:10.1080/16000870.2018.1433433.
Leighton, H, S. Gopalakrishnan, J. A. Zhang, R. F. Rogers, Z. Zhang, and V. Tallapragada, 2018: Azimuthal distribution of deep convection, environmental factors, and tropical cyclone rapid intensification: A perspective from HWRF ensemble forecasts of Hurricane Edouard (2014). *J. Atmos. Sci.*, **75**, 275–295, doi:10.1175/JAS-D-17-0171.1.
Leroux, M.-D., J. Meister, D. Mekies, and P. Caroff, 2018: A climatology of Southwest Indian Ocean tropical systems: Their number, tracks, impacts, sizes, empirical maximum potential intensity and intensity changes. *J. Appl. Meteor. Climatol.*, **57**, 1021–1041, doi:10.1175/JAMC-D-17-0094.1.
Li, M., F. Ping, Chen, J, and L. Xu, 2016: A simulation study on the rapid intensification of Typhoon Megi (2010) in vertical wind shear. *Atmos.Sci.Lett.*, **17**, 630–638, doi:10.1002/asl.713.
Li, Q., and Y. Wang, 2012a: Formation and quasi-periodic behavior of outer spiral rainbands in a numerically simulated tropical cyclone. *J. Atmos. Sci.,* **69**, 997–1020, doi:10.1175/2011jas3690.1.
Li, Q., and Y. Wang, 2012b: A comparison of inner and outer spiral rainbands in a numerically simulated tropical cyclone. *Mon. Wea. Rev.,* **140**, 2782–2805, doi: 10.1175/MWR-D-11-00237.1.
Li, Q., Y. Wang, and Y. Duan, 2014a: Effects of diabatic heating and cooling in the rapid filamentation zone on structure and intensity of a simulated tropical cyclone. *J. Atmos. Sci.,* **71**, 3144–3163, doi:10.1175/JAS-D-13-0312.1.
Li, Q., Y., Wang, and Y. Duan, 2015: Impacts of evaporation of rainwater on tropical cyclone structure and intensity—A revisit. *J. Atmos. Sci.*, **72**, 1323–1345, doi:10.1175/jas-d-14-0224.1.
Li, Q., Y. Wang, and Y. Duan, 2017: A numerical study of outer rainband formation in a sheared tropical cyclone. *J. Atmos. Sci.,* **74**, 203–227, doi:10.1175/jas-d-16-0123.1.
Li, Y., S. Peng, J. Wang, and J. Yan, 2014b: Impacts of nonbreaking wave-stirring-induced mixing on the upper ocean thermal structure and typhoon intensity in the South China Sea. *J. Geophys. Res.-Oceans*, **119**, 5052-5070, doi:10.1002/2014JC009956.
Liu, J. J., F. M. Zhang, and Z. X. Pu, 2017: Numerical simulation of the rapid intensification of Hurricane Katrina (2005): Sensitivity to boundary layer parameterization schemes. *Adv. Atmos. Sci.*, **34**, 482–496, doi:10.1007/s00376-016-6209-5.
Ma, Z. H., J. F. Fei, X. P. Cheng, Y. Q., Wang, and X. G. Huang, 2015: Contributions of surface sensible heat fluxes to tropical cyclone. Part II: The sea spray processes. *J. Atmos. Sci.*, **72**, 4218-4236, doi:10.1175/JAS-D-15-0058.1.
Ma, Y. M., N. E. Davidson, Y. Xiao, and J. W. Bao, 2017: Revised parameterization of air–sea exchanges in high winds for operational numerical prediction: Impact on tropical cyclone track, intensity, and rapid intensification. *Wea. Forecasting*, **32**, 821–848, doi:10.1175/WAF-D-15-0109.1.

Malkus, J. S., and H. Riehl, 1960: On the dynamics and energy transformations in steady-state hurricanes. *Tellus*, **12**, 1–20, doi: 10.1111/j.2153-3490.1960.tb01279.x.

Martinez, J., M. M. Bell, J. Vigh, and R. Rogers, 2017: Examination of Tropical Cyclone Structure and Intensification with the Extended Flight Level Dataset (FLIGHT+) from 1999 to 2012. *Mon. Wea. Rev.,* **145**, 4401–4421, doi.org/10.1175/MWR-D-17-0011.1

Menelaou, K., D. A. Schecter, and M. K. Yau, 2016: On the relative contribution of inertia-gravity wave radiation to asymmetric instabilities in tropical cyclone-like vortices. *J. Atmos. Sci.*, **73**, 3345–3370, doi:10.1175/JAS-D-15-0360.1.

Menelaou, K. and M. K. Yau, 2018: Spontaneous emission of spiral inertia-gravity waves and formation of elliptical eyewalls in tropical cyclone-like vortices: Three-dimensional nonlinear simulations. *J. Atmos. Sci.*, **75**, 2635–2658, doi:10.1175/JAS-D-17-0341.1.

Merrill, R. T., 1988a: Environmental influences on hurricane intensification. *J. Atmos. Sci.*, **45**, 1678–1687, doi:10.1175/1520-0469(1988)045<1678:EIOHI>2.0.CO;2

Merrill, R. T., 1988b: Characteristics of the upper-tropospheric environmental flow around hurricanes. *J. Atmos. Sci.*, **45**, 1665–1677, doi:10.1175/1520-0469(1988)045<1665:COTUTE>2.0.CO;2

Ming, J. and J. A. Zhang, 2016: Effects of surface flux parameterization on the numerically simulated intensity and structure of Typhoon Morakot (2009). *Adv. Atmos. Sci.*, **33**, 58-72, doi:10.1007/s00376-015-4202-z.

Miller, W., H. Chen, and D.-L. Zhang, 2015: On the rapid intensification of Hurricane Wilma (2005). Part III: Effects of latent heat of fusion. *J. Atmos. Sci*., **72**, 3829–3849, doi:10.1175/JAS-D-14-0386.1.

Miyamoto, Y., and T. Takemi, 2015: A triggering mechanism for rapid intensification of tropical cyclones. *J. Atmos. Sci.*, **72**, 2666–2681, doi:10.1175/JAS-D-14-0193.1.

Miyamoto, Y, G. H. Bryan, and R. Rotunno, 2017: An analytical model of maximum potential intensity for tropical cyclones incorporating the effect of ocean mixing. *Geophys. Res. Lett.*, **44**, 5826-5835, doi:10.1002/2017GL073670.

Miyamoto, Y., and D. Nolan, 2018: Structural changes preceding rapid intensification in tropical cyclones as shown in a large ensemble of idealized simulations. *J. Atmos. Sci.*, **75**, 555–569, doi:10.1175/JAS-D-17-0177.1.

Möller, J. D., and L. J. Shapiro, 2002: Balanced contributions to the intensification of Hurricane Opal as diagnosed from a GFDL model forecast. *Mon. Wea. Rev.*, **130**, 1866–1881, doi:10.1175/1520-0493(2002)130<1866:bcttio>2.0.co;2.

Montgomery, M. T., N. V. Sang, R. K. Smith, and J. Persing, 2009: Do tropical cyclones intensify by WISHE? *Q. J. Roy. Meteor. Soc.*, **135**, 1697–1714, doi:10.1002/qj.459.

Montgomery M. T. and R. K. Smith, 2014: Paradigms for tropical-cyclone intensification. *Aust. Meteor. Ocean. Journl.* (Bruce Morton Memorial Volume), **64**, 37-66.

Montgomery, M. T., J. A. Zhang, and R. K. Smith, 2014: An analysis of the observed low-level structure of rapidly intensifying and mature Hurricane Earl (2010). *Q. J. Roy. Meteor. Soc.*, **140**, 2132-2146, doi:10.1002/qj.2283.

Montgomery, M. T., J. Persing, and R. K. Smith, 2015: Putting to rest WISHE-ful misconceptions for tropical cyclone intensification. *J. Adv. Model. Earth Syst.*, **7**, 92–109, doi:10.1002/2014MS000362.

Montgomery M.T., 2016: Introduction to Hurricane Dynamics: Tropical Cyclone Intensification. In: Mohanty U.C., Gopalakrishnan S.G. (eds) Advanced Numerical Modeling and Data Assimilation Techniques for Tropical Cyclone Prediction. Springer, Dordrecht, doi:10.5822/978-94-024-0896-6_21.

Montgomery M. T. and R. K. Smith, 2017: Recent developments in the fluid dynamics of tropical cyclones. *Annu. Rev. Fluid Mech.*, **49**, 541-574, doi:10.1146/annurev-fluid-010816-060022.

Montgomery, M. T., and R. K. Smith, 2018: Comments on "Revisiting the balanced and unbalanced aspects of tropical cyclone intensification." *J. Atmos. Sci.*, **75**, 2491–2496, doi:10.1175/JAS-D-17-0323.1.

Moon, Y., and D. S. Nolan, 2010: The dynamic response of the hurricane wind field to spiral rainband heating. *J. Atmos. Sci.*, **67**, 1779–1805, doi:10.1175/2010jas3171.1.

Moon, Y., and D. S. Nolan, 2015a: Spiral rainbands in a numerical simulation of Hurricane Bill (2009). Part I: Structures and comparisons to observations. *J. Atmos. Sci.,* **72**, 164–190, doi: 10.1175/JAS-D-14-0058.1.

Moon, Y., and D. S. Nolan, 2015b: Spiral rainbands in a numerical simulation of Hurricane Bill (2009). Part II: Propagation of inner rainbands. *J. Atmos. Sci.,* **72**, 191–215, doi:10.1175/jas-d-14-0056.1.

Mueller, J. A., and F. Veron, 2014: Impact of sea spray on air-sea fluxes. Part II: Feedback effects. *J. Phys. Oceanogr.*, **44**, 2835-2853, doi:10.1175/JPO-D-13-0246.1.

Munsell, E. B., F. Zhang, J. A. Sippel, S. A. Braun, and Y. Weng, 2017: Dynamics and predictability of the intensification of Hurricane Edouard (2014). *J. Atmos. Sci.*, **74**, 573–595, doi:10.1175/JAS-D-16-0018.1.

Murthy, V. S., and W. R. Boos, 2018: Role of surface enthalpy fluxes in idealized simulations of tropical depression spinup. *J. Atmos. Sci.*, **75**, 1811–1831, doi:10.1175/JAS-D-17-0119.1.

Musgrave, K. D., R. K. Taft, J. L. Vigh, B. D. McNoldy, and W. H. Schubert, 2012: Time evolution of the intensity and size of tropical cyclones. *J. Adv. Model. Earth Syst.*, **4**, M08001, doi:10.1029/2011MS000104.

Navarro, E. L., and G. J. Hakim, 2016: Idealized numerical modeling of the diurnal cycle of tropical cyclones. *J. Atmos. Sci.*, **73**, 4189–4201, doi:10.1175/JAS-D-15-0349.1.

Navarro, E. L., G. J. Hakim, and H. E. Willoughby, 2017: Balanced response of an axisymmetric tropical cyclone to periodic diurnal heating. *J. Atmos. Sci.*, **74**, 3325–3337, doi: 10.1175/JAS-D-16-0279.1.

Naylor, J., and D. A. Schecter, 2014: Evaluation of the impact of moist convection on the development of asymmetric inner core instabilities in simulated tropical cyclones. *J. Adv. Model. Earth Syst.*, **6**, 1027–1048, doi:10.1002/2014MS000366.

Neelin, J. D., I. M. Held, and K. H. Cook, 1987: Evaporation-wind feedback and low-frequency variability in the tropical atmosphere. *J. Atmos. Sci.*, **44**, 2341–2348, doi:10.1175/1520-0469(1987)044<2341:EWFALF>2.0.CO;2

Ooyama, K. V., 1964: A dynamical model for the study of tropical cyclone development. *Geofis. Int.*, **4**, 187–198.

Ooyama, K. V., 1969: Numerical simulation of the life cycle of tropical cyclones. *J. Atmos. Sci.*, **26**, 3–40, doi:10.1175/1520-0469(1969)026<0003:NSOTLC>2.0.CO;2.

Ooyama, K. V., 1982: Conceptual evolution of the theory and modeling of the tropical cyclone. *J. Meteor. Soc. Japan*, **60**, 369–380, doi:10.2151/jmsj1965.60.1_369.

Osuri, K. K., R. Nadimpalli, U.C. Mohanty, and D. Niyogi, 2017: Prediction of rapid intensification of tropical cyclone Phailin over the Bay of Bengal using the HWRF modelling system. *Q. J. Roy. Meteor. Soc.,* **143**, 678–690, doi:10.1002/qj.2956.

Oyama, R., 2017: Relationship between tropical cyclone intensification and cloud-top outflow revealed by upper-tropospheric atmospheric motion vectors. *J. Appl. Meteorol. Climatol.*, **56**, 2801–2819, doi:10.1175/JAMC-D-17-0058.1.

Ozawa, H., and S. Shimokawa, 2015: Thermodynamics of a tropical cyclone: generation and dissipation of mechanical energy in a self-driven convection system. *Tellus A*, **67**, 24216, doi:10.3402/tellusa.v67.24216.

Pendergrass, A. G., and H. E. Willoughby, 2009: Diabatically induced secondary flows in tropical cyclones. Part I: Quasi-steady forcing. *Mon. Wea. Rev.*, **137**, 805–821, doi: 10.1175/2008MWR2657.1.

Peng, K., R. Rotunno, and G. H. Bryan, 2018: Evaluation of a time-dependent model for the intensification of tropical cyclones. *J. Atmos. Sci.*, **75**, 2125–2138, doi:10.1175/JAS-D-17-0382.1.

Persing, J., M. T. Montgomery, J. McWilliams, and R. K. Smith, 2013: Asymmetric and axisymmetric dynamics of tropical cyclones. *Atmos. Chem. Phys.*, **13**, 12 299–12 341, doi:10.5194/acp-13-12299-2013.

Potter, H., H. C. Graber, N. J. Williams, C. O. Collins, R. J. Ramos, and W. M. Drennan, 2015: In situ measurements of momentum fluxes in typhoons. *J. Atmos. Sci.*, **72**, 104–118, doi:10.1175/JAS-D-14-0025.1.

Potter, H. W. M. Drennan, and H. C. Graber, 2017: Upper ocean cooling and air-sea fluxes under typhoons: A case study. *J. Geophys. Res.-Oceans*, **122**, 7237–7252, doi:10.1002/2017JC012954.

Powell, M. D., P. J. Vickery, and T. A. Reinhold, 2003: Reduced drag coefficient for high wind speeds in tropical cyclones. *Nature,* **422,** 279-283, 10.1038/nature01481.

Powell, M. D., E. W. Uhlhorn, and J. D. Kepert, 2009: Estimating maximum surface winds from hurricane reconnaissance measurements. *Wea. Forecasting,* **24,** 868-883, 10.1175/2008WAF2007087.1.

Qin, N., D.-L. Zhang, and Y. Li, 2016: A statistical analysis of steady eyewall sizes associated with rapidly intensifying hurricanes. *Wea. Forecasting*, **31**, 737–742, doi:10.1175/WAF-D-16-0016.1.

Qin, N., and D.-L. Zhang, 2018: On the extraordinary intensification of Hurricane Patricia (2015). Part I: Numerical experiments. *Wea. Forecasting*, **33**, 1205–1224, doi:10.1175/WAF-D-18-0045.1.

Qin, N., D.-L. Zhang, W. Miller, and C. Q. Kieu, 2018: On the rapid intensification of Hurricane Wilma (2005). Part IV: Inner-core dynamics during the steady RMW stage. *Q. J. Roy. Meteor. Soc.,* in press, doi:10.1002/qj.3339.

Ranalkar, M. R., S. D. Pawar, and P. P. Kumar, 2017: Characteristics of lightning activity in tropical cyclones developed over North Indian Ocean basin during 2010–2015. *Atmos. Res.*, **187**, 16–32, doi:10.1016/j.atmosres.2016.12.003.

Rappin, E. D., M. C. Morgan, and G. J. Tripoli, 2011: The impact of outflow environment on tropical cyclone intensification and structure. *J. Atmos. Sci.*, **68**, 177–194, doi:10.1175/2009JAS2970.1.

Rastigejev, Y. and S. A. Suslov, 2014: E-ϵ model of spray-laden near-sea atmospheric layer in high wind conditions. *J. Phys. Oceanogr.,* **44,** 742-763, 10.1175/JPO-D-12-0195.1.

Raymond, D. J. and M. J. Herman, 2012: Frictional convergence, atmospheric convection, and causality. *Atmósfera*, **25**, 253-267.

Reasor, P. D., and M. T. Montgomery, F. D. Marks, and J. F. Gamache, 2000: Low-wavenumber structure and evolution of the hurricane inner core observed by airborne dual-Doppler radar. *Mon. Wea. Rev.*, **128**, 1653–1680, doi:1520-0493(2000)128<1653:LWSAEO>2.0.CO;2.

Riehl, H., and J. S. Malkus, 1961: Some aspects of Hurricane Daisy, 1958. *Tellus*, **13**, 181–213, doi:10.3402/tellusa.v13i2.9495.

Rogers, R. F., P. D. Reasor, and S. Lorsolo, 2013: Airborne Doppler observations of the inner-core structural differences between intensifying and steady-state tropical cyclones. *Mon. Wea. Rev.*, **141**, 2970–2991, doi:10.1175/MWR-D-12-00357.1.

Rogers, R. F., P. D. Reasor, and J. A. Zhang, 2015: Multi-scale structure and evolution of Hurricane Earl (2010) during rapid intensification. *Mon. Wea. Rev.*, **143**, 536–562, doi:10.1175/MWR-D-14-00175.1.

Rogers R. F., J. A. Zhang, J. Zawislak, H. Jiang, G. R. Alvey, E. J. Zipser, and S. N. Stevenson, 2016: Observations of the structure and evolution of Hurricane Edouard (2014) during intensity change. Part II: Kinematic structure and the distribution of deep convection. *Mon. Wea. Rev.*, **144**, 3355–3376, 10.1175/MWR-D-16-0017.1.

Rozoff, C. M., W. H. Schubert, B. D. McNoldy, and J. P. Kossin, 2006: Rapid filamentation zones in intense tropical cyclones. *J. Atmos. Sci.,* **63**, 325–340, doi:10.1175/JAS3595.1.

Rozoff, C. M., D. S. Nolan, J. P. Kossin, F. Zhang, and J. Fang, 2012: The roles of an expanding wind field and inertial stability in tropical cyclone secondary eyewall formation. *J. Atmos. Sci.*, **69**, 2621–2643, doi:10.1175/JAS-D-11-0326.1.

Rozoff, C. M., C. S. Velden, J. Kaplan, J. P. Kossin, and A. J. Wimmers, 2015: Improvements in the probabilistic prediction of tropical cyclone rapid intensification resulting from inclusion of passive microwave observations. *Wea. Forecasting,* **30**, 1016–1038, doi:10.1175/WAF-D-14-00109.1.

Salmon, R., 2014: Analogous formulation of electrodynamics and two-dimensional fluid dynamics. *J. Fluid Mech.*, **761**, R2, doi:10.1017/jfm.2014.642.

Sanger, N. T., M. T. Montgomery, R. K. Smith, and M. M. Bell, 2014: An observational study of tropical cyclone spinup in Supertyphoon Jangmi (2008) from 24 to 27 September. *Mon. Weather Rev.*, **142**, 3–28, doi:10.1175/MWR-D-12-00306.1.

Schecter, D. A., and M. T. Montgomery, 2004: Damping and pumping of a vortex Rossby wave in a monotonic cyclone: Critical layer stirring versus inertia-buoyancy wave emission. *Phys. Fluids*, **16**, 1334–1348, doi:10.1063/1.1651485.

Schecter, D. A., and K. Menelaou, 2017: Note on analyzing perturbation growth in a tropical cyclone-like vortex radiating inertia-gravity waves. *J. Atmos. Sci.*, **74**, 1561–1571, doi:10.1175/JAS-D-16-0289.1.

Schecter, D. A., 2018: On the instabilities of tropical cyclones generated by cloud resolving models. *Tellus A*, doi:10.1080/16000870.2018.1525245.

Schubert, W. H., and J. J. Hack, 1982: Inertial stability and tropical cyclone development. *J. Atmos. Sci.*, **39**, 1687–1697, doi:10.1175/1520-0469(1982)039<1687:ISATCD>2.0.CO;2.

Schubert, W. H., M. T. Montgomery, R. K. Taft, T. A. Guinn, S. R. Fulton, J. P. Kossin, and J. P. Edwards, 1999: Polygonal eyewalls, asymmetric eye contraction, and potential vorticity mixing in hurricanes. *J. Atmos. Sci.*, **56**, 1197–1223, doi:10.1175/1520-0469(1999)056<1197:PEAECA>2.0.CO;2.

Schubert, W. H., C. J. Slocum, and R. K. Taft, 2016: Forced, balanced model of tropical cyclone intensification. *J. Meteor. Soc. Japan*, **94**, 119–135, doi:10.2151/jmsj.2016-007.

Seroka, G., T. Miles, Y. Xu, J. Kohut, O. Schofield, and S. Glenn, 2016: Hurricane Irene Sensitivity to Stratified Coastal Ocean Cooling. *Mon. Weather Rev.*, **144**, 3507-3530, doi:10.1175/MWR-D-15-0452.1.

Seroka, G., T. Miles, Y. Xu, J. Kohut, O. Schofield, and S. Glenn, 2017: Rapid shelf-wide cooling response of a stratified coastal ocean to hurricanes. *J. Geophys. Res.-Oceans*, **122**, 4845-4867, doi:10.1002/2017JC012756.

Shapiro, L. J., and H. E. Willoughby, 1982: The response of balanced hurricanes to local sources of heat and momentum. *J. Atmos. Sci.*, **39**, 378–394, doi:10.1175/1520-0469(1982)039<0378:TROBHT>2.0.CO;2.

Shimada, U., K. Aonashi, and Y. Miyamoto, 2017: Tropical cyclone intensity change and axisymmetricity deduced from GSMaP. *Mon. Wea. Rev.*, **145**, 1003–1017, doi:10.1175/MWR-D-16-0244.1.

Shimada, U., M. Sawada,and H. Yamada, 2018: Doppler radar analysis of the rapid intensification of Typhoon Goni (2015) after eyewall replacement. *J. Atmos. Sci.*, **75**, 143–162, doi:10.1175/JAS-D-17-0042.1.

Shu, S., J. Ming, and P. Chi, 2012: Large-scale characteristics and probability of rapidly intensifying tropical cyclones in the Western North Pacific basin. *Mon. Wea. Rev.*, **27**, 411–423, doi:10.1175/WAF-D-11-00042.1.

Sitkowski, M., J. P. Kossin, and C. M. Rozoff, 2011: Intensity and structure changes during hurricane eyewall replacement cycles. *Mon. Wea. Rev.*, **139**, 3829–3847, doi:10.1175/MWR-D-11-00034.1.

Sitkowski, M., J. P. Kossin, C. M. Rozoff, and J. A. Knaff, 2012: Hurricane eyewall replacement cycle thermodynamics and the relict inner eyewall circulation. *Mon. Wea. Rev.*, **140**, 4035–4045, doi:10.1175/MWR-D-11-00349.1.

Slocum, C. J., G. J. Williams, R. K. Taft, and W. H. Schubert, 2014: Tropical cyclone boundary layer shocks. arXiv, http://arxiv.org/abs/1405.7939.

Smith, R. K., and S. Vogl, 2008: A simple model of the hurricane boundary layer revisited. *Q. J. Roy. Meteor. Soc.*, **134**, 337–51, doi:10.1002/qj.216.

Smith, R. K., M. T. Montgomery, and S. V. Nguyen, 2009: Tropical cyclone spin-up revisited. *Q. J. Roy. Meteor. Soc.*, **135**, 1321–1335, doi:10.1002/qj.428.

Smith, R. K. and M. T. Montgomery, 2015: Toward clarity on understanding tropical cyclone intensification. *J. Atmos. Sci.*, **72**, 3020–3031, doi:10.1175/JAS-D-15-0017.1.

Smith, R. K., M. T. Montgomery, G. Kilroy, S. Tang, and S. Müller, 2015: Tropical low formation during the Australian monsoon: the events of January 2013. *Aust. Meteor. Ocean. Journl.*, **65**, 318–341.

Smith, R. K. and M. T. Montgomery, 2016a: Comments on: Nonlinear response of a tropical cyclone vortex to prescribed eyewall heating with and without surface friction in TCM4: Implications for tropical cyclone intensification, by J. Heng and Y. Wang. *J. Atmos. Sci.*, **73**, 5101–5103.

Smith, R. K., and M. T. Montgomery, 2016b: The efficiency of diabatic heating and tropical cyclone intensification. *Q. J. Roy. Meteor. Soc.*, 142, 2081–2086, 10.1002/qj.2804.

Smith R. K. and M. T. Montgomery, 2016c: Understanding hurricanes. *Weather*, **71**, 219–223, doi:10.1002/wea.2776.

Smith, R. K., J. A. Zhang and M. T. Montgomery, 2017: The dynamics of intensification in an HWRF simulation of Hurricane Earl (2010). *Q. J. Roy. Meteor. Soc.*, **143**, 293-308, doi:10.1002/qj.2922.

Smith, R. K., M. T. Montgomery, and H. Bui, 2018: Axisymmetric balance dynamics of tropical cyclone intensification and its breakdown revisited. *J. Atmos. Sci.*, **75**, 3169–3189, doi:10.1175/JAS-D-17-0179.1.

Soloviev, A. V., R. Lukas, M. A. Donelan, B. K. Haus, and I. GinisI, 2017: Is the state of the air-sea interface a factor in rapid intensification and rapid decline of tropical cyclones? *J. Geophys. Res.-Oceans*, **122**, 10174–10183, doi:10.1002/2017JC013435.

Stern, D., J. Dunion, M. Bell, E. Hendricks, Y.-H. Huang, H. Jiang, J. Kossin, J. Kepert, Y. Miyamoto, and Y. Wang, 2014: Subtopic 2.6. Intensity change: Internal processes. Report for the Eighth WMO International Workshop on Tropical Cyclones IWTC-VIII, World Meteorological Organization, Jeju Island, South Korea, 26 pp.

Stern, D. P., and F. Zhang, 2016: The warm-core structure of Hurricane Earl (2010). *J. Atmos. Sci*., **73**, 3305–3328, doi:10.1175/JAS-D-15-0328.1.

Stern, D. P., J. L. Vigh, D. S. Nolan, and F. Zhang, 2015: Revisiting the relationship between eyewall contraction and intensification. *J. Atmos. Sci.*, **72**, 1283–1306, doi:10.1175/JAS-D-14-0261.1.

Stevenson, S. N., K. L. Corbosiero, and J. Molinari, 2014: The convective evolution and rapid intensification of Hurricane Earl (2010). *Mon. Wea. Rev.*, **142**, 4364–4380, doi:10.1175/MWR-D-14-00078.1.

Stevenson, S. N., K. L. Corbosiero, and S. F. Abarca, 2016: Lightning in eastern North Pacific tropical cyclones: A comparison to the North Atlantic. *Mon. Wea. Rev.*, **144**, 225–239, doi:10.1175/MWR-D-15-0276.1.

Stevenson, S. N., K. L. Corbosiero, M. DeMaria, and J. L. Vigh, 2018: A 10-Year survey of tropical cyclone inner-core lightning bursts and their relationship to intensity change. *Wea. Forecasting*, **33**, 23-36, 10.1175/WAF-D-17-0096.1.

Strazzo, S. E., J. B. Elsner, and T. E. LaRow, 2015: Quantifying the sensitivity of maximum, limiting, and potential tropical cyclone intensity to SST: Observations versus the FSU/COAPS global climate model. *J. Adv. Model. Earth Syst.*, **7**, 586-599, doi:10.1002/2015MS000432.

Sun, Y., Z. Zhong, L. Yi, Y. Ha, and Y. M. Sun, 2014: The opposite effects of inner and outer sea surface temperature on tropical cyclone intensity. *J. Geophys. Res.-Atmos.*, **119**, 2193-2208, doi:10.1002/2013JD021354.

Susca-Lopata, G., J. Zawislak, E. J. Zipser, R. F. Rogers, 2015: The role of observed environmental conditions and precipitation evolution in the rapid intensification of Hurricane Earl (2010). *Mon. Wea. Rev.*, **143**, 2207–2223, doi: 10.1175/MWR-D-14-00283.1.

Tao, C., and H. Jiang, 2015: Distributions of shallow to very deep precipitation–convection in rapidly intensifying tropical cyclones. *J. Climate*, **28**, 8791–8824. doi:10.1175/JCLI-D-14-00448.1.

Tao, C., H. Jiang, and J. Zawislak, 2017: The relative importance of stratiform and convective rainfall in rapidly intensifying tropical cyclones, *Mon. Wea. Rev.*, **145**, 795–809, doi: 10.1175/MWR-D-16-0316.1.

Tao, D., and F. Zhang, 2014: Effect of environmental shear, sea-surface temperature, and ambient moisture on the formation and predictability of tropical cyclones: An ensemble-mean perspective. *J. Adv. Model. Earth Syst.*, **6**, 384–404, doi:10.1002/2014MS000314.

Tao, D., and F. Zhang, 2015: Effects of vertical wind shear on the predictability of tropical cyclones: Practical versus intrinsic limit. *J. Adv. Model. Earth Syst.*, **7**, 1534–1553, doi:10.1002/2015MS000474.

Tang S., R. K. Smith, M. T. Montgomery and M. Gu, 2016: Numerical study of the spin up of a tropical low over land during the Australian monsoon. *Q. J. Roy. Meteor. Soc.*, **142**, 2021-2032, doi:10.1002/qj.2797.

Tang, X., W. Lee, and M. Bell, 2014: A Squall-Line-Like Principal Rainband in Typhoon Hagupit (2008) Observed by Airborne Doppler Radar. *J. Atmos. Sci.,* **71**, 2733–2746, doi:10.1175/JAS-D-13-0307.1.

Tang, X., Z.-M. Tan, J. Fang, Y. Q. Sun, and F. Zhang, 2017: Impact of the diurnal radiation cycle on secondary eyewall formation. *J. Atmos. Sci.*, **74**, 3079–3098, doi:10.1175/JAS-D-17-0020.1

Tang, X., F. Ping, S. Yang, M. Li, and J. Peng, 2018a: Relationship between convective bursts and the rapid intensification of Typhoon Mujigae (2015). *Atmos. Sci. Lett.*, doi:10.1002/asl.811.

Tang, X., W.-C. Lee, and M. Bell, 2018b: Subrainband structure and dynamic characteristics in the principal rainband of Typhoon Hagupit (2008). *Mon. Wea. Rev.,* **146**, 157–173, doi:10.1175/MWR-D-17-0178.1.

Torn, R. D., 2016: Evaluation of atmosphere and ocean initial condition uncertainty and stochastic exchange coefficients on ensemble tropical cyclone intensity forecasts. *Mon. Weather Rev.*, **144**, 3487-3506, doi:10.1175/MWR-D-16-0108.1.

Tsujino, S., K. Tsuboki, and H. Kuo, 2017: Structure and maintenance mechanism of long-lived concentric eyewalls associated with simulated Typhoon Bolaven (2012). *J. Atmos. Sci.*, **74**, 3609–3634, doi:10.1175/JAS-D-16-0236.1.

Vickery, P. J., P. F. Skerjl, A. C. Stechley, and L. A. Twisdale, 2000: Hurricane wind field model for use in hurricane simulations. *J. Eng. Structures.* **126,** 1203-1221, doi:10.1061/(ASCE)0733-9445(2000)126:10(1203).

Vigh, J. L., and W. H. Schubert, 2009: Rapid development of the tropical cyclone warm core. *J. Atmos. Sci.*, **66**, 3335–3350, doi:10.1175/2009JAS3092.1.

Vigh, J. L., J. A. Knaff, and W. H. Schubert, 2012: A Climatology of Hurricane Eye Formation. *Mon. Wea. Rev.*, **140**, 1405–1426, doi:10.1175/MWR-D-11-00108.1.

Wada, A., 2015a: Unusually rapid intensification of Typhoon Man-yi in 2013 under preexisting warm-water conditions near the Kuroshio front south of Japan. *J. Oceanogr.*, **71**, 597-622, doi:10.1007/s10872-015-0273-9.

Wada, A., 2015b: Verification of tropical cyclone heat potential for tropical cyclone intensity forecasting in the Western North Pacific. *J. Oceanogr.*, **71**, 373-387, doi:10.1007/s10872-015-0298-0.

Wang, H., and Y. Q. Wang, 2014: A numerical study of Typhoon Megi (2010). Part I: Rapid intensification. *Mon. Wea. Rev.*, **142**, 29–48, doi:10.1175/MWR-D-13-00070.1.

Wang, X., C. Wang, L. Zhang,, and X. Wang, 2015: Multidecadal variability of tropical cyclone rapid intensification in the western North Pacific. *J. Clim.*, **28**, 3806–3820, doi:10.1175/JCLI-D-14-00400.1.

Wang, Y., 2008: Rapid filamentation zone in a numerically simulated tropical cyclone. *J. Atmos. Sci.,* **65**, 1158–1181, doi:10.1175/2007JAS2426.1.

Wang, Y., 2009: How do outer spiral rainbands affect tropical cyclone structure and intensity? *J. Atmos. Sci.,* **66**, 1250–1273, doi:10.1175/2008JAS2737.1.

Wang, Y., 2012: Recent research progress on tropical cyclone structure and intensity. *Trop. Cyclone Res. and Rev.*, **1**, 254-275, doi:10.6057/2012TCRR02.05.

Wang, Y., 2015: Hurricane Dynamics. *Encyclopedia of Atmospheric Sciences*, 2nd edition, Vol. 6, 8–29, Gerald R. North (editor-in-chief), John Pyle and Fuqing Zhang (eds). Elsevier Ltd, doi:10.1016/B978-0-12-382225-3.00488-6

Wang, Y., Y. Rao, Z.-M. Tan, and D. Schenomann, 2015. A statistical analysis of the effects of vertical wind shear on tropical cyclone intensity change over the western North Pacific. *Month. Wea. Rev.*, **143**, 3434–3453, doi:10.1175/MWR-D-15-0049.1.

Wang, Y., and J.-Y. Heng, 2016: Contribution of eye excess energy to the intensification rate of tropical cyclones – A numerical study. *J. Adv. Mod. Earth Sys.*, **8**, 1953–1968, doi:10.1002/2016MS000709.

Wang, M., K. Zhao, M. Xue, G. Zhang, S. Liu, L. Wen, and G. Chen, 2016: Precipitation microphysics characteristics of a Typhoon Matmo (2014) rainband after landfall over eastern China based on polarimetric radar observations. *J. Geophys. Res. Atmos.*, **121**, 12415–12433, doi:10.1002/2016JD025307.

Wei, J., and G. Q. Jiang, and X. Liu, 2017: Parameterization of typhoon-induced ocean cooling using temperature equation and machine learning algorithms: an example of Typhoon Soulik (2013). *Ocean Dyn.*, **67**, 1179-1193, doi:10.1007/s10236-017-1082-z.

Willoughby, H. E., J. A. Clos, and M. G. Shoreibah, 1982: Concentric eye walls, secondary wind maxima, and the evolution of the hurricane vortex. *J. Atmos. Sci.*, **39**, 395–411, doi:10.1175/1520-0469(1982)039<0395:CEWSWM>2.0.CO;2.

Wimmers, A. J., and C. S. Velden, 2016: Advancements in objective multisatellite tropical cyclone center fixing. *J. Appl. Meteor. Climatol.*, **55**, 197–212, doi:10.1175/JAMC-D-15-0098.1.

Wu, D., K. Zhao, M.R. Kumjian, X. Chen, H. Huang, M. Wang, A.C. Didlake, Y. Duan, and F. Zhang, 2018: Kinematics and microphysics of convection in the outer rainband of Typhoon Nida (2016) revealed by polarimetric radar. *Mon. Wea. Rev.,* **146**, 2147–2159, doi:10.1175/MWR-D-17-0320.1.

Wu, C.-C., S.-N. Wu, H.-H. Wei, and S. F. Abarca, 2016: The role of convective heating in tropical cyclone eyewall ring evolution. *J. Atmos. Sci.*, **73**, 319–330, doi:10.1175/JAS-D-15-0085.1.

Xu, H. X., 2015: A numerical study on impact of Taiwan Island surface heat flux on Super Typhoon Haitang (2005). *Adv. Meteorol.*, **2015**, 710348, 11 pp., doi:10.1155/2015/710348.

Xu, J., and Y. Wang 2015: A statistical analysis on the dependence of tropical cyclone intensification rate on the storm intensity and size in the North Atlantic. *Wea. Forecasting*, **30**, 692–701, doi:10.1175/WAF-D-14-00141.1.

Xu, J., Y. Wang, and Z.-M. Tan, 2016: The relationship between sea surface temperature and maximum potential intensification rate of tropical cyclones over the North Atlantic. *J. Atmos. Sci.*, **73**, 4979–4988, doi:10.1175/JAS-D-16-0164.1.

Xu, J. and Y. Wang, 2018a: Dependence of tropical cyclone intensification rate on sea surface temperature, storm intensity, and size in the western North Pacific. *Wea. Forecasting*, **33**, 523–537, doi:10.1175/WAF-D-17-0095.1.

Xu, J., and Y. Wang, 2018b: Effect of the initial vortex structure on intensification of a numerically simulated tropical cyclone. *J. Meteor. Soc. Japan*, **96**, 111–126, doi:10.2151/jmsj.2018-014.

Xu, W., S. A. Rutledge, and W. Zhang, 2017: Relationships between total lightning, deep convection, and tropical cyclone intensity change. *J. Geophys. Res. Atmos.*, **122**, 7047–7063, doi:10.1002/2017JD027072.

Yanai, M., 1961: A detailed analysis of typhoon formation. *J. Meteor. Soc. Japan*, **39**, 187–214, doi:10.2151/jmsj1923.39.4_187.

Yang, Y.-T., H.-C. Kuo, E. A. Hendricks, and M.S. Peng, 2013: Structural and intensity changes of concentric eyewall typhoons in the Western North Pacific basin. *Mon. Wea. Rev.*, **141**, 2632–2648, doi:10.1175/MWR-D-12-00251.1.

Yang, Z., T. Yuan, H. Jiang, L. Zhang, and C. Zhang, 2018: Stratiform and convective precipitation properties of tropical cyclones in the northwest pacific. *J. Geophys. Res. Atmos.*, **123**, 3513–3529, doi:10.1002/2017JD027174.

Yano, J.-I., and K.A. Emanuel, 1991: An improved WISHE model of the equatorial atmosphere and its coupling with the stratosphere. *J. Atmos. Sci.*, **48**, 377-389, doi:10.1175/1520-0469(1991)048<0377:AIMOTE>2.0.CO;2.

Yaukey, P. H., 2014: Intensification and rapid intensification of North Atlantic tropical cyclones: geography, time of year, age since genesis, and storm characteristics. *Int. J. Climatol.*, **34,** 1038–1049, doi:10.1002/joc.3744.

Yu, C.-Y., C.-Y. Lin, L.-W. Cheng, J.-S. Luo, C.-C. Wu, and Y. Chen, 2018: The degree of prevalence of similarity between outer tropical cyclone rainbands and squall lines. *Sci. Rep.*, **8**, 8248, doi:10.1038/s41598-018-26553-8.

Zagrodnik, J., and H. Jiang, 2014: Rainfall, convection, and latent heating distributions in rapidly intensifying tropical cyclones. *J. Atmos. Sci.*, **71**, 2789–2809, doi:10.1175/JAS-D-13-0314.1

Zawislak, J., H. Jiang, G. R. Alvey III, E. J. Zipser, R. F. Rogers, J. Zhang, and S. Stevenson, 2016: Observations of the structure and evolution of Hurricane Edouard (2014) during intensity change. Part I: Relationship between the thermodynamic structure and precipitation. *Mon. Wea. Rev.*, **144**, 3333–3354, doi: 10.1175/MWR-D-16-0018.1.

Zhang, D.-L., Y. Liu, and M. K. Yau, 2001: A multiscale numerical study of Hurricane Andrew (1992). Part IV: Unbalanced flows. *Mon. Wea. Rev.*, **129**, 92–107, doi:10.1175/1520-0493(2001)129,0092:AMNSOH.2.0.CO;2.

Zhang, F., and K. A. Emanuel, 2016: On the role of surface fluxes and WISHE in tropical cyclone intensification. *J. Atmos. Sci.*, **73**, 2011–2019, doi:10.1175/JAS-D-16-0011.1.

Zhang, F., D. Tao, Y. Q. Sun, and J. D. Kepert, 2017a: Dynamics and predictability of secondary eyewall formation in sheared tropical cyclones. *J. Adv. Model. Earth Syst.*, **9**, 89–112, doi:10.1002/2016MS000729.

Zhang, G., and Perrie, W., 2018: Effects of asymmetric secondary eyewall on tropical cyclone evolution in Hurricane Ike (2008). *Geophys. Res. Lett.*, **45**, 1676–1683. doi:10.1002/2017GL076988.

Zhang, L., X. Zhang, P. C. Chu, C. Guan, H. Fu, G. Chao, G. Han, and W. Li, 2017b: Impact of sea spray on the Yellow and East China Seas thermal structure during the passage of Typhoon Rammasun (2002). *J. Geophys. Res.-Oceans*, **122**, 7783-7802, doi:10.1002/2016JC012592.

Zhang, J. A., R. F. Rogers, D. S. Nolan, and F. D. Marks, 2011: On the characteristic height scales of the hurricane boundary layer. *Mon. Wea. Rev.*, **139**, 2523–2535, doi:10.1175/MWR-D-10-05017.1.

Zhang, J. A., J. J. Cione, E. A. Kalina, E. W. Uhlhorn, T. Hock, and J. A. Smith, 2017c: Observations of infrared sea surface temperature and air-sea interaction in Hurricane Edouard (2014) using GPS dropsondes. *J. Atmos. Ocean. Technol.*, **34**, 1333-1349, doi:10.1175/JTECH-D-16-0211.1.

Zhang, J. A., R. F. Rogers, and V. Tallapragada, 2017d: Impact of parameterized boundary layer structure on tropical cyclone rapid intensification forecasts in HWRF. *Mon. Wea. Rev.*, **145**, 1413–1426, doi:10.1175/MWR-D-16-0129.1.

Zhang, S. J., Y. Z. Qian, Y. W. Huang, and J. M. Guo, 2017e: Numerical simulation study on the rapid intensification of Typhoon Haikui (1211) off the shore of China. *J. Trop. Meteor.*, doi:10.16555/j.1006-8775.2017.03.004.

Zhang, X., Y. Duan, Y. Wang, N. Wei, and H. Hu, 2017f: A high-resolution simulation of Supertyphoon Rammasun (2014)—Part I: Model verification and surface energetics analysis. *Adv. Atmos. Sci.*, **34**, 757–770, doi:10.1007/s00376-017-6255-7.

Zhang, W., Y. Zhang, D. Zheng, F. Wang, and L. Xu, 2015: Relationship between lightning activity and tropical cyclone intensity over the northwest Pacific. *J. Geophys. Res. Atmos.*, **120**, 40724089, doi:10.1002/2014JD022334.

Zhao, X. H. and J. C. L. Chan, 2017: Effect of the initial vortex size on intensity change in the WRF-ROMS coupled model. *J. Geophys. Res.-Oceans*, **122**, 9636-9648, doi:10.1002/2017JC013283.

Zhou, X., and B. Wang, 2013: Large-scale influences on secondary eyewall size. *J. Geophys. Res. Atmos.*, **118**, 11,088–11,097, doi:10.1002/jgrd.50605.

Zhu, P., Y. T. Wang, S. S. Chen, M. Curcic, and C. Gao, 2016: Impact of storm-induced cooling of sea surface temperature on large turbulent eddies and vertical turbulent transport in the atmospheric boundary layer of Hurricane Isaac. *J. Geophys. Res.-Oceans*, **121**, 861-876, doi:10.1002/2015JC011320.

Zhu, Z., and P. Zhu, 2014: The role of outer rainband convection in governing the eyewall replacement cycle in numerical simulations of tropical cyclones. *J. Geophys. Res. Atmos.*, **119**, 8049–8072, doi:10.1002/2014JD021899.

Zhu, Z., and P. Zhu, 2015: Sensitivities of eyewall replacement cycle to model physics, vortex structure, and background winds in numerical simulations of tropical cyclones. *J. Geophys. Res. Atmos.*, **120**, 590–622, doi:10.1002/2014JD022056.

Zhuge, X., J. Ming, and Y. Wang, 2015: Reassessing the use of inner-core hot towers to predict tropical cyclone rapid intensification. *Wea. Forecasting*, **30**, 1265–1279, doi:10.1175/WAF-D-15-0024.1.

Zweers, N. C., V. K. Makin, J. W. de Vries, and V. N. Kudryavtsev, 2015: The impact of spray-mediated enhanced enthalpy and reduced drag coefficients in the modelling of tropical cyclones. *Bound.-Layer Meteor.*, **155**, 501-514, doi:10.1007/s10546-014-9996-1.